National Library of Canada
Acquisitions and Bibliographic Services Branch
395 Wellington Street
Ottawa, Ontario
K1A 0N4

Bibliothèque nationale du Canada
Direction des acquisitions et des services bibliographiques
395, rue Wellington
Ottawa (Ontario)
K1A 0N4

Your file Votre référence

Our file Notre référence

NOTICE

The quality of this microform is heavily dependent upon the quality of the original thesis submitted for microfilming. Every effort has been made to ensure the highest quality of reproduction possible.

If pages are missing, contact the university which granted the degree.

Some pages may have indistinct print especially if the original pages were typed with a poor typewriter ribbon or if the university sent us an inferior photocopy.

Reproduction in full or in part of this microform is governed by the Canadian Copyright Act, R.S.C. 1970, c. C-30, and subsequent amendments.

AVIS

La qualité de cette microforme dépend grandement de la qualité de la thèse soumise au microfilmage. Nous avons tout fait pour assurer une qualité supérieure de reproduction.

S'il manque des pages, veuillez communiquer avec l'université qui a conféré le grade.

La qualité d'impression de certaines pages peut laisser à désirer, surtout si les pages originales ont été dactylographiées à l'aide d'un ruban usé ou si l'université nous a fait parvenir une photocopie de qualité inférieure.

La reproduction, même partielle, de cette microforme est soumise à la Loi canadienne sur le droit d'auteur, SRC 1970, c. C-30, et ses amendements subséquents.

Canada

Finite Element Vorticity-Based Methods for the Solution of the Incompressible and Compressible Navier-Stokes Equations

Grant Guèvremont

A Thesis

in

The Department

of

Mechanical Engineering

Presented in Partial Fulfillment of the Requirements
for the Degree of Doctor of Philosophy at
Concordia University
Montréal, Québec, Canada

August 1993

© Grant Guèvremont, 1993

National Library
of Canada

Acquisitions and
Bibliographic Services Branch

395 Wellington Street
Ottawa, Ontario
K1A 0N4

Bibliothèque nationale
du Canada

Direction des acquisitions et
des services bibliographiques

395, rue Wellington
Ottawa (Ontario)
K1A 0N4

Your file Votre référence

Our file Notre référence

The author has granted an irrevocable non-exclusive licence allowing the National Library of Canada to reproduce, loan, distribute or sell copies of his/her thesis by any means and in any form or format, making this thesis available to interested persons.

L'auteur a accordé une licence irrévocable et non exclusive permettant à la Bibliothèque nationale du Canada de reproduire, prêter, distribuer ou vendre des copies de sa thèse de quelque manière et sous quelque forme que ce soit pour mettre des exemplaires de cette thèse à la disposition des personnes intéressées.

The author retains ownership of the copyright in his/her thesis. Neither the thesis nor substantial extracts from it may be printed or otherwise reproduced without his/her permission.

L'auteur conserve la propriété du droit d'auteur qui protège sa thèse. Ni la thèse ni des extraits substantiels de celle-ci ne doivent être imprimés ou autrement reproduits sans son autorisation.

ISBN 0-315-87265-9

Canada

ABSTRACT

Finite Element Vorticity-Based Methods for the Solution of the Incompressible and Compressible Navier-Stokes Equations

Grant Guèvremont, Ph.D.
Concordia University, 1993

Finite element vorticity-based methods are applied to the analysis of viscous flows. This is carried out in terms of a stream function-vorticity formulation for 2-D flows and a velocity-vorticity formulation for 2-D and 3-D flows. Second order equations are obtained for the variables and the discretization is based on the weak-Galerkin weighted residual method.

The stream function-vorticity approach proposed in this thesis reverses the traditional imposition of wall boundary conditions. The finite element method is used to naturally impose the no-slip condition on the stream function equation accurate for complex geometries. This method is extended to two-dimensional subsonic external lifting flow. The unknown stream function value on the airfoil, for lifting flow, is obtained by enforcing a continuous pressure distribution over the entire airfoil. This is imposed naturally through the finite element discretized vorticity transport equation.

The velocity-vorticity scheme proposed in this thesis was the first to use a finite element weak-Galerkin method. This method is extended beyond incompressible flow to two- and three-dimensional subsonic internal flow. A new accurate wall vorticity boundary condition is also proposed. The

finite element discretization is chosen to have equal order interpolation for the vorticity and the first derivatives of velocity.

The stream function and vorticity or the velocity and vorticity are solved simultaneously using a Newton method. At each iteration, the linear algebraic system is solved by either a direct or an iterative matrix solver. For subsonic flows, the iteration is completed by obtaining the pressure, temperature, density and viscosity. Although it was found necessary in some cases to obtain solutions at intermediary Reynolds numbers, no artificial viscosity was required to stabilize the iteration algorithm.

The schemes demonstrate the advantages of the finite element method in providing natural boundary conditions for such problems.

Acknowledgments

I would first like to thank my supervisor Dr. W.G. (Fred) Habashi for his guidance and support throughout my graduate studies and for providing the opportunity, the environment and the resources to do this research. A special thanks goes to Dr. Mohammed Hafez for the many useful and invaluable technical discussions concerning my thesis work.

Many of my colleagues working for Dr. Habashi helped with the computer programs that were put together, most notably Peter Kotiuga of Pratt&Whitney Canada (PWC) for the compressible 3-D code, and Billy Sotirakos and Demetra Moutis for the stream function-vorticity lifting code. Other contributors include Dr. Jack Strigberger of the Concordia CFD Lab for his iterative matrix solver and Viet-Nam Nguyen of PWC for his CRAY-YMP parallel-vector direct matrix solver. I would also like to thank Martin Peeters for the useful technical discussions on his work with vorticity-based methods as well as my colleagues Bao Nguyen and Guido Baruzzi for their assistance and suggestions throughout my studies and research.

I would like to acknowledge the gracious donation of computer time from CRAY on their YMP/8-128. Much of the work in this thesis could not have been performed without this donation and it is very much appreciated. I would also like to acknowledge the donation of computer time from the Centre de Recherche en Informatique de Montreal (CRIM) on their VAX-8600.

This work was partially supported under Operating Grant OGPIN013 and Strategic Grants G-1613 and STR0040696 of the Natural Sciences and Engineering Research Council of Canada (NSERC). I would also like to personally acknowledge NSERC and Concordia University for financial support through scholarships.

This thesis is dedicated to Gerard, Louise, Paul, Dennis, Martin and Celine.

Table of Contents

List of Figures

List of Tables

Nomenclature

a_i	unknown coefficients of the element distribution
A	domain area
b	matrix bandwidth
c	airfoil chord length
C	solution domain contour
C_p, C_v	specific heat coefficients
C_p	coefficient of pressure
d	exact differential
E	total number of elements
E_{mass}	error norm in conservation of mass
$\vec{F}$	non-pressure terms of the momentum equations
H_o	stagnation enthalpy
$\vec{i}, \vec{j}, \vec{k}$	Cartesian unit vectors
I()	variational principle
k	element influence matrix
k	thermal conductivity
^oK	degrees Kelvin
L	length
L[]	differential operator
L_2	residual norm
M	Mach number
n	outward normal to domain boundary
n	exponent with which the CPU time increases with respect to the matrix bandwidth

$\vec{n}, \vec{s}$	unit vectors in normal and tangential directions at the domain boundaries
N	finite element shape function
N	number of unknowns in the matrix system
O( )	term of a specified order
p	pressure
Pr	Prandtl number
q	absolute velocity
R	gas constant
R	residual of a differential equation
Re	Reynolds number
s	distance along boundary of domain
S	solution domain surface
S^{ρ}	compressibility source term
S^{μ}	viscosity source term
$S^{\mu 1}, S^{\mu 2}, S^{\mu 3}$	components of the viscosity source term
t	CPU time
T	temperature
u,v,w	Cartesian velocity components
U,V,W	specified boundary velocities
$\vec{V}$	velocity vector
W	weight function
x,y,z	Cartesian coordinates

Greek symbols

α	angle of attack of free stream

∂	partial derivative
δ	variation
δ	boundary layer thickness
ξ,η,ζ	non-dimensional coordinates of the undistorted element
Δ	change in a variable
∇	Del operator
μ	viscosity
ρ	density
$\overline{\rho}$	inverse of the density
Ψ	stream function
ω	two-dimensional vorticity
$\vec{\Omega}$	vorticity vector
Ω_i	ith vorticity component
ϕ	unknown finite element variable
Φ	viscous dissipation function
ϑ	domain volume

Subscripts

i,j	nodal indices
LS	least-squares
n	derivative in the direction normal to the domain boundary
o	constant or reference value
ref	reference value
u,v,w	related to the x, y and z components of the velocity equation respectively

u,v,w	related to the x, y and z components of the velocity vector respectively
$\vec{V}$	related to the velocity equation
$\vec{V}$	related to the velocity vector
w	wall nodal index
ψ	related to the stream function equation
ψ	related to the stream function
ω	related to the two-dimensional vorticity transport equation
ω	related to the two-dimensional vorticity
$\vec{\Omega}$	related to the vorticity transport equation
$\vec{\Omega}$	related to the vorticity vector
Ω_i	related to the ith vorticity transport equation
Ω_i	related to the ith vorticity component
∞	free stream or reference value

Superscripts

e	element index
n	related to the outward normal to domain boundary
n	iteration number
$\vec{V}$	related to the velocity equation
$\vec{V}$	related to the velocity vector
ψ	related to the stream function equation
ψ	related to the stream function
ω	related to the two-dimensional vorticity transport equation

ω	related to the two-dimensional vorticity
$\vec{\Omega}$	related to the vorticity transport equation
$\vec{\Omega}$	related to the vorticity vector

1. Introduction

1.1 Historical Development of Vorticity-based Methods for the Navier-Stokes Equations

Viscous fluid flow, under the assumption of a continuum, is governed by a set of differential equations known as the Navier-Stokes equations. Strictly speaking, the Navier-Stokes equations refer only to those representing the conservation of momentum but generally also include the equations representing the conservation of mass and energy. Any numerical formulation requires the selection of the variables to be used as well as a discretization scheme. Since the governing equations, in any form, are generally non-linear, an iterative algorithm must also be selected. The choice of variables determines the form of the governing equations and greatly influences the choice of discretization and iterative algorithm.

For the two-dimensional incompressible Navier-Stokes equations, the most often used sets of variables have been either the primitive variables, i.e., velocity and pressure, the stream function and vorticity, or the stream function. The governing equations, in primitive variables form, consist of the continuity equation, a first order differential equation, and two momentum equations, each a second order differential equation. The energy equation is decoupled for incompressible flow. The pressure variable is not present in the continuity equation and is only present as a first order derivative in each momentum equation. If no special treatment is introduced into the numerical formulation, the solution will exhibit the

classical "checkerboarding" of the pressure [1]. Most primitive variables algorithms have attempted to avoid this phenomena through modification of the governing equations and/or through a non-standard discretization. Among the modifications of the governing equations are:

1) replacing the continuity equation with a Poisson pressure equation [2],
2) adding a pressure time derivative to the continuity equation (artificial compressibility [3]),
3) projection methods [4], and
4) penalty methods [4].

Discretization schemes include staggered finite difference grids where the velocity component and the pressure nodes are at different locations [2]. Similarly, for finite element discretizations, the pressure and velocity are represented by different interpolation functions [5].

The governing equations, in stream function-vorticity form, consist of two second order differential equations. The first equation is formed from the definitions of the vorticity and of the stream function and thus does not contain the pressure. The second equation is derived from the curl of the momentum equations which decouples the pressure variable from the governing system. After the stream function and vorticity have been converged upon, the pressure is recovered from a Poisson equation which is the divergence of the momentum equations. The major advantage of using the stream function is that it automatically satisfies the continuity equation through its definition.

The governing equations, in stream function form, reduce to only one fourth order differential equation. As with the stream function-vorticity equations,

this equation is derived from the curl of the momentum equations which decouples the pressure variable from the governing system. After the stream function has been converged upon, the pressure is recovered from a Poisson equation which is the divergence of the momentum equations. The continuity equation is also automatically satisfied which is a major advantage with respect to primitive variables. Solving for the stream function alone, compared to solving for both the stream function and the vorticity, has the advantage of only having to solve for one variable but has the disadvantage of having to solve a fourth order differential equation.

For the three-dimensional incompressible Navier-Stokes equations, most of the numerical formulations have been in terms of either primitive variables, stream functions (or vector potential) and vorticity, or velocity and vorticity. Vorticity-based methods form the vorticity transport equations by taking the curl of the momentum equations thus eliminating the pressure term. The pressure variable is not present in the governing equations for the stream function-vorticity and velocity-vorticity systems.

The compressible Navier-Stokes equations, in both two- and three-dimensions, have been formulated numerically almost exclusively using primitive variables. The governing equations, in primitive variables form, consist of the continuity equation, the momentum equations, the energy equation, an equation of state and an empirical relation for viscosity.

For vorticity-based methods, the vorticity transport equations are formed by taking the curl of the momentum equations and thus, as for incompressible flows, the pressure term is eliminated. As a result, the pressure is not

explicitly present in the governing equations. For compressible flow, however, the pressure is implicitly coupled through the presence of the density. As for incompressible flow, the pressure is recovered from a Poisson equation which is the divergence of the momentum equations. Unlike incompressible flow, the pressure must be updated during the iteration process. As with primitive variables formulations, the thermodynamic variables are updated during the iteration process using the energy equation, equation of state and viscosity relation.

The numerical formulation of the Navier-Stokes equations, by means of the stream function-vorticity approach, has traditionally suffered from some drawbacks, among them:

- The need to calculate vorticity at solid walls, which can only be done approximately and iteratively,
- The need for upwind discretization of the convective terms in the vorticity transport equation, in order to stabilize the iteration algorithm at high Reynolds numbers,
- The non-uniqueness of mass flow versus Mach number for transonic flows,
- The complexity of applying stream function formulations to three-dimensional flows.

For viscous flows, the stream function-vorticity approach has been efficiently applied to two-dimensional incompressible flows [6-8]. Despite the advantage of guaranteeing mass conservation, stream function-vorticity formulations have received limited attention for three-dimensional flows [9-

19] and have rarely been applied to subsonic flows [20,21]. Transonic stream function solvers have only been developed for inviscid flows [22].

Traditionally, for 2-D incompressible flows, the vorticity and the stream function were solved separately. The physical boundary conditions of no-penetration and no-slip velocities, when translated to stream function and vorticity variables, produce two boundary conditions on the stream function variable but none on the vorticity variable. The vorticity transport equation requires, however, a boundary condition on walls. By solving the two variables separately, it was only natural to impose the Dirichlet stream function boundary condition (no-penetration) on the stream function equation and use the Neumann stream function boundary condition (no-slip) to estimate the vorticity at a wall. Roache even goes as far as to claim that this is "the only correct distribution of these conditions" [23]. Traditionally, therefore, in finite difference methods, a Taylor's expansion for the stream function normal to the wall is formed. This series is modified by imposing the no-slip boundary condition and is used to obtain a wall vorticity formula. This vorticity value, which must be evaluated at each iteration, is then imposed as a Dirichlet boundary condition for the solution of the vorticity transport equation. This segregated solution method has been the source of instabilities at high Reynolds number requiring the use of upwinding, or artificial viscosity, to obtain convergence. Second order wall vorticity formulae have not produced better solutions than first order wall vorticity formulae [23,24] and have even worsened stability when the equations are solved in a segregated manner [23].

Although upwinding or artificial viscosity stabilizes such segregated schemes, the accuracy of the final solution will be affected. Strikwerda shows that the solution to a problem with upwinding on a given geometry is equivalent to the same problem with no upwinding but with the length scales of the geometry changed [25]. It can also be shown to be equivalent to lowering the effective Reynolds number [23]. Upwinding has also been used to suppress wiggles in the final solution. These wiggles, however, are a sign that the grid is too coarse and that it is preferable to refine the grid than suppress them artificially [23,26].

The cure to the instability problem with respect to the wall vorticity boundary condition is the coupling of the vorticity and the stream function equations. The two equations cannot be treated in isolation. The stream function appears to be over-specified and the vorticity under-specified. This is not the case when one views the entire stream function-vorticity system together. There are two boundary conditions on the wall which are indeed sufficient for the solution of the problem [27]. High Reynolds number solutions have been obtained in this thesis, without any use of upwinding or artificial viscosity, by solving the stream function and the vorticity simultaneously [7,8,21,28].

The extension of such alternative formulations to primitive variables, for 3-D flows, has been made but is, to a large degree, not simple. For example, either a vector potential [9,10,16,17,19], a scalar and vector potential [11,12,13,18], or a two-stream function [14,15] approach is used to represent arbitrary three-dimensional flows. The imposition of the boundary conditions, especially for internal flows, is quite complicated.

A logical extension of the stream function-vorticity approach could, however, be done through the velocity-vorticity formulation, initially suggested by Markham and Lewis [29] and Fasel [30] for two-dimensional flows and by Cook [31] and Dennis et al. [32] for three-dimensional Navier-Stokes equations. The boundary conditions for velocity-vorticity formulations remain simple for three-dimensions, which is not the case for stream function-vorticity formulations.

Among the advantages of the velocity-vorticity approach, over primitive variables, one should mention:

- Boundary conditions implementation is simpler for second order equations,
- For incompressible flows, the pressure does not need to be solved for as one of the variables and non-inertial effects do not change the form of the equations [33].

This last point is encouraging for turbomachinery applications for which it is desirable to solve an entire stage simultaneously. A turbomachinery stage is comprised of both a stator (stationary frame of reference) and a rotor (rotating frame of reference). Speziale [33] shows that, contrary to primitive variable formulations, the velocity-vorticity equations do not change form for a rotating frame of reference and hence the numerical formulation can be independent of the frame of reference.

The velocity-vorticity formulation has since become an attractive alternative and incompressible velocity-vorticity approaches using finite difference

[29,34-50], finite element [51-57], boundary element [58,59], vortex-particle [60,61] and other schemes [62] have been proposed.

There are two sets of differential equations that use velocity and vorticity variables for the Navier-Stokes equations. The first set is comprised of;

- Vorticity transport equation (second order PDE)
- Continuity equation (first order PDE)
- Definition of vorticity (first order PDE)

while the second set is comprised of;

- Vorticity transport equation (second order PDE)
- Poisson velocity equations (second order PDE)

Both sets include the second order vorticity transport equations. The difference is in the choice of equations for the velocity vector. The first set includes the first order differential equations; the continuity equation and the definition of vorticity. The second set includes the second order Poisson equations derived from the continuity equation and the definition of vorticity. It has been shown that if the proper boundary conditions are used, the second order set of partial differential equations will give back the same solution as the first order set [46,50]. On the discrete level, however, this is not necessarily the case. This constitutes a major problem, especially with respect to the conservation of mass. Second order partial differential equations are, however, preferable to solve numerically.

For two-dimensional problems, there are three governing equations for the velocity-vorticity system. The first order set of equations include the continuity equation, the definition of vorticity and the vorticity transport equation. The second order set of equations include two Poisson equations, one for each velocity component, and the vorticity transport equation.

For three-dimensional problems, there are six variables, three velocity components and three vorticity components, and thus six independent equations. The first order set of equations include the continuity equation, a vector equation defining vorticity and three vorticity transport equations. There is also an additional constraint on the vorticity vector; the vorticity must be solenoidal. This last constraint is a direct consequence of the definition of vorticity. This is redundant on a differential level, but may not be exact on a discrete level. This leaves a total of eight equations for six unknowns and requires either an elimination of two equations or a merging of some of the equations to form six. The second order set of equations merge the continuity equation and the three vorticity definitions into three Poisson equations for velocity. This still leaves a total of seven equations including the three vorticity transport equations and the vorticity vector constraint. Some authors start with the first order set of equations and then use a least-squares method to merge the continuity equation and the three definitions of vorticity. Hafez et al. [55] and Gunzburger and Peterson [52] have shown that the least-squares finite element equations using the original first order differential equations are identical to the Galerkin finite element equations using the second order Poisson equations for velocity. The vorticity remains solenoidal if the conservative form of the unsteady vorticity transport equation is used, assuming the flow at the initial time has

a solenoidal vorticity [39,46,49]. As a result of the vorticity vector being solenoidal, Osswald et al. eliminate one of the components of the definition of vorticity [39]. Gunzburger and Peterson [52] use the non-conservative form of the steady vorticity transport equation and impose the solenoidal condition on vorticity at the boundaries and show that this ensures a solenoidal vorticity in the field on the differential level. Gatski et al. solve a Poisson equation for a scalar potential to project the vorticity onto a solenoidal field at each time step [36].

The first papers on velocity-vorticity used the second order Poisson equations for velocity discretized by finite differences on regular (non-staggered) grids [30-32,34,35,37]. These formulations, although not acknowledging it, suffer mass loss for through-flow problems [41]. Daube explains that the gradient of the continuity equation, which is set to zero in the derivation of the second order Poisson equations, is not discretized correctly on a non-staggered grid [50]. Dacles and Hafez explain that the discretization of the divergence of the curl must be exactly zero [46]. Osswald et al. [39] introduced a scheme using the first order equations on a staggered grid where the velocities and vorticities nodes are not at the same location. This allows 'exact' mass conservation locally based on a finite volume analysis [40,42]. Several authors used the second order Poisson velocity equations on a staggered grid and obtained 'exact' or machine accurate mass conservation locally [42-44,46,47,50]. Napolitano and Catalano [45] found that the staggered grid results using the Poisson velocity equations recovered the definition of vorticity exactly for two-dimensional flows but not for three-dimensional flows. The experience with finite difference schemes using regular grids is that the final solution is very sensitive to the discretization of the vorticity

boundary condition and may not even obtain second order accuracy with respect to mass conservation [44]. A major disadvantage with using finite difference staggered grids is the discretization of the convective terms of the vorticity transport equation. The scheme must use velocities at points where they are not computed [43,50]. A similar problem arises at boundaries where not all the variables are defined and may cause inaccuracies in implementing known boundary conditions. For example, Osswald et al. [39] impose the normal velocity (no-penetration) explicitly at walls, but impose the no-slip condition implicitly through the tangential vorticities definition imposed at the walls.

The Galerkin finite element method, when applied to the velocity-vorticity system using the second order Poisson equations, experiences the same problem as with the finite difference methods on regular grids. The discretization of the vorticity boundary condition is critical for any success with this method [54].

The same conclusion concerning the importance of the vorticity boundary condition is reached by those using other methods of discretization such as the boundary element method [59] and the pseudo-spectral method [62].

In conclusion, it should be remarked that very few authors to date have solved the velocity-vorticity equations and only for moderate Reynolds number (3 000 - 7 000) flows. The unsteady equations have also been solved for, but require a restrictive time step [38,40,42,44,45], with convergence to steady-state requiring thousands of time steps. As examples, Orlandi [38] and Huang et al. [40] use a second order time stepping scheme with the intention

of accurately modeling unsteady flows, while Napolitano uses upwinding on the convective operator only such that the final steady-state solution is free of any upwinding or artificial viscosity [44,45].

1.2 Advantages of Proposed Stream Function-Vorticity Scheme

The proposed approach eliminates two of the traditional difficulties with the stream function-vorticity method mentioned in the previous section. It is based on a coupled solution of the equations, with the following consequences:

- The natural boundary conditions of a finite element formulation eliminate the need for explicit wall vorticity formulae and are ideal for the solution of the pressure equation,
- The upwinding required for the stabilization of the iterative procedure at high Reynolds numbers is unnecessary in this formulation.

Coupled stream function-vorticity solution schemes were initiated by Campion-Renson and Crochet [6] and Dhatt et al. [7]. Dhatt et al. demonstrated stable solutions at high Reynolds numbers without using upwinding, but their scheme still requires the use of wall vorticity formulae and hence leads to important, if not impossible, approximations in implementing the no-slip condition for complex geometries. Campion-Renson and Crochet, on the other hand, suggested that the Dirichlet boundary condition on the stream function replace the vorticity transport equation at solid wall boundaries, with the no-slip condition satisfied naturally by the stream function equation. This provided the key to

avoidance of wall vorticity formulae, but their results, somewhat erroneously, indicated that stability problems existed even at low Reynolds numbers.

Mizukami extended Campion-Renson's method to multiply connected domains but did not attempt a moderate or high Reynolds number problem [63]. Gunzburger also suggested a method for multiply connected domains [64] but is more difficult to implement. Tezduyar later used a method for multiply connected domains similar to that of Mizukami but for unsteady flows [65].

Peeters et al. first extended Campion-Renson's method to high Reynolds number incompressible flows without any need for upwinding or artificial viscosity and showed that the key was in the selection of the element discretizations for the stream function and the vorticity [8]. This part of the thesis is an extension of these methods to subsonic, high Reynolds number external lifting flows [21].

For vorticity-based methods, the pressure is generally solved from a Poisson equation. The boundary conditions for this equation are difficult and may lead to inaccuracies. A finite element formulation for this Poisson equation for pressure whose natural boundary conditions automatically satisfy the momentum equations is presented. For incompressible flows, the pressure is decoupled from the vorticity and is obtained as a post-processing exercise. It proves to be particularly useful for compressible flows, where pressure must be repeatedly solved for.

1.3 Advantages of Proposed Velocity-Vorticity Scheme

A finite element formulation is presented in this thesis for 2-D and 3-D, incompressible and subsonic flows [66-71]. Artificial viscosity, which is not present in any form in this formulation, would have to be added in order to be applied to transonic flows. Second order Poisson equations, derived from the continuity equation and the definition of vorticity, are used for the velocity vector. Satisfying the continuity equation, the definition of vorticity and a solenoidal vorticity relies on grid refinement and on an accurate implementation of the wall vorticity boundary condition.

Based on the experience of stream function-vorticity methods, the vorticity should be solved simultaneously with the velocity for stability at high Reynolds number. The wall boundary conditions, i.e., no-penetration and no-slip, are imposed directly on the velocities as Dirichlet boundary conditions. The vorticity at the walls is evaluated directly from the definition of vorticity in terms of velocity first order derivatives. The accuracy of this vorticity boundary condition is critical to the accuracy of the final solution. The numerical vorticity boundary condition is derived from a variational principle for the kinematics of the flow, i.e., the velocity equations, by minimizing it with respect to the unknown nodal vorticities at the walls. The choice of element, based on the stream function-vorticity experience and the need for an accurate vorticity boundary condition, is done such that the order of approximation for the vorticity and the first order derivatives of velocity are the same [53,66-71].

The numerical method for obtaining the pressure is the same as for the stream function-vorticity formulation with the stream function replaced by the velocity vector.

1.4 Brief Overview of Thesis

The second chapter describes in detail the stream function-vorticity finite element algorithm for solving two-dimensional subsonic flows. The governing differential equations and the associated boundary conditions in terms of stream function and vorticity are first derived. The finite element equations are derived including boundary condition implementation. A detailed discussion on the treatment of wall boundary conditions is then done. Finally, the overall subsonic iterative algorithm is shown.

The third chapter describes in detail the velocity-vorticity finite element algorithm for solving three-dimensional subsonic flows. The structure of this chapter is similar to that of Chapter 2.

The fourth chapter describes the finite element algorithm for solving the pressure for vorticity-based methods. The energy equation and thermodynamic relations necessary to complete the numerical model for subsonic flow are shown and/or derived.

The fifth and sixth chapters present the results for the stream function-vorticity and velocity-vorticity methods respectively. The stream function-vorticity method is tested for 2-D laminar subsonic external flows. The

velocity-vorticity method is tested for 2-D and 3-D laminar incompressible and subsonic internal flows.

The seventh and final chapter states the major conclusions and briefly describes some ideas on future work for both 2-D stream function-vorticity and 3-D velocity-vorticity methods.

2. Stream Function-Vorticity Formulation

2.1 Governing Equations

2.1.1 Governing Equations in Primitive Variables

The governing equations for two-dimensional, steady, compressible subsonic viscous flow, in terms of the primitive variables (u, v, p, ρ), are:

Continuity:

$$\frac{\partial(\rho u)}{\partial x} + \frac{\partial(\rho v)}{\partial y} = 0 \tag{2.1}$$

Momentum:

$$\rho\left(u\frac{\partial u}{\partial x} + v\frac{\partial u}{\partial y}\right) = -\frac{\partial p}{\partial x} + \frac{1}{Re}\left\{\frac{\partial}{\partial x}\left[2\mu\frac{\partial u}{\partial x} - \frac{2}{3}\mu\left(\frac{\partial u}{\partial x} + \frac{\partial v}{\partial y}\right)\right] + \frac{\partial}{\partial y}\left[\mu\left(\frac{\partial u}{\partial y} + \frac{\partial v}{\partial x}\right)\right]\right\} \tag{2.2a}$$

$$\rho\left(u\frac{\partial v}{\partial x} + v\frac{\partial v}{\partial y}\right) = -\frac{\partial p}{\partial y} + \frac{1}{Re}\left\{\frac{\partial}{\partial x}\left[\mu\left(\frac{\partial u}{\partial y} + \frac{\partial v}{\partial x}\right)\right] + \frac{\partial}{\partial y}\left[2\mu\frac{\partial v}{\partial y} - \frac{2}{3}\mu\left(\frac{\partial u}{\partial x} + \frac{\partial v}{\partial y}\right)\right]\right\} \tag{2.2b}$$

where Re is the Reynolds number. The external body forces are assumed negligible. For compressible flows, these equations are complemented by the energy equation, an equation of state and a relation for the viscosity.

The energy equation under the assumption of constant total enthalpy along streamlines takes the form:

$$H_o = C_pT + \frac{1}{2}(u^2 + v^2) \tag{2.3}$$

The equation of state for an ideal gas is:

$$\rho = \frac{p}{RT} \tag{2.4}$$

The empirical Sutherland's law for air [72] is used for the viscosity relation:

$$\frac{\mu}{\mu_\infty} = \left(\frac{T}{T_\infty}\right)^{1.5}\left(\frac{T_\infty + 110°K}{T + 110°K}\right) \tag{2.5}$$

2.1.2 Definition of Stream Function and Vorticity

The stream function is defined to identically satisfy the continuity equation:

$$\frac{\partial \Psi}{\partial y} \equiv \rho u \qquad\qquad \frac{\partial \Psi}{\partial x} \equiv -\rho v \tag{2.6}$$

The vorticity is defined as the curl of the velocity vector. For two-dimensional flow, the vorticity is the z-component of the vorticity vector:

$$\omega \equiv \frac{\partial v}{\partial x} - \frac{\partial u}{\partial y} \tag{2.7}$$

2.1.3 Stream Function-Vorticity Equations

The stream function equation is obtained by substituting the definition of the stream function (equation 2.6) into the definition of vorticity (equation 2.7):

$$\frac{\partial}{\partial x}\left(\frac{1}{\rho}\frac{\partial \Psi}{\partial x}\right) + \frac{\partial}{\partial y}\left(\frac{1}{\rho}\frac{\partial \Psi}{\partial y}\right) + \omega = 0 \tag{2.8}$$

The vorticity transport equation is obtained by taking the curl of the momentum equations (2.2a,b), thus eliminating the pressure term. After substituting the definition of the stream function (equation 2.6) and the definition of the vorticity (equation 2.7), the vorticity transport equation is:

$$\nabla^2(\mu\omega) - Re\left\{\frac{\partial \Psi}{\partial y}\frac{\partial \omega}{\partial x} - \frac{\partial \Psi}{\partial x}\frac{\partial \omega}{\partial y} + S^{\rho}\right\} + S^{\mu} = 0 \tag{2.9}$$

where

$$S^{\rho} = \frac{\partial}{\partial y}\left(\frac{1}{\rho}\right)\frac{\partial}{\partial x}\left(\frac{(\rho q)^2}{2}\right) - \frac{\partial}{\partial x}\left(\frac{1}{\rho}\right)\frac{\partial}{\partial y}\left(\frac{(\rho q)^2}{2}\right)$$

$$S^{\mu} = 2\left[\frac{\partial}{\partial x}\left(\frac{\partial \mu}{\partial x}\frac{\partial u}{\partial y} - \frac{\partial \mu}{\partial y}\frac{\partial u}{\partial x}\right) + \frac{\partial}{\partial y}\left(\frac{\partial \mu}{\partial x}\frac{\partial v}{\partial y} - \frac{\partial \mu}{\partial y}\frac{\partial v}{\partial x}\right)\right]$$

$$= \frac{\partial}{\partial x}(S^{\mu 1}) + \frac{\partial}{\partial y}(S^{\mu 2})$$

$$(\rho q)^2 = \left(\frac{\partial \Psi}{\partial x}\right)^2 + \left(\frac{\partial \Psi}{\partial y}\right)^2$$

The detailed derivation is shown in Appendix A. The incompressible laminar equations are obtained by setting the density and viscosity to unity ($\rho=\mu=1$) for which the compressibility source term S^{ρ} and the viscosity source term S^{μ} are both zero. No additional assumptions are made in deriving the

stream function-vorticity system of equations (2.8,2.9) from the primitive variable system of equations (2.1,2.2). Both equations (2.8) and (2.9) contain the stream function and the vorticity and are thus fully-coupled. The convective term, although linear in terms of one variable, is highly nonlinear for the coupled system.

For subsonic flows, this system is incomplete since the density and viscosity are variables that each require an extra relation. Although the pressure is explicitly decoupled from the stream function-vorticity equations, it is implicitly coupled through the density. The numerical solution of the pressure thus becomes crucial for the solution of the stream function and the vorticity. A method for recovering the pressure which takes advantage of natural boundary conditions will be presented in Chapter 4.

2.2 Finite Element Method : Method of Weighted Residuals

The finite element method first breaks up a given domain into a number of elements. Within each element, the unknown variable is approximated by a simple function, usually a polynomial, with a finite number of undetermined coefficients. For example, in two-dimensions, the variable could be represented with a bilinear polynomial distribution:

$$\phi^e(x,y) = a_1^e + a_2^e x + a_3^e y + a_4^e x y \qquad (2.10)$$

where

$\phi^e(x,y)$ is the variable approximation inside element e

a_i are the unknown coefficients of the distribution inside element e

These simple functions are usually expressed in terms of shape functions with the unknown coefficients being the variable ϕ at the nodal points of a given element:

$$\begin{aligned}\phi^e(x,y) &= N_1^e(x,y)\,\phi_1^e + N_2^e(x,y)\,\phi_2^e + N_3^e(x,y)\,\phi_3^e + N_4^e(x,y)\,\phi_4^e \\ &= \sum_{i=1}^{ndperl} N_i^e(x,y)\,\phi_i^e\end{aligned} \tag{2.11}$$

where

$N_i^e(x,y)$ is the shape function corresponding to node i of element e

ϕ_i^e is the variable at node i of element e (unknown)

ndperl is the number of nodes per element (4 in this case)

The shape functions have certain properties in order to be consistent with the prescribed variable distribution within the element:

1. $$\sum_{i=1}^{ndperl} N_i^e(x,y) = 1.0 \tag{2.12}$$

at any point (x,y) in the element. This property follows from the special case of $\phi^e(x,y)$ = constant = ϕ_i^e.

2. $$N_i^e(x_j,y_j) = \begin{cases} 1.0 & j = i \\ 0.0 & j \neq i \end{cases} \tag{2.13}$$

where (x_j,y_j) are the coordinates of node j. This property follows from the definition of $\phi_i^e \equiv \phi^e(x_i,y_i)$.

The weighted residual method orthogonalizes the discrete governing equation with a finite set of weight functions:

$$\int_A W_i(x,y)\, L[\phi(x,y)]\, dA = 0 \qquad (2.14)$$

where

$L[\phi] = 0$	is the governing equation
$\phi(x,y)$	is the unknown variable to be solved for
$W_i(x,y)$	is the weight function associated with global node i

Each governing discrete integral equation (2.14) is evaluated element by element:

$$\sum_{e=1}^{E} \left\{ \int_{A^e} W_i^e(x,y)\, L[\phi^e(x,y)]\, dA \right\} = 0 \qquad (2.15)$$

where

E	is the number of elements
$W_i^e(x,y)$	is the weight function corresponding to node i of element e

The number of weight functions per element, which equals the number of equations in a given element, must equal the number of unknown coefficients of the variable ϕ. These weight functions must form an

independent set in order to produce a set of independent equations. For the Galerkin weighted residual method, the weight functions are the shape functions:

$$W_i^e(x,y) = N_i^e(x,y) \tag{2.16}$$

2.2.1 Stream Function Equation

The weighted residual form of the stream function equation can be written as:

$$\int_A W_i^{\Psi}\left[\frac{\partial}{\partial x}\left(\frac{1}{\rho}\frac{\partial \Psi}{\partial x}\right) + \frac{\partial}{\partial y}\left(\frac{1}{\rho}\frac{\partial \Psi}{\partial y}\right) + \omega\right] dA = 0 \tag{2.17}$$

where W_i^{Ψ} is the weight function at node i, selected to correspond to the finite element shape function, N_i.

The integration by parts of equation (2.17) yields the weak-Galerkin form:

$$\int_A \left[\frac{1}{\rho}\left(\frac{\partial W_i^{\Psi}}{\partial x}\frac{\partial \Psi}{\partial x} + \frac{\partial W_i^{\Psi}}{\partial y}\frac{\partial \Psi}{\partial y}\right) - W_i^{\Psi}\omega\right] dA - \oint_C W_i^{\Psi}\left[\frac{1}{\rho}\frac{\partial \Psi}{\partial n}\right] ds = 0 \tag{2.18}$$

2.2.2 Vorticity Equation

The Galerkin weighted residual form of the vorticity transport equation can be written as:

$$\int_A W_i^{\omega}\left[\nabla^2(\mu\omega) - Re\left\{\frac{\partial\Psi}{\partial y}\frac{\partial\omega}{\partial x} - \frac{\partial\Psi}{\partial x}\frac{\partial\omega}{\partial y} + S^{\rho}\right\} + S^{\mu}\right] dA = 0 \qquad (2.19)$$

where W_i^{ω} is the weight function at node i, selected to correspond to the finite element shape function, N_i.

The integration by parts of equation (2.19) yields the weak-Galerkin form:

$$\int_A\left[\frac{\partial W_i^{\omega}}{\partial x}\left(\frac{\partial(\mu\omega)}{\partial x} + S^{\mu 1} - Re\frac{(\rho q)^2}{2}\frac{\partial}{\partial y}\left(\frac{1}{\rho}\right)\right) + \right.$$
$$\left.\frac{\partial W_i^{\omega}}{\partial y}\left(\frac{\partial(\mu\omega)}{\partial y} + S^{\mu 2} + Re\frac{(\rho q)^2}{2}\frac{\partial}{\partial x}\left(\frac{1}{\rho}\right)\right) + W_i^{\omega} Re\left\{\frac{\partial\Psi}{\partial y}\frac{\partial\omega}{\partial x} - \frac{\partial\Psi}{\partial x}\frac{\partial\omega}{\partial y}\right\}\right] dA$$
$$- \oint_C W_i^{\omega}\left[\frac{\partial(\mu\omega)}{\partial n} + S^{\mu n} - Re\frac{(\rho q)^2}{2}\frac{\partial}{\partial s}\left(\frac{1}{\rho}\right)\right] ds = 0 \qquad (2.20)$$

where

$$S^{\mu n} = \left(S^{\mu 1}\,\vec{i} + S^{\mu 2}\,\vec{j}\right)\cdot\vec{n}$$

Details of the integration by parts of the compressibility source term is given in Appendix B.

2.2.3 Element Discretization

In [8] numerical experiments were carried out with several combinations of weight functions and elements and it was concluded that bilinear shape functions should preferably be used for the vorticity, while the stream

function representation should be biquadratic. For accuracy, the geometry is described with curvilinear biquadratic elements. Hence:

$$\Psi = \sum_{j=1}^{8} N_j^{\Psi}(\xi,\eta)\,\Psi_j \qquad\qquad \omega = \sum_{j=1}^{4} N_j^{\omega}(\xi,\eta)\,\omega_j \qquad (2.21a,b)$$

$$x = \sum_{j=1}^{8} N_j^{\Psi}(\xi,\eta)\,x_j \qquad\qquad y = \sum_{j=1}^{8} N_j^{\Psi}(\xi,\eta)\,y_j \qquad (2.22a,b)$$

where (ξ,η) are the non-dimensional coordinates of the undistorted element.

These same numerical experiments [8] also demonstrated that the selection of the weight functions for the finite element governing equations (2.18,2.20) should be;

$$W_i^{\Psi} = N_i^{\Psi} \qquad\qquad W_i^{\omega} = N_i^{\omega} \qquad (2.23a,b)$$

2.3 General Boundary Conditions

2.3.1 Inlet, Infinite and Symmetry Boundaries

On the inlet for internal flows, the normal velocity and the density are prescribed profiles and the tangential velocity is assumed zero. For the case where the inlet normal is in the x-direction, the stream function and vorticity are :

$$\Psi = \Psi(y) = \int_0^y \rho(y)\,U(y)\,dy \qquad (2.24a)$$

$$\omega = \omega(y) = -\frac{dU(y)}{dy} \tag{2.24b}$$

For external flows, the actual domain of influence is infinite. For most computational models, the far-field boundary is set at a finite distance away from the body. On this boundary, free stream velocity and density are assumed, hence:

$$\Psi = y\cos(\alpha) - x\sin(\alpha) \tag{2.25a}$$

$$\omega = 0 \tag{2.25b}$$

On symmetry boundaries, the normal velocity, its tangential derivative and the tangential velocity's normal derivative are all zero, hence:

$$\Psi = \Psi_o \tag{2.26a}$$

$$\omega = \left(\vec{\nabla} \times \vec{V}\right) \bullet \vec{k} = \frac{\partial\left(\vec{V} \bullet \vec{n}\right)}{\partial s} - \frac{\partial\left(\vec{V} \bullet \vec{s}\right)}{\partial n} = 0 - 0 = 0 \tag{2.26b}$$

All these boundaries have Dirichlet boundary conditions for both the stream function and the vorticity. These are very easy to implement for any chosen numerical algorithm and discretization.

2.3.2 Exit Boundary

On the exit, the streamlines are parallel and the normal derivative of most quantities are assumed zero:

$$\frac{\partial \Psi}{\partial n} = 0 \tag{2.27a}$$

$$\frac{\partial \omega}{\partial n} = 0 \tag{2.27b}$$

Physically, the first boundary condition assumes zero transverse velocity while the second boundary condition assumes zero normal derivatives of the velocities. Since in reality the flow gradients are zero only at infinity, the above boundary conditions are approximate. Outflow or exit boundary conditions are a source of ongoing debates [27], especially for flows where recirculation reaches the exit. To avoid such a case, the exit is placed far downstream of the disturbance (airfoil) such that the gradients of the flow quantities are very low.

The first boundary condition (2.27a) is implemented by not evaluating the contour integral of the stream function equation (2.18). The second boundary condition (2.27b) is implemented by not evaluating the first term in the contour integral of the vorticity transport equation (2.20). It is assumed that the normal derivative of the viscosity is also zero. The second term in the vorticity transport contour integral ($S^{\mu n}$) is neglected as a result of assuming zero normal derivatives (see Appendix C). The third term in the vorticity transport contour integral only contains a tangential derivative and is

evaluated analytically. Implementing Neumann boundary conditions for finite element methods is usually done naturally through the contour integral of the governing equations. For zero Neumann boundary conditions, which is often the case, the implementation is done very easily by not evaluating the contour integral.

2.4 Wall Boundary Conditions

For viscous flows, the boundary conditions on a stationary wall are;

$$u = 0 \qquad\qquad v = 0 \qquad\qquad (2.28a,b)$$

or in local coordinates

$$\vec{V} \cdot \vec{n} = \vec{V} \cdot \vec{s} = 0 \qquad\qquad (2.29a,b)$$

Translating into stream function and vorticity variables;

$$\text{no-penetration} : \quad \frac{\partial \Psi}{\partial s} = \rho\left(\vec{V} \cdot \vec{n}\right) = 0 \quad \text{or} \quad \Psi = \text{constant} \qquad (2.30a)$$

$$\text{no-slip} : \quad \frac{\partial \Psi}{\partial n} = -\rho\left(\vec{V} \cdot \vec{s}\right) = 0 \qquad (2.30b)$$

There are two boundary conditions on the stream function and none on the vorticity. This is perfectly consistent with respect to the overall system of equations. If either variable is taken in isolation, then the stream function is over-specified and the vorticity under-specified.

2.4.1 Segregated Methods for Stream Function-Vorticity

Traditionally, the two equations were solved sequentially [27]. The Dirichlet boundary condition for the stream function representing no-penetration was imposed on the Poisson stream function equation. The Neumann boundary condition for the stream function representing no-slip was used to create a formula to evaluate the vorticity at a wall node. This wall vorticity value was imposed as a Dirichlet vorticity boundary condition to solve the vorticity transport equation.

For demonstration purposes, the most basic first order wall vorticity formula is derived here [23]. A Taylor's series expansion for the stream function node adjacent to the wall results in;

$$\Psi_{w+1} = \Psi_w + (\Delta n)\left(\frac{\partial \Psi}{\partial n}\right)_w + \frac{(\Delta n)^2}{2!}\left(\frac{\partial^2 \Psi}{\partial n^2}\right)_w + \ldots \qquad (2.31)$$

The no-slip boundary condition is imposed on this expansion by eliminating the first derivative term. The second derivative of stream function is replaced with the definition of vorticity using the no-penetration condition to remove tangential derivatives;

$$\left(\frac{\partial \Psi}{\partial n}\right)_w = 0 \qquad -\omega_w = \left(\frac{\partial^2 \Psi}{\partial n^2}\right)_w + \left(\frac{\partial^2 \Psi}{\partial s^2}\right)_w = \left(\frac{\partial^2 \Psi}{\partial n^2}\right)_w \qquad (2.32a,b)$$

Higher derivatives are removed which forms the truncation error. After rearranging, this results in a first order accurate wall vorticity formula;

$$-\omega_w = \frac{2(\Psi_{w+1} - \Psi_w)}{\Delta n^2} + O(\Delta n) \tag{2.33}$$

By using more points, second order wall vorticity formulae can be derived. Many authors have found that these second order formulae do not create more accurate final solutions than the first order formulae and may even cause instability [23,24]. The wall vorticity boundary condition, unlike the two boundary conditions on the stream function, changes in value every iteration.

The procedure is to first solve for the stream function in the field using the Poisson stream function equation, then evaluate the vorticity at walls and then solve for the vorticity in the field using the vorticity transport equation. The lagging of the wall vorticity is thought to be the main culprit in preventing convergence at high Reynolds number flows [6-8,27,28].

The wall vorticity formulae derivation requires that the grid line be normal to the wall boundary. For complex geometries, this would require a global grid transformation or association to more neighboring points.

2.4.2 Simultaneous Methods for Stream Function-Vorticity Using Finite Elements

To eliminate the stability problem associated with the lagging of the iterative vorticity wall boundary condition, the stream function and the vorticity can be solved simultaneously [6-8,27,28]. This statement is independent of the discretization (finite difference or finite element) of the governing equations

and boundary conditions. Although this increases the stability of the scheme, the computational cost per iteration increases due to the larger size of the matrix. It is felt that the overall computational cost will be lower for moderate Reynolds number and that convergence can be obtained for high Reynolds number which may not be the case for segregated methods.

The stream function-vorticity system of two second order differential equations requires two independent boundary conditions at the wall. There is no need that one boundary condition be on the stream function and one on the vorticity. The two boundary conditions replace the two unknowns at the wall. The stream function is known from the Dirichlet no-penetration condition. This leaves the no-slip condition to be imposed in place of the wall vorticity unknown.

Dhatt et al. [7] simply set the discrete version of the normal derivative of the stream function at the wall node to zero;

$$\sum_j \left[\frac{1}{E_i} \sum_{e=1}^{E_i} \frac{\partial N_j^e}{\partial n} \right] \Psi_j = 0 \qquad \text{at wall node } i \tag{2.34}$$

where

E_i is the number of elements connected to node i

and places this equation in the matrix row of the unknown wall vorticity. Since the stream function-vorticity system is solved simultaneously, the absence of the wall vorticity unknown in its own equation does not prevent a solution of the problem. Dhatt's discretization is however inaccurate due to two reasons; 1) derivatives are less accurate on the sides of elements and least accurate at the corners, and 2) for curved geometries, there will be a

discontinuity in slope between elements at the nodes on the boundary and thus a singularity in the normal direction.

Campion-Renson and Crochet [6] use the stream function equation to impose the Neumann stream function no-slip boundary condition by simply neglecting the contour integral at walls;

$$\int_A \left[\frac{\partial W_i}{\partial x}\frac{\partial \Psi}{\partial x} + \frac{\partial W_i}{\partial y}\frac{\partial \Psi}{\partial y} - W_i\,\omega \right] dA = \oint_C W_i \frac{\partial \Psi}{\partial n} ds = 0 \qquad (2.35)$$

The stream function equation at the wall is placed in the matrix row of the unknown wall vorticity. This is more accurate than Dhatt's method and doesn't require any treatment for complex geometries as this is handled by the finite element discretization directly. The mathematical reasoning behind this choice will be given in the next section.

2.4.3 Variational Principle for Stokes Flow

The scheme is first discussed for Stokes flow (Re=0) to illustrate the proper imposition of boundary conditions. The governing stream function-vorticity equations for two-dimensional incompressible flow are:

$$\nabla^2 \Psi + \omega = 0 \qquad (2.36)$$

$$\nabla^2 \omega = 0 \qquad (2.37)$$

where

$$\frac{\partial \Psi}{\partial y} \equiv u \quad , \quad \frac{\partial \Psi}{\partial x} \equiv - v$$

$$\omega \equiv \frac{\partial v}{\partial y} - \frac{\partial u}{\partial x}$$

Multiplying (2.36) by ω and (2.37) by Ψ, summing and integrating by parts leads to the variational principle:

$$I(\Psi,\omega) = \int_A \left[- \nabla\omega \cdot \nabla\Psi + \frac{1}{2}\omega^2 \right] dA + \oint_C \left[\omega \frac{\partial \Psi}{\partial n} + \Psi \frac{\partial \omega}{\partial n} \right] ds \qquad (2.38)$$

Taking the variation of (2.38):

$$\delta I = \int_A \left[- \frac{\partial(\delta\omega)}{\partial x}\frac{\partial \Psi}{\partial x} - \frac{\partial(\delta\omega)}{\partial y}\frac{\partial \Psi}{\partial y} + \omega\,\delta\omega \right] dA + \oint_C \delta\omega \frac{\partial \Psi}{\partial n} ds + \int_A \left[- \frac{\partial \omega}{\partial x}\frac{\partial(\delta\Psi)}{\partial x} - \frac{\partial \omega}{\partial y}\frac{\partial(\delta\Psi)}{\partial y} \right] dA + \oint_C \delta\Psi \frac{\partial \omega}{\partial n} ds \qquad (2.39)$$

Using Green's theorem, the governing equations can be recovered:

$$\delta I = \int_A \delta\omega \left[\nabla^2\Psi + \omega \right] dA + \int_A \delta\Psi \left[\nabla^2\omega \right] dA = 0 \qquad (2.40)$$

Since the variations $\delta\Psi$ and $\delta\omega$ are arbitrary, both integrals will have to be zero. The governing variational equations are therefore:

$$\int_A \left[\frac{\partial(\delta\omega)}{\partial x}\frac{\partial \Psi}{\partial x} + \frac{\partial(\delta\omega)}{\partial y}\frac{\partial \Psi}{\partial y} - \omega\,\delta\omega \right] dA = \oint_C \delta\omega \frac{\partial \Psi}{\partial n} ds \qquad (2.41a)$$

$$\int_A \left[\frac{\partial \omega}{\partial x}\frac{\partial(\delta\Psi)}{\partial x} + \frac{\partial \omega}{\partial y}\frac{\partial(\delta\Psi)}{\partial y} \right] dA = \oint_C \delta\Psi \frac{\partial \omega}{\partial n} ds \qquad (2.41b)$$

The variations $\delta\Psi$ and $\delta\omega$ are arbitrary except that $\delta\Psi=0$ when Ψ is specified and $\delta\omega=0$ when ω is specified. At solid walls Ψ is specified thus equation (2.41b) becomes trivial since $\delta\Psi=0$ and is replaced by the Dirichlet condition $\Psi=\Psi(s)$. The second boundary condition, $\Psi_n = 0$ or $\Psi_n = \Psi_n(s)$, is satisfied naturally by the contour integral of equation (2.41a). The key to the avoidance of wall vorticity formulae is seen therefore to be the reversal, as compared to traditional methods, of applying the no-slip and no-penetration stream function boundary conditions to the governing equations. Since the (Ψ-ω) system is solved in a coupled manner there is no need to identify which boundary condition applies to which equation. The coupled approach thus dispenses with the evaluation of complex wall vorticity formulae and all their associated inaccuracies and instabilities.

2.4.4 Present Method for Navier-Stokes Equations

For the full compressible stream function-vorticity system of equations, there exists no variational principle. It is assumed that the reasoning behind the application of the wall boundary conditions for the incompressible Stokes flow analysis remain the same for subsonic viscous flows.

The wall boundary conditions are imposed without wall vorticity formulae. At solid walls, the vorticity transport equation (2.20) is ignored and replaced by the no-penetration condition (2.30a). Neglecting the contour integral in the stream function equation (2.18) implicitly satisfies the no-slip condition (2.30b). Should the velocity of the wall not be zero, for example along a moving wall, the contour integral is evaluated analytically for such contours;

$$\oint_C W_i^{\Psi}\left[\frac{1}{\rho}\frac{\partial \Psi}{\partial n}\right] ds = \oint_C W_i^{\Psi}\, U(s)\, ds \tag{2.42}$$

2.5 Multiply Connected Domains

For simply connected domains such as symmetric airfoils at zero angle of attack, the stream function along walls is constant and its value is known. For multiply connected domains such as asymmetric airfoils or symmetric airfoils at non-zero angles of attack, the stream function along walls is also constant but its value is unknown. This requires one extra constraint in the domain to determine this value. This constraint requires the pressure, which is not solved for directly, to be continuous along the airfoil:

$$\oint_C dp = 0 \tag{2.43}$$

The pressure gradients are replaced using the momentum equations (2.2). Assuming a stationary airfoil, the convective terms are removed since the integration is only along the airfoil. The viscous terms are recast using the definition of vorticity (equation 2.7) giving:

$$0 = \oint_C dp = \oint_C \left[\frac{\partial p}{\partial x} dx + \frac{\partial p}{\partial y} dy\right]$$

$$= \oint_C \left[-\frac{\partial(\mu\omega)}{\partial y} + 2\left(\frac{\partial \mu}{\partial y}\frac{\partial v}{\partial x} - \frac{\partial \mu}{\partial x}\frac{\partial v}{\partial y}\right)\right] dx \qquad (2.44)$$

$$+ \left[\frac{\partial(\mu\omega)}{\partial x} + 2\left(\frac{\partial \mu}{\partial x}\frac{\partial u}{\partial y} - \frac{\partial \mu}{\partial y}\frac{\partial u}{\partial x}\right)\right] dy$$

Mizukami introduced a method for implementing this constraint into a finite element stream function-vorticity incompressible formulation [63]. The same ideas are used to implement this constraint into the present subsonic formulation.

All the derivatives in equation (2.44) must be evaluated at the wall. Derivatives of finite element distributions are considered more accurate inside the element than on the boundary of elements for C^o elements. For C^o elements, only the variable itself is required to be continuous between elements. The normal derivatives of the variable are generally discontinuous between elements. Mizukami, for incompressible flows, replaced the line integral with an area integral using the weak-Galerkin form of the vorticity transport equation (2.20). The vorticity shape function must be introduced into the line integral of equation (2.44) to make it compatible with the contour integral of equation (2.20). This is achieved by using the property that the summation of all the finite element shape functions at a given point is unity (equation 2.12). As a consequence of equation (2.13), the only shape functions that are non-zero along a boundary are those whose corresponding nodes are on the boundary. Equation (2.43) is thus modified as follows:

$$0 = \oint_C (1)\,dp = \oint_C \left(\sum_{i=1}^{nnodea} N_i^{\omega} \right) dp$$
$$= \sum_{i=1}^{nnodea} \oint_C N_i^{\omega}\,dp \tag{2.45}$$

where nnodea is the number of vorticity nodes on the airfoil.

Replacing equation (2.44) into equation (2.45) gives a finite element form of the constraint:

$$0 = \sum_{i=1}^{nnodea} \oint_C N_i^{\omega} \left\{ \left[-\frac{\partial(\mu\omega)}{\partial y} + 2\left(\frac{\partial \mu}{\partial y}\frac{\partial v}{\partial x} - \frac{\partial \mu}{\partial x}\frac{\partial v}{\partial y} \right) \right] dx \right.$$
$$\left. + \left[\frac{\partial(\mu\omega)}{\partial x} + 2\left(\frac{\partial \mu}{\partial x}\frac{\partial u}{\partial y} - \frac{\partial \mu}{\partial y}\frac{\partial u}{\partial x} \right) \right] dy \right\} \tag{2.46}$$

The above line integral for the subsonic formulation is the contour integral of the weak-Galerkin form of the vorticity transport equation (2.20) for walls with zero velocity. Replacing equation (2.20) into equation (2.46) gives the final form of the constraint equation which is implemented in the present subsonic finite element formulation:

$$0 = \sum_{i=1}^{nnodea} \int_A \left[\frac{\partial N_i^{\omega}}{\partial x} \left(\frac{\partial(\mu\omega)}{\partial x} + S^{\mu 1} - Re\,\frac{(\rho q)^2}{2}\frac{\partial}{\partial y}\left(\frac{1}{\rho}\right) \right) \right.$$
$$+ \frac{\partial N_i^{\omega}}{\partial y} \left(\frac{\partial(\mu\omega)}{\partial y} + S^{\mu 2} + Re\,\frac{(\rho q)^2}{2}\frac{\partial}{\partial x}\left(\frac{1}{\rho}\right) \right)$$
$$\left. + N_i^{\omega}\,Re \left(\frac{\partial \Psi}{\partial y}\frac{\partial \omega}{\partial x} - \frac{\partial \Psi}{\partial x}\frac{\partial \omega}{\partial y} \right) \right] dA \tag{2.47}$$

This equation connects all the nodes along the isolated body (airfoil). This requires the use of a matrix solver with skyline storage, with this particular equation placed in the last row to minimize the memory requirements. This last unknown in the matrix system is the stream function value on the airfoil surface.

2.6 Newton Linearization

The nonlinear system of equations (2.18,2.20) is linearized by a Newton method. The stream function and the vorticity are solved simultaneously. Each variable is expressed in Δ form as follows:

$$\Delta\Psi \equiv \Psi^{n+1} - \Psi^{n} \tag{2.48a}$$

$$\Delta\omega \equiv \omega^{n+1} - \omega^{n} \tag{2.48b}$$

After neglecting second order terms, the Newton-Galerkin form of the governing finite element equations can be written as:

$$\int_A \left[\frac{1}{\rho}\left(\frac{\partial W_i^{\Psi}}{\partial x}\frac{\partial(\Delta\Psi)}{\partial x} + \frac{\partial W_i^{\Psi}}{\partial y}\frac{\partial(\Delta\Psi)}{\partial y}\right) - W_i^{\Psi}\Delta\omega\right] dA = -R_i^{\Psi} \tag{2.49}$$

$$\begin{aligned}\int_A \Bigg[&\frac{\partial W_i^{\omega}}{\partial x}\left(\frac{\partial(\mu\Delta\omega)}{\partial x} - Re\,\frac{\partial}{\partial y}\left(\frac{1}{\rho}\right)\left(\frac{\partial\Psi}{\partial x}\frac{\partial(\Delta\Psi)}{\partial x} + \frac{\partial\Psi}{\partial y}\frac{\partial(\Delta\Psi)}{\partial y}\right)\right)\\ &+ \frac{\partial W_i^{\omega}}{\partial y}\left(\frac{\partial(\mu\Delta\omega)}{\partial y} + Re\,\frac{\partial}{\partial x}\left(\frac{1}{\rho}\right)\left(\frac{\partial\Psi}{\partial x}\frac{\partial(\Delta\Psi)}{\partial x} + \frac{\partial\Psi}{\partial y}\frac{\partial(\Delta\Psi)}{\partial y}\right)\right) +\\ &W_i^{\omega}\,Re\left(\frac{\partial\Psi}{\partial y}\frac{\partial(\Delta\omega)}{\partial x} + \frac{\partial\omega}{\partial x}\frac{\partial(\Delta\Psi)}{\partial y} - \frac{\partial\Psi}{\partial x}\frac{\partial(\Delta\omega)}{\partial y} - \frac{\partial\omega}{\partial y}\frac{\partial(\Delta\Psi)}{\partial x}\right)\Bigg] dA = -R_i^{\omega}\end{aligned} \tag{2.50}$$

where R_i^{Ψ} and R_i^{ω} are the residuals, at node i, of equations (2.18) and (2.20), respectively. Substituting the shape functions of equation (2.21), one obtains the following discretized matrix equations (i=row, j=column) :

$$\sum_{e=1}^{E}\left[\sum_{j=1}^{8}\left[k_{\psi\psi}\right]_{ij}\Delta\Psi_j + \sum_{j=1}^{4}\left[k_{\psi\omega}\right]_{ij}\Delta\omega_j\right] = -R_i^{\Psi} \qquad (2.51)$$

where

$$\left[k_{\psi\psi}\right]_{ij} = \int_A\left[\frac{1}{\rho}\left(\frac{\partial W_i^{\psi}}{\partial x}\frac{\partial N_j^{\psi}}{\partial x} + \frac{\partial W_i^{\psi}}{\partial y}\frac{\partial N_j^{\psi}}{\partial y}\right)\right]dA$$

$$\left[k_{\psi\omega}\right]_{ij} = \int_A -\left[W_i^{\psi}\, N_j^{\omega}\right]dA$$

and

$$\sum_{e=1}^{E}\left[\sum_{j=1}^{8}\left[k_{\omega\psi}\right]_{ij}\Delta\Psi_j + \sum_{j=1}^{4}\left[k_{\omega\omega}\right]_{ij}\Delta\omega_j\right] = -R_i^{\omega} \qquad (2.52)$$

where

$$\left[k_{\omega\psi}\right]_{ij} = \int_A\left[W_i^{\omega}\,\mathrm{Re}\left(\frac{\partial\omega}{\partial x}\frac{\partial N_j^{\psi}}{\partial y} - \frac{\partial\omega}{\partial y}\frac{\partial N_j^{\psi}}{\partial x}\right)\right]dA$$

$$[k_{\omega\omega}]_{ij} = \int_A \left[\frac{\partial W_i^\omega}{\partial x} \left(\frac{\partial \mu}{\partial x} N_j^\omega + \mu \frac{\partial N_j^\omega}{\partial x} \right) + \frac{\partial W_i^\omega}{\partial y} \left(\frac{\partial \mu}{\partial y} N_j^\omega + \mu \frac{\partial N_j^\omega}{\partial y} \right) + W_i^\omega \, Re \left(\frac{\partial \Psi}{\partial y} \frac{\partial N_j^\omega}{\partial x} - \frac{\partial \Psi}{\partial x} \frac{\partial N_j^\omega}{\partial y} \right) \right] dA$$

The integrals are evaluated numerically by Gauss-Legendre quadrature, using a 3x3 grid in each element.

3. Velocity-Vorticity Formulation

3.1 Governing Equations

3.1.1 Governing Equations in Primitive Variables

The governing equations for three-dimensional, steady, compressible subsonic viscous flow, in terms of the primitive variables ($\vec{V}$, p, ρ), are [73]:

Continuity:

$$\nabla \cdot (\rho \vec{V}) = 0 \tag{3.1}$$

Momentum:

$$\begin{aligned}(\rho \vec{V} \cdot \nabla)\vec{V} = -\nabla p + \frac{1}{Re}\Big\{\nabla\Big[\frac{4}{3}\mu(\nabla \cdot \vec{V}) + \vec{V} \cdot \nabla\mu\Big] - \vec{V}\big[\nabla^2\mu\big] \\ - \big[\nabla \cdot \vec{V}\big]\nabla\mu + \nabla\mu \times \big[\nabla \times \vec{V}\big] - \nabla \times \big[\nabla \times (\mu\vec{V})\big]\Big\}\end{aligned} \tag{3.2}$$

where Re is the Reynolds number. The external body forces are assumed negligible. For compressible flows, these equations are complemented by the energy equation, an equation of state and a relation for the viscosity.

The energy equation under the assumption of constant total enthalpy along streamlines takes the form:

$$H_o = C_p T + \frac{1}{2}\vec{V} \cdot \vec{V} \tag{3.3}$$

The equation of state for an ideal gas is given by equation (2.4) while the empirical Sutherland's law for air [72] is used for the viscosity relation (equation 2.5).

3.1.2 Velocity-Vorticity Equations

The vorticity vector is defined as the curl of the velocity vector:

$$\vec{\Omega} \equiv \nabla \times \vec{V} \tag{3.4}$$

Using the vorticity definition and the continuity equation, a second order form of the velocity-vorticity equations, appropriate for a finite element formulation, can be obtained. For the velocity equations:

$$\begin{aligned} \nabla \times (\rho\vec{\Omega}) &= \nabla \times (\rho\, \nabla \times \vec{V}) = \nabla \times [\nabla \times (\rho\vec{V}) - \nabla\rho \times \vec{V}] \\ &= \nabla [\nabla \cdot (\rho\vec{V})] - \nabla^2(\rho\vec{V}) - \nabla \times (\nabla\rho \times \vec{V}) \\ &= -\nabla^2(\rho\vec{V}) - \nabla \times (\nabla\rho \times \vec{V}) \end{aligned}$$

or:

$$\nabla^2(\rho\vec{V}) + \nabla \times (\rho\vec{\Omega}) + \nabla \times (\nabla\rho \times \vec{V}) = 0 \tag{3.5}$$

The vorticity transport equation can be derived by taking the curl of the momentum equations, hence eliminating the pressure as a variable. After substituting the definition of the vorticity (equation 3.4), the vorticity transport equation takes the form:

$$\nabla^2(\mu\vec{\Omega}) - \mathrm{Re}\left\{(\rho\vec{V} \cdot \nabla)\vec{\Omega} - (\vec{\Omega} \cdot \nabla)(\rho\vec{V}) + \vec{S}^{p}\right\} + \vec{S}^{\mu} = 0 \tag{3.6}$$

where:

$$\vec{S}^{\rho} = \frac{1}{2}\nabla\rho\times\left(\nabla V^2\right)$$

$$\vec{S}^{\mu} = -2\nabla\times\left[\left(\nabla\bullet\vec{V}\right)\nabla\mu + \left(\vec{V}\bullet\nabla\right)\nabla\mu\right] - \nabla\left(\vec{\Omega}\bullet\nabla\mu\right)$$

$$= \frac{\partial\vec{S}^{\mu 1}}{\partial x} + \frac{\partial\vec{S}^{\mu 2}}{\partial y} + \frac{\partial\vec{S}^{\mu 3}}{\partial z} \qquad \text{in Cartesian coordinates}$$

The detailed derivation is shown in Appendix D. The incompressible laminar equations are obtained by setting the density and viscosity to unity ($\rho=\mu=1$) for which the compressibility source term S^{ρ} and the viscosity source term S^{μ} are both zero. No additional assumptions are made in deriving the velocity-vorticity system of equations (3.5,3.6) from the primitive variable system of equations (3.1,3.2). As with the stream function-vorticity system, the velocity-vorticity system is coupled and highly nonlinear.

For subsonic flows, this system is still incomplete since the density and viscosity are variables that each require an extra relation. Although the pressure is explicitly decoupled from the velocity-vorticity equations, it is implicitly coupled through the density. The numerical solution of the pressure, as with the stream function-vorticity system, becomes crucial for the solution of the velocity and the vorticity and will be shown in Chapter 4.

3.2 Finite Element Method : Method of Weighted Residuals

3.2.1 Velocity Equations

The weighted residual form is obtained by minimizing the residuals of the system of equations over the solution domain. The velocity equation (3.5) is

multiplied by a weight function, W_i, and integrated over the domain as follows:

$$\int_{\vartheta} W_i^{\vec{V}}\left[\nabla^2\left(\rho\vec{V}\right) + \nabla\times\left(\rho\vec{\Omega}\right) + \nabla\times\left(\nabla\rho\times\vec{V}\right)\right]d\vartheta = 0 \qquad (3.7)$$

The weak form of equation (3.7) is obtained after integration by parts of second order terms:

$$\int_{\vartheta}\left[\nabla W_i^{\vec{V}}\bullet\nabla\left(\rho\vec{V}\right) - W_i^{\vec{V}}\left(\nabla\times\left(\rho\vec{\Omega}\right)\right) + \nabla W_i^{\vec{V}}\times\left(\nabla\rho\times\vec{V}\right)\right]d\vartheta$$

$$- \oint_S W_i^{\vec{V}}\left[\vec{n}\bullet\nabla\left(\rho\vec{V}\right) + \vec{n}\times\left(\nabla\rho\times\vec{V}\right)\right]dS = 0 \qquad (3.8)$$

3.2.2 Vorticity Equations

The vorticity transport equation (3.6) is multiplied by a weight function, W_i, and integrated over the domain as follows:

$$\int_{\vartheta} W_i^{\vec{\Omega}}\left[\nabla^2\left(\mu\vec{\Omega}\right) - Re\left\{\left(\rho\vec{V}\bullet\nabla\right)\vec{\Omega} - \left(\vec{\Omega}\bullet\nabla\right)\left(\rho\vec{V}\right) + \vec{S}^{\rho}\right\} + \vec{S}^{\mu}\right]d\vartheta = 0 \qquad (3.9)$$

The weak form of equation (3.9) is obtained after integration by parts of second order terms:

$$\int_{\vartheta}\Big[\nabla W_i^{\vec{\Omega}}\cdot\nabla\left(\mu\vec{\Omega}\right)+W_i^{\vec{\Omega}}\,Re\left\{\left(\rho\vec{V}\cdot\nabla\right)\vec{\Omega}-\left(\vec{\Omega}\cdot\nabla\right)\left(\rho\vec{V}\right)+\vec{S}^{p}\right\}$$
$$+\frac{\partial W_i^{\vec{\Omega}}}{\partial x}\vec{S}^{\mu 1}+\frac{\partial W_i^{\vec{\Omega}}}{\partial y}\vec{S}^{\mu 2}+\frac{\partial W_i^{\vec{\Omega}}}{\partial z}\vec{S}^{\mu 3}\Big]d\vartheta$$
$$-\oint_S W_i^{\vec{\Omega}}\Big[\vec{n}\cdot\nabla\left(\mu\vec{\Omega}\right)dS+\vec{S}^{\mu 1}dydz+\vec{S}^{\mu 2}dzdx+\vec{S}^{\mu 3}dxdy\Big]=0 \qquad (3.10)$$

3.2.3 Element Discretization

For equal degree of approximation of vorticity and derivatives of velocity, the former is represented by trilinear shape functions, while the velocity is approximated by triquadratic shape functions. The advantage of using this element discretization over trilinear interpolation for both vorticity and velocity is higher accuracy of the wall vorticity boundary condition which derives from the definition of vorticity (equation 3.4). For some preliminary through-flow cases in two dimensions, the mixed interpolation was compared, on the same grid, to equal order trilinear interpolation. The error in conservation of mass was significantly greater for the equal order trilinear element than for the mixed element.

Hence for the velocity and vorticity vectors:

$$\vec{V}=\sum_{j=1}^{20}N_j^{\vec{V}}(\xi,\eta,\zeta)\,\vec{V}_j \qquad\qquad \vec{\Omega}=\sum_{j=1}^{8}N_j^{\vec{\Omega}}(\xi,\eta,\zeta)\,\vec{\Omega}_j \qquad (3.11a,b)$$

The geometry discretization is based on curvilinear twenty node elements:

$$x = \sum_{j=1}^{20} N_j^{\vec{V}}(\xi,\eta,\zeta)\, x_j \qquad y = \sum_{j=1}^{20} N_j^{\vec{V}}(\xi,\eta,\zeta)\, y_j$$

$$z = \sum_{j=1}^{20} N_j^{\vec{V}}(\xi,\eta,\zeta)\, z_j \qquad (3.12a,b,c)$$

The weight functions in the Galerkin finite element scheme are chosen to be the corresponding shape functions:

$$W_i^{\vec{V}} = N_i^{\vec{V}} \qquad W_i^{\vec{\Omega}} = N_i^{\vec{\Omega}} \qquad (3.13a,b)$$

3.3 Boundary Conditions

3.3.1 Inlet Boundary

For through-flow type problems, the velocity distribution is specified at inlet and the vorticity is therefore known:

$$\vec{V} = \vec{V}(y,z) \qquad (3.14a)$$

$$\vec{\Omega} = \vec{\Omega}(y,z) \qquad (3.14b)$$

These are very easy to implement for any chosen numerical algorithm and discretization.

3.3.2 Symmetry Boundary

The boundary conditions for a symmetry boundary are that the normal velocity and the normal derivative of scalar quantities are zero. In terms of velocity and vorticity, this translates to;

$$\vec{V} \cdot \vec{n} = 0 \qquad \vec{\Omega} \times \vec{n} = 0 \qquad (3.15a,b)$$

$$\frac{\partial(\vec{V} \times \vec{n})}{\partial n} = 0 \qquad \frac{\partial(\vec{\Omega} \cdot \vec{n})}{\partial n} = 0 \qquad (3.16a,b)$$

The first set, equations (3.15a,b), are Dirichlet boundary conditions and are very easy to implement no matter what discretization method is chosen. The second set, equations (3.16a,b), are Neumann boundary conditions which happen to be present in the boundary surface integrals of the velocity and vorticity transport equations (3.8,3.10). These boundary conditions are implemented by simply neglecting these boundary integrals, i.e. treating the boundary as any other point in the field.

3.3.3 Exit Boundary

In the derivation of the second order velocity equations (3.5), while it has been implicitly recognized that the gradient of the continuity equation is zero, the continuity equation itself is no longer part of the system. Mass continuity is thus accounted for only to within an arbitrary constant [41] and must therefore be explicitly imposed, at least at one point, to remove the arbitrariness of the solution. This can be done by using the continuity equation to modify the original surface integral of the normal velocity

equation at exit (equation 3.8). For example, for an exit normal aligned with the x-axis, the original surface integral of the x-velocity equation:

$$\oint_S W_i^{\vec{v}}\left[\vec{n}\cdot\nabla\left(\rho\vec{V}\right) + \vec{n}\times\left(\nabla\rho\times\vec{V}\right)\right] dS\cdot\vec{i} = \oint_S W_i^{\vec{v}}\left[\frac{\partial(\rho u)}{\partial x} + 0\right] dydz \quad (3.17)$$

is modified using the continuity equation, to yield:

$$\oint_S W_i^{\vec{v}}\left[\frac{\partial(\rho u)}{\partial x} + 0\right] dydz = -\oint_S W_i^{\vec{v}}\left[\frac{\partial(\rho v)}{\partial y} + \frac{\partial(\rho w)}{\partial z}\right] dydz \quad (3.18)$$

For the transverse velocity equations, the exit boundary condition is that the normal derivative vanishes. This is accounted for by dropping the first term in the surface integral of the transverse velocity equations (3.8). The second term, however, only contains transverse derivatives and must be evaluated at exit.

The vorticity boundary condition is applied by dropping the first term of the surface integral of equation (3.10), since on the exit boundary the normal derivative of the vorticity is assumed zero:

$$\frac{\partial\left(\mu\vec{\Omega}\right)}{\partial n} = 0 \quad (3.19)$$

The remaining viscosity source terms in the surface integrals are neglected at the exit.

The assumption of zero normal derivatives is only exact if the exit is placed at an infinite distance downstream of the disturbance. In practice, the exit is placed at a finite distance downstream where the flow quantities no longer change significantly.

3.3.4 Wall Boundary

On walls, no-slip and no-penetration are implemented as Dirichlet conditions on the velocity components:

$$u = 0 \quad \text{or} \quad u = U(S) \tag{3.20a}$$

$$v = 0 \quad \text{or} \quad v = V(S) \tag{3.20b}$$

$$w = 0 \quad \text{or} \quad w = W(S) \tag{3.20c}$$

The vorticity has no explicit wall boundary condition and is derived from the kinematics of the flow. Hafez et al. show that the kinematics can be governed by a least-squares variational principle [55];

$$I_{LS} = \int_{\vartheta} \left[\left| \nabla \cdot \vec{V} \right|^2 + \left| \vec{\Omega} - \nabla \times \vec{V} \right|^2 \right] d\vartheta \tag{3.21}$$

Minimizing with respect to the interior nodal velocities will give the same finite element governing equations as using the Galerkin weighted residual method applied to the second order Poisson velocity equations [52,55]. Minimizing the least-squares variational with respect to a wall vorticity node i results in the vorticity definition applied in the following manner at walls:

$$\sum_{e=1}^{E_i} \int_{\vartheta'} N_i^{\vec{\Omega}} \left[\vec{\Omega} - \nabla \times \vec{V} \right] d\vartheta = 0 \qquad (3.22)$$

where E_i is the total number of elements connected to wall node i. As mentioned in the introduction, the discretization of the wall vorticity boundary condition is critical for success in the velocity-vorticity system. This is the main reason for the choice of element discretizations (equations 3.11) for the velocity and vorticity vectors. The advantage of equation (3.22) is that the derivatives of velocity are evaluated in the interior of the element and not on its boundary. Since normal derivatives are not continuous between elements, they are not formally defined and thus least accurate at element boundaries.

3.4 Newton Linearization

The nonlinear system of equations (3.8,3.10) is linearized by a Newton method. All three velocity components with all three vorticity components are solved simultaneously. Each vector is expressed in Δ form as follows:

$$\Delta \vec{V} \equiv \vec{V}^{n+1} - \vec{V}^{n} \qquad (3.23)$$

$$\Delta \vec{\Omega} \equiv \vec{\Omega}^{n+1} - \vec{\Omega}^{n} \qquad (3.24)$$

Upon substitution in equations (3.8,3.10) and retaining only first order terms, the system of equations can be re-expressed as follows:

$$\int_{\vartheta} \left[\nabla W_i^{\vec{V}} \bullet \nabla \left(\rho \, \Delta \vec{V} \right) - W_i^{\vec{V}} \left(\nabla \times \left(\rho \, \Delta \vec{\Omega} \right) \right) + \nabla W_i^{\vec{V}} \times \left(\nabla \rho \times \Delta \vec{V} \right) \right] d\vartheta = - R_i^{\vec{V}} \qquad (3.25)$$

$$\int_{\vartheta}\Big[\nabla W_i^{\vec{\Omega}}\cdot\nabla\left(\mu\Delta\vec{\Omega}\right)+W_i^{\vec{\Omega}}\,Re\left\{\left(\rho\vec{V}\cdot\nabla\right)\Delta\vec{\Omega}+\left(\rho\,\Delta\vec{V}\cdot\nabla\right)\vec{\Omega}-\left(\vec{\Omega}\cdot\nabla\right)\left(\rho\,\Delta\vec{V}\right)-\left(\Delta\vec{\Omega}\cdot\nabla\right)\left(\rho\vec{V}\right)+\Delta\vec{S}^{\rho}\right\}+\frac{\partial W_i^{\vec{\Omega}}}{\partial x}\Delta\vec{S}^{\mu 1}+\frac{\partial W_i^{\vec{\Omega}}}{\partial y}\Delta\vec{S}^{\mu 2}+\frac{\partial W_i^{\vec{\Omega}}}{\partial z}\Delta\vec{S}^{\mu 3}\Big]d\vartheta=-R_i^{\vec{\Omega}}\qquad(3.26)$$

where:

$$\Delta\vec{S}^{\rho}=\nabla\rho\times\nabla\left(\vec{V}\cdot\Delta\vec{V}\right)$$

$$\Delta\vec{S}^{\mu}=2\left[\nabla\times\left(\mu\,\nabla^2\left(\Delta\vec{V}\right)\right)+\nabla\times\left(\nabla\mu\cdot\nabla\right)\Delta\vec{V}-\nabla^2\mu\,\Delta\vec{\Omega}\right]+\nabla\left(\nabla\mu\cdot\Delta\vec{\Omega}\right)$$

$$=\frac{\partial\Delta\vec{S}^{\mu 1}}{\partial x}+\frac{\partial\Delta\vec{S}^{\mu 2}}{\partial y}+\frac{\partial\Delta\vec{S}^{\mu 3}}{\partial z}$$

and R_i's are the residuals, at node i, of the discretized governing equations.

Substituting the shape functions (equation 3.11) and weight functions (equations 3.13) and assembling over the elements, one obtains the following set of discretized equations for the velocity vector:

$$\sum_{e=1}^{E}\left[\sum_{j=1}^{20}\left[k_{\vec{V}\vec{V}}\right]_{ij}\Delta\vec{V}_j+\sum_{j=1}^{8}\left[k_{\vec{V}\vec{\Omega}}\right]_{ij}\Delta\vec{\Omega}_j\right]=-R_i^{\vec{V}}\qquad(3.27)$$

where, for example, for the w-velocity component:

$$\left[k_{wu}\right]_{i,j}=\int_{\vartheta}\left[\frac{\partial N_i^{\vec{V}}}{\partial x}\frac{\partial\rho}{\partial z}N_j^{\vec{V}}\right]d\vartheta$$

$$[k_{wv}]_{i,j} = \int_{\vartheta} \left[\frac{\partial N_i^{\vec{V}}}{\partial y} \frac{\partial \rho}{\partial z} N_j^{\vec{V}} \right] d\vartheta$$

$$[k_{ww}]_{i,j} = \int_{\vartheta} \left[\rho \left(\frac{\partial N_i^{\vec{V}}}{\partial x} \frac{\partial N_j^{\vec{V}}}{\partial x} + \frac{\partial N_i^{\vec{V}}}{\partial y} \frac{\partial N_j^{\vec{V}}}{\partial y} + \frac{\partial N_i^{\vec{V}}}{\partial z} \frac{\partial N_j^{\vec{V}}}{\partial z} \right) + \frac{\partial N_i^{\vec{V}}}{\partial z} \frac{\partial \rho}{\partial z} N_j^{\vec{V}} \right] d\vartheta$$

$$[k_{w\Omega_1}]_{i,j} = \int_{\vartheta} \left[N_i^{\vec{V}} \left(\rho \frac{\partial N_j^{\vec{\Omega}}}{\partial y} + \frac{\partial \rho}{\partial y} N_j^{\vec{\Omega}} \right) \right] d\vartheta$$

$$[k_{w\Omega_2}]_{i,j} = - \int_{\vartheta} \left[N_i^{\vec{V}} \left(\rho \frac{\partial N_j^{\vec{\Omega}}}{\partial x} + \frac{\partial \rho}{\partial x} N_j^{\vec{\Omega}} \right) \right] d\vartheta$$

$$[k_{w\Omega_3}]_{i,j} = 0$$

The following set of discretized equations is obtained for the vorticity vector:

$$\sum_{e=1}^{E} \left[\sum_{j=1}^{8} [k_{\vec{\Omega}\vec{\Omega}}]_{ij} \Delta\vec{\Omega}_j + \sum_{j=1}^{20} [k_{\vec{\Omega}\vec{V}}]_{ij} \Delta\vec{V}_j \right] = - R_i^{\vec{\Omega}} \qquad (3.28)$$

where, for example, for the Ω_1-vorticity component:

$$[k_{\Omega_1 u}]_{i,j} = \int_{\vartheta} \left[N_i^{\vec{\Omega}} \, Re \left\{ \rho \frac{\partial \Omega_1}{\partial x} N_j^{\vec{v}} - \Omega_1 \left(\rho \frac{\partial N_j^{\vec{v}}}{\partial x} + \frac{\partial \rho}{\partial x} N_j^{\vec{v}} \right) - \Omega_2 \left(\rho \frac{\partial N_j^{\vec{v}}}{\partial y} + \frac{\partial \rho}{\partial y} N_j^{\vec{v}} \right) \right.$$

$$\left. - \Omega_3 \left(\rho \frac{\partial N_j^{\vec{v}}}{\partial z} + \frac{\partial \rho}{\partial z} N_j^{\vec{v}} \right) + \frac{\partial \rho}{\partial y} \left(u \frac{\partial N_j^{\vec{v}}}{\partial z} + \frac{\partial u}{\partial z} N_j^{\vec{v}} \right) - \frac{\partial \rho}{\partial z} \left(u \frac{\partial N_j^{\vec{v}}}{\partial y} + \frac{\partial u}{\partial y} N_j^{\vec{v}} \right) \right\}$$

$$+ 2 \frac{\partial N_i^{\vec{\Omega}}}{\partial x} \left(\frac{\partial \mu}{\partial y} \frac{\partial N_j^{\vec{v}}}{\partial z} - \frac{\partial \mu}{\partial z} \frac{\partial N_j^{\vec{v}}}{\partial y} \right) \Big] d\vartheta$$

$$[k_{\Omega_1 v}]_{i,j} = \int_{\vartheta} \left[N_i^{\vec{\Omega}} \, Re \left\{ \rho \frac{\partial \Omega_1}{\partial y} N_j^{\vec{v}} + \frac{\partial \rho}{\partial y} \left(v \frac{\partial N_j^{\vec{v}}}{\partial z} + \frac{\partial v}{\partial z} N_j^{\vec{v}} \right) \right.$$

$$\left. - \frac{\partial \rho}{\partial z} \left(v \frac{\partial N_j^{\vec{v}}}{\partial y} + \frac{\partial v}{\partial y} N_j^{\vec{v}} \right) \right\} + 2 \frac{\partial N_i^{\vec{\Omega}}}{\partial y} \left(\frac{\partial \mu}{\partial y} \frac{\partial N_j^{\vec{v}}}{\partial z} - \frac{\partial \mu}{\partial z} \frac{\partial N_j^{\vec{v}}}{\partial y} \right) \Big] d\vartheta$$

$$[k_{\Omega_1 w}]_{i,j} = \int_{\vartheta} \left[N_i^{\vec{\Omega}} \, Re \left\{ \rho \frac{\partial \Omega_1}{\partial z} N_j^{\vec{v}} + \frac{\partial \rho}{\partial y} \left(w \frac{\partial N_j^{\vec{v}}}{\partial z} + \frac{\partial w}{\partial z} N_j^{\vec{v}} \right) \right.$$

$$\left. - \frac{\partial \rho}{\partial z} \left(w \frac{\partial N_j^{\vec{v}}}{\partial y} + \frac{\partial w}{\partial y} N_j^{\vec{v}} \right) \right\} + 2 \frac{\partial N_i^{\vec{\Omega}}}{\partial z} \left(\frac{\partial \mu}{\partial y} \frac{\partial N_j^{\vec{v}}}{\partial z} - \frac{\partial \mu}{\partial z} \frac{\partial N_j^{\vec{v}}}{\partial y} \right) \Big] d\vartheta$$

$$[k_{\Omega_1 \Omega_1}]_{i,j} = \int_{\vartheta} \left[N_i^{\vec{\Omega}} \, Re \left\{ \rho u \frac{\partial N_j^{\vec{\Omega}}}{\partial x} + \rho v \frac{\partial N_j^{\vec{\Omega}}}{\partial y} + \rho w \frac{\partial N_j^{\vec{\Omega}}}{\partial z} - \left(\frac{\partial \rho}{\partial x} u + \rho \frac{\partial u}{\partial x} \right) N_j^{\vec{\Omega}} \right\} \right.$$

$$+ \frac{\partial N_i^{\vec{\Omega}}}{\partial x} \mu \frac{\partial N_j^{\vec{\Omega}}}{\partial x} + \frac{\partial N_i^{\vec{\Omega}}}{\partial y} \left(\mu \frac{\partial N_j^{\vec{\Omega}}}{\partial y} + \frac{\partial \mu}{\partial y} N_j^{\vec{\Omega}} \right)$$

$$\left. + \frac{\partial N_i^{\vec{\Omega}}}{\partial z} \left(\mu \frac{\partial N_j^{\vec{\Omega}}}{\partial z} + \frac{\partial \mu}{\partial z} N_j^{\vec{\Omega}} \right) \right] d\vartheta$$

$$[k_{\Omega_1\Omega_2}]_{i,j} = -\int_{\vartheta}\left[N_i^{\vec{\Omega}}\,\mathrm{Re}\left(\frac{\partial\rho}{\partial y}u + \rho\frac{\partial u}{\partial y}\right)N_j^{\vec{\Omega}} + \frac{\partial N_i^{\vec{\Omega}}}{\partial x}\frac{\partial\mu}{\partial y}N_j^{\vec{\Omega}}\right]d\vartheta$$

$$[k_{\Omega_1\Omega_3}]_{i,j} = -\int_{\vartheta}\left[N_i^{\vec{\Omega}}\,\mathrm{Re}\left(\frac{\partial\rho}{\partial z}u + \rho\frac{\partial u}{\partial z}\right)N_j^{\vec{\Omega}} + \frac{\partial N_i^{\vec{\Omega}}}{\partial x}\frac{\partial\mu}{\partial z}N_j^{\vec{\Omega}}\right]d\vartheta$$

The integrals are evaluated numerically by Gauss-Legendre quadrature, using a 3x3x3 grid in each element.

4. Solution Procedure

4.1 General Algorithm

The iterative procedure is outlined in the flowchart of Figure 4.1. At every iteration, a coupled system is solved. For the stream function-vorticity formulation, the stream function and vorticity are solved simultaneously. For the velocity-vorticity formulation, the velocity vector and the vorticity vector are solved simultaneously. For subsonic flow, the thermodynamic variables are then evaluated in the following sequence;

1) the pressure is solved for from the divergence of momentum,
2) the temperature is solved for from the energy equation,
3) the density is obtained from the equation of state,
4) the viscosity, thermal conductivity and specific heat coefficients are obtained from empirical relations.

For the stream function-vorticity formulation, the velocities and their first derivatives must be evaluated from the updated stream function and the previous density before solving for the pressure. The velocities are first evaluated at the Gauss integration points inside the element from the stream function and density. These values are then extrapolated to the nodes and finally the nodal values are averaged between the elements connected to that given node [74]. The first derivatives of the velocity are obtained at the nodes in the same manner. The first derivatives of the velocity are necessary at the nodes in order to evaluate the second derivatives inside the element. Note also that the thermodynamic variables do not have to be solved for at every

iteration since the coupled stream function-vorticity or velocity-vorticity systems are themselves internally nonlinear.

Stokes flow (Re=0) is used as an initial guess for flows at all Reynolds numbers. For high Reynolds numbers, obtaining solutions at progressively increasing Reynolds numbers may be required. Since the solution at an intermediary Reynolds number is only used as a better initial guess for the next higher Reynolds number, the convergence criteria for these intermediary steps can be somewhat relaxed. The initial incompressible Stokes flow is a linear problem and therefore machine accuracy is achieved after one matrix solution.

Convergence is considered obtained when the sum of the squares of the residuals of all the equations is less than a prescribed value. For the stream function-vorticity system, equations (2.49,2.50), the convergence criterion is;

$$\sum_{i}^{nnode} \left(R_i^{\psi}\right)^2 + \sum_{j}^{nnodev} \left(R_j^{\omega}\right)^2 \leq R_{criterion} \tag{4.1}$$

where

nnode	is the total number of stream function nodes in the domain
nnodev	is the total number of vorticity nodes in the domain
$R_{criterion}$	is the convergence criterion

4.2 Pressure

To complete the iteration, for subsonic flow, the density needs to be updated and this requires the solution for the pressure. This is obtained from a Poisson equation derived by taking the divergence of the momentum equations:

$$\nabla \cdot \left(\nabla p + \vec{F} \right) = 0 \tag{4.2}$$

where $\vec{F}$ is the remainder of the momentum equations (2.2,3.2).

The weighted residual form of the pressure equation is:

$$\int_{\vartheta} W_i \left[\nabla \cdot \left(\nabla p + \vec{F} \right) \right] d\vartheta = 0 \tag{4.3}$$

Upon integration of the entire equation by parts, one obtains:

$$\int_{\vartheta} \left[\nabla W_i \cdot \left(\nabla p + \vec{F} \right) \right] d\vartheta = \int_{S} \left[W_i \left(\nabla p + \vec{F} \right) \cdot \vec{n} \right] dS \tag{4.4}$$

It is seen that the surface boundary integral contains the normal momentum equation. Hence, by neglecting this surface integral on boundaries where pressure is unknown, the normal momentum equation is automatically satisfied. Such natural boundary conditions of finite element methods are an advantage over schemes where unknowns at a wall, such as pressure, may have to be extrapolated from their values in the field.

To avoid the arbitrariness of the pressure Poisson problem, the pressure level is set by specifying its value at one point of the flow.

4.3 Energy Equation

The temperature is updated using the energy equation once the pressure has been determined. For most of the test cases, the assumption of constant total enthalpy along streamlines is used:

$$H_o = C_pT + \frac{1}{2}\vec{V}\cdot\vec{V} \tag{3.3}$$

This simplified energy equation is a reasonable approximation for the viscous energy equation in the absence of heat exchange. This particular relation is only valid for an ideal gas.

The complete energy equation is solved for in a few test cases, in the form :

$$Re\left(\rho\vec{V}\cdot\nabla\right)(C_vT) - \frac{1}{Pr}\nabla\cdot\left(k\,\nabla T\right) = \Phi - Re\left(p\,\nabla\cdot\vec{V}\right) \tag{4.5}$$

where

Re	is the Reynolds number
Pr	is the Prandtl number
C_v	is the constant volume specific heat
k	is the thermal conductivity
Φ	is the viscous dissipation term

The weighted residual form of the complete energy equation, after integration by parts of the second order terms, is :

$$\int_{\vartheta}\left[W_i\,\mathrm{Re}\left(\rho\vec{V}\cdot\nabla\right)(C_vT) + \frac{1}{\mathrm{Pr}}\nabla W_i\cdot\left(k\,\nabla T\right)\right]d\vartheta$$

$$= \int_{\vartheta}\left[W_i\left(\Phi - \mathrm{Re}\left(p\,\nabla\cdot\vec{V}\right)\right)\right]d\vartheta + \oint_S W_i\,\frac{1}{\mathrm{Pr}}\left[\vec{n}\cdot\left(k\,\nabla T\right)\right]dS \qquad (4.6)$$

The boundary conditions are that either the temperature or the heat flux is specified. The surface integral contains the heat flux allowing a natural implementation of the latter boundary condition. All the temperature unknowns in the domain are solved simultaneously.

4.4 Thermodynamic Variables

The density is evaluated from the updated pressure and temperature using the equation of state for a perfect gas;

$$\rho = \frac{p}{RT} \qquad (2.4)$$

The viscosity is obtained from the updated temperature using the empirical Sutherland's law for air [72]:

$$\frac{\mu}{\mu_\infty} = \left(\frac{T}{T_\infty}\right)^{1.5}\left(\frac{T_\infty + 110°K}{T + 110°K}\right) \qquad (2.5)$$

The thermal conductivity and specific heat coefficients are assumed constant for the given test cases.

It is recognized that more accurate relations for all the thermodynamic properties can be used. Since the primary purpose of this research concerns the continuity and momentum equations, the simplest thermodynamic relations are used for completion.

4.5 Element Discretization

4.5.1 Stream Function-Vorticity

Recalling from section 2.2.3, the stream function and geometry are discretized using biquadratic eight node elements (equations 2.21a, 2.22a,b) and the vorticity using bilinear four node elements (equation 2.21b). The velocities, pressure, temperature, density and viscosity are all chosen to follow biquadratic eight node elements;

$$u = \sum_{j=1}^{8} N_j^{\psi}(\xi,\eta)\, u_j \qquad v = \sum_{j=1}^{8} N_j^{\psi}(\xi,\eta)\, v_j \qquad (4.7a,b)$$

$$p = \sum_{j=1}^{8} N_j^{\psi}(\xi,\eta)\, p_j \qquad T = \sum_{j=1}^{8} N_j^{\psi}(\xi,\eta)\, T_j \qquad (4.8a,b)$$

$$\bar{\rho} = \sum_{j=1}^{8} N_j^{\psi}(\xi,\eta)\, \bar{\rho}_j \qquad \mu = \sum_{j=1}^{8} N_j^{\psi}(\xi,\eta)\, \mu_j \qquad (4.9a,b)$$

where

$$\bar{\rho} \equiv \frac{1}{\rho}$$

The inverse of the density is discretized since it consistently shows up in this form in the stream function-vorticity equations.

4.5.2 Velocity-Vorticity

Recalling from section 3.2.3, the velocity vector and geometry are discretized using triquadratic twenty node elements (equations 3.11a, 3.12a,b,c) and the vorticity vector using trilinear eight node elements (equation 3.11b). The pressure, temperature, density and viscosity are all chosen to follow triquadratic twenty node elements;

$$p = \sum_{j=1}^{20} N_j^{\vec{v}}(\xi,\eta,\zeta)\, p_j \qquad T = \sum_{j=1}^{20} N_j^{\vec{v}}(\xi,\eta,\zeta)\, T_j \qquad (4.10a,b)$$

$$\rho = \sum_{j=1}^{20} N_j^{\vec{v}}(\xi,\eta,\zeta)\, \rho_j \qquad \mu = \sum_{j=1}^{20} N_j^{\vec{v}}(\xi,\eta,\zeta)\, \mu_j \qquad (4.11a,b)$$

5. Stream Function-Vorticity Results

5.1 Summary of Test Cases

To illustrate the application of the method to external aerodynamics, laminar flow over a symmetric NACA 0012 airfoil is computed for the following three flow conditions;

1)	$Re_\infty = 10\,000$	$M_\infty = 0.2$	$\alpha = 0°$
2)	$Re_\infty = 10\,000$	$M_\infty = 0.5$	$\alpha = 0°$
3)	$Re_\infty = 5\,000$	$M_\infty = 0.5$	$\alpha = 3°$

The free stream Reynolds number Re_∞ is defined as follows:

$$Re_\infty = \frac{\rho_\infty U_\infty c}{\mu_\infty} \tag{5.1}$$

where U_∞, ρ_∞ and μ_∞ are, respectively, the dimensional velocity, density and viscosity of the undisturbed free stream flow. The reference length, c, is the dimensional chord length of the airfoil.

The geometry and boundary conditions of the airfoil test cases are shown in Figure 5.1. These test cases have the desired properties of a curved geometry, flow separation, a moderate Reynolds number to test iterative stability, a moderate subsonic Mach number and a non-zero angle of attack to test the multiply connected domain algorithm.

Comparison to experiments requires the implementation of a turbulence model. If turbulence is introduced, then the numerical results depend on the turbulence model chosen. Any inaccuracy in the final solution could be due to the stream function-vorticity discretization or the turbulence model or both. It would be very difficult, if not impossible, to determine which is the case. Turbulence also produces a much higher effective viscosity which tends to stabilize any stream function-vorticity iterative scheme, so that even a 'bad' scheme might converge for turbulent flows. Laminar cases show the true stability and accuracy properties of a given stream function-vorticity formulation.

C-type grids are preferred for the isolated NACA 0012 airfoil. The leading edge elements are not skewed with respect to the surface as with H-type grids. Unlike O-type grids, the exit boundary of a C-type grid is a straight line normal to the flow which is better suited for viscous flow exit boundary conditions. The C-grid of Figure 5.2 is generated by a method, programmed by the author, similar to the one outlined in Rizzi [75].

All flow and thermodynamic variables are non-dimensionalized with respect to free-stream values and the geometry with respect to the airfoil chord.

5.2 Test Case #1 : Re = 10 000 , M = 0.20 , $\alpha = 0°$

The outer boundary is taken 8 airfoil chords away from the leading edge to 10 chords radially from the trailing edge. The exit boundary is placed 2 chords from the trailing edge. The exit boundary condition of parallel streamlines

allows the exit boundary to be placed closer to the airfoil than the outer boundary. Due to the symmetry of the problem, only half the domain is solved for.

There are 35 elements in the radial direction, including 15 placed within the estimated boundary layer thickness of 0.050 from the airfoil. The estimate is taken from flat plate boundary layer theory;

$$\delta \approx \frac{5}{Re^{0.5}} \tag{5.2}$$

The radial length of the elements expand from 0.0013 at the leading edge to 2.2 at the outer boundary. There are 30 elements along the upper half of the airfoil surface expanding in length from 0.0065 at the leading edge to 0.050 at the trailing edge. There are 16 columns of elements downstream of the airfoil expanding in length from 0.050 at the trailing edge to 0.26 at the exit boundary. A total of 1610 elements are used, yielding 6685 degrees of freedom for the half-problem.

Among the attempts that diverged, only the following two are significant for establishing approximately the stability limits for this particular test case. For the first attempt, incompressible Stokes flow (Re=0) was solved during the first iteration. The iterative Reynolds number was increased to 1 000 from the second iteration until the L_2 residual reached the intermediary convergence criteria of 10^0. The iterative Reynolds number was then increased to the solution Reynolds number of 10 000. No under-relaxation was used for this attempt. The second attempt first solved for incompressible Stokes flow and then jumped directly to the solution Reynolds number of

10 000 where an under-relaxation of 0.6 was imposed. Both attempts diverged rapidly at the target Reynolds number.

The third attempt first solved incompressible Stokes flow and then increased to an intermediary Reynolds number of 1 000 with no under-relaxation. After the L_2 residual decreased below 10^0, the iterative Reynolds number was increased to 10 000 and an under-relaxation of 0.6 was imposed. Convergence to machine accuracy was obtained after a total of 42 iterations, including 35 iterations at the final Reynolds number.

The fourth attempt was identical to the third attempt except that at the final Reynolds number, under-relaxation was removed as soon as the L_2 residual reached below 10^0. A savings of 17 iterations was obtained. The convergence history for the successful attempts are shown in Figure 5.3.

The C_p distribution over the airfoil surface is shown in Figure 5.4. The results compare well to those of Steger [76]. The vorticity distribution over the airfoil surface is shown in Figure 5.5. The separation point on the surface of the airfoil is clearly identified by the point of zero vorticity. The absolute vorticity increases dramatically towards the leading edge stagnation point due to the reduction of the boundary layer thickness. At the leading edge itself, there is, in theory, a singularity in vorticity. Due to the symmetry of the problem, however, the vorticity at the leading edge node was set to zero.

5.3 Test Case #2 : Re = 10 000 , M = 0.50 , $\alpha = 0°$

The numerical domain and the grid are identical to those chosen for the previous test case.

The first attempt at convergence was to repeat what had been successful for the previous test case at Re = 10 000 and M = 0.20. Incompressible Stokes flow was obtained during the first iteration. The iterative Reynolds number was increased to 1 000, with no under-relaxation, from the second iteration until the L_2 residual reached 10^0. The iterative Reynolds number was then increased to the solution Reynolds number of 10 000, with an under-relaxation factor of 0.6, where the run quickly diverged.

The second attempt was to repeat the first attempt with an added intermediary Reynolds number of 5 000 after the intermediary Reynolds number of 1 000 was solved to an L_2 residual of 10^{-3}. No under-relaxation was used for either intermediary Reynolds number. This attempt quickly diverged at the intermediary Reynolds number of 5 000.

The third attempt was to start again with incompressible Stokes Flow followed by an intermediary Reynolds number of 1 000 with no under-relaxation. After the L_2 residual reached 10^{-3}, the intermediary Reynolds number was again increased to 5 000 but with an under-relaxation of 0.6. After the L_2 residual reached 10^{-3}, the iterative Reynolds number was increased to the solution Reynolds number of 10 000 keeping an under-relaxation of 0.6. When the L_2 residual got down below 10^0, the under-relaxation was removed. Convergence to machine accuracy was obtained

after a total of 43 iterations, including a total of 21 iterations at the final Reynolds number. The convergence history for this final attempt is shown in Figure 5.6.

No attempt was made in any of the test cases to find an optimum under-relaxation factor. The value of 0.6 was chosen based on the experience of Peeters et al. with the incompressible driven cavity problem [8]. For the external flows tested, there is no need to impose under-relaxation at the intermediary Reynolds number of 1 000. For Reynolds numbers of 5 000 and 10 000, under-relaxation is required to stabilize the iterative process.

The C_p distribution over the airfoil surface is shown in Figure 5.4. Due to compressibility of streamlines, the values are slightly higher than for the results at M = 0.20. The streamlines and recirculation zones are shown in Figure 5.7. The vorticity distribution over the airfoil surface is shown in Figure 5.5. At the higher Mach number, the separation point, indicated by zero vorticity, moves further upstream than the M = 0.20 case. The lower surface pressure and the larger separation zone are consistent with higher compressibility, which results in higher velocities and thus greater acceleration.

5.4 Test Case #3 : Re = 5 000 , M = 0.50 , $\alpha = 3°$

Due to the expected larger separation zone than in the previous cases, the outer boundary is taken 15 airfoil chords away from the airfoil. The exit boundary is placed 5 chords from the trailing edge. The exit boundary condition of parallel streamlines allows the exit boundary to be placed closer

to the airfoil than the outer boundary. Unlike the zero angle of attack cases, there is no symmetry in this problem and the full domain is solved for.

There are 35 elements in the radial direction, including 15 placed within a distance of 0.040 from the airfoil. The radial length of the elements expand from 0.0011 at the airfoil surface to 4.5 at the outer boundary. There are 50 elements along the upper and lower halves of the airfoil surface expanding in length from 0.0044 at the leading edge to 0.030 at the trailing edge. There are 24 columns of elements downstream of the airfoil expanding in length from 0.030 at the trailing edge to 0.70 at the exit boundary. The exit boundary is a straight line at an angle of 3° with respect to the y-axis and is thus normal to the free stream flow for ease of application of the exit boundary conditions. A total of 5180 elements are used, yielding 20 751 degrees of freedom.

The first and only attempt repeated what was successful for the zero angle of attack test cases. Incompressible Stokes flow was first obtained followed by an increase to an intermediary Reynolds number of 1 000 with no under-relaxation. After the L_2 residual decreased below 10^{-3}, the iterative Reynolds number was increased to the target value of 5 000 and an under-relaxation of 0.6 was imposed. At this final Reynolds number, under-relaxation was removed as soon as the L_2 residual reached below 10^{-1}. Figure 5.8 shows that convergence to machine accuracy was obtained after a total of 34 iterations, including 24 iterations at the final Reynolds number.

The C_p distribution over the airfoil surface is shown in Figure 5.9 and naturally indicates lower pressure values on the top surface than on the lower surface, resulting in a lifting force on the airfoil. Figure 5.10 shows the

streamline patterns over the airfoil including the large separation zone near the trailing edge. The results compare well to those of Venkatakrishnan [77], who used Roe's flux difference splitting technique with a GMRES iterative matrix solver on a 128*32 grid. The vorticity distribution over the airfoil surface is shown in Figure 5.11. The separation point on the top surface of the airfoil is clearly identified by the point of zero vorticity. Unlike the symmetric cases (zero angle of attack), the stagnation point, again indicated by zero vorticity, occurs on the bottom surface. On either side of the stagnation point are regions of very high vorticities (opposite signs) as a result of the thin boundary layers in this region.

6. Velocity-Vorticity Results

6.1 Summary of Test Cases

Results have been obtained for laminar two-dimensional incompressible and subsonic flows. The cases investigated are: flow in a driven cavity, over a trough and through a nozzle. Flow in a driven cavity is then analyzed for three-dimensional flows, both incompressible and subsonic, and compared to the results of other numerical methods. Incompressible results for all the test cases were obtained by explicitly setting the density and viscosity to unity everywhere in the domain. The Reynolds number is defined as:

$$Re = \frac{\rho_{ref} U_{ref} L_{ref}}{\mu_{ref}} \tag{6.1}$$

where the reference values are defined for each test case in Table 6.1:

Test case	U_{ref}	ρ_{ref}	μ_{ref}	L_{ref}
Cavity (2-D and 3-D)	Lid velocity	Lid density at p_{ref}	Lid viscosity	Cavity height
Nozzle	average inlet velocity	inlet density at U_{ref}	inlet viscosity at U_{ref}	Inlet height
Trough	average inlet velocity	inlet density at U_{ref}	inlet viscosity at U_{ref}	Inlet height

Table 6.1 Reference Values

For the compressible cases, the stagnation temperature (298°K), reference pressure (p_{ref} = 101 325.0 Pa), Reynolds number, and the Mach number are all

specified. The remaining reference values are derived from these specified quantities.

6.2 Test Case #1 : 2-D Driven Cavity

The two-dimensional driven cavity problem is tested for incompressible flow at a Reynolds number of 400. Figure 6.1 shows the geometry, boundary conditions and the grid used for the problem. There is a discontinuity in velocity at the two upper corners. As a result, the vorticity has a singularity at these two points. For this test case, the discontinuous velocity is arbitrarily chosen to be unity at these two corner nodes.

Figure 6.2 shows that convergence to machine accuracy is attained in 9 iterations on the (15*15) element grid. The first iteration is the solution of Stokes flow (Re=0) followed by quadratic convergence at the target Reynolds number. Figures 6.3 and 6.4 compare equi-vorticity contours and center-line velocities of the present solution to results using the stream function-vorticity method [8]. The difference between the center-line velocity profiles at the point of minimum velocity may be due to a slight difference in vorticity at the bottom wall. This would result in slightly different velocity gradients at the wall which eventually creates a difference in the two profiles at the point of minimum velocity. This is not too surprising as the wall vorticity is obtained from different approaches in the two formulations. The difference in the velocity in the upper region of the profile is a direct result of the difference in the lower region as mass must be conserved.

Figure 6.3 shows that the vorticity values are quite high at the upper corners due to the presence of a singularity in vorticity. The zero vorticity contours near the two lower corners, indicating the presence of secondary corner vorticities, compare very well with the stream function-vorticity results. Both formulations seem to indicate the faint presence of a very small vortex at the two corners. This is consistent with the findings of Ghia et al. [78]. The concentration of the highest vorticity value contours occurs near the lid, which is the region of highest shear, while the relatively lower value contours are within the large vortex in the center of the cavity. The lid drives the fluid toward the right stationary wall where the flow must turn abruptly down into the lower part of the cavity. This creates a second region of high vorticity along the upper right wall. It is reasonable to expect some differences in the vorticity contours between the two formulations in these regions of high vorticity and vorticity gradients, especially due to the coarseness of the grid. It can be somehow concluded, after the fact, that the stream function-vorticity values are probably more accurate.

6.3 Test Case #2 : 2-D Trough

Flow over a trough is selected to test the stability of the method for high Reynolds number separated flows. Figure 6.5a shows the geometry, boundary conditions and the grid used for the problem. The bottom wall geometry is given by;

$$y = \frac{-0.15}{\cosh(\,6[2(x - x_o) - 1]\,)} \tag{6.2}$$

where x_0 is the x-coordinate value at the start of the trough. The trough has a length of one inlet height and the y-coordinate is explicitly set to zero at the two ends of the trough. The inlet and exit are placed three channel heights from the trough.

For a Reynolds number of 10 000, convergence is attained in 7 iterations to machine accuracy on the 420 element grid and is shown in Figure 6.6. The initial guess of uniform flow is close enough to the solution to achieve quadratic convergence. The velocity vectors are shown, in the region of the trough, in Figure 6.5b. As expected at such a high Reynolds number, a recirculation zone is contained within the trough. The results are meant to be only illustrative since at such a Reynolds number the flow would actually be turbulent.

6.4 Test Case #3 : 2-D Nozzle

For subsonic flow, a converging-diverging nozzle with an inlet Mach number of 0.2 and a Reynolds number of 100 is tested. Figure 6.7 shows the geometry, boundary conditions and the grid used for the problem. The upper boundary is set at the symmetry line so that only half the problem need be solved. The Reynolds number is based on the full inlet channel height (diameter) so that the non-dimensional distance from the wall to the symmetry line is 0.5. The inlet and exit sections are both of constant cross-sectional area and are 20 diameters long. The nozzle length is one diameter and the bottom wall geometry is given by;

$$y = 0.2[\,1 - \cos(2\pi(x - x_0))\,] \qquad (6.3)$$

where x_o is the x-coordinate value at the start of the nozzle. The cross-sectional area at the throat is 60% of the inlet cross-sectional area.

Convergence is attained in 23 iterations to machine accuracy on the 930 element stretched grid and is compared, in Figure 6.8, to the convergence of the incompressible case, with the same initial guess. As expected, convergence is quadratic for the incompressible case and drops to linear for the subsonic case, since density is lagged one iteration. Despite this, the convergence is quite fast, justifying the solution strategy chosen for subsonic flows, at least for this test case. Figure 6.9 shows the velocity vectors in the nozzle region for incompressible flow, including the separation zone and reattachment after the nozzle, while Figure 6.10 compares the incompressible and subsonic results. The length of the separation zone for the incompressible and subsonic cases are 0.53 and 0.55 diameters respectively. The maximum Mach number in the subsonic flow case was 0.54. The results indicate, as expected, that compressibility raises the levels of velocity and thus creates a larger separation zone and higher levels of vorticity than for the corresponding incompressible case.

The continuity equation is not solved for explicitly, as shown in section 3.1. To assess the error in mass conservation, the mass flux was calculated at each grid station and is shown for the incompressible case in Figure 6.11. The mass flux at the exit is 1.28% lower than at the inlet. For the subsonic case, the mass flux is 1.22% lower at the exit than at the inlet. The incompressible case was tested using bilinear elements for both velocity and vorticity on exactly the same grid (930 elements) and also on a grid twice as fine in both the axial and tangential directions (3720 elements). The mass flux at exit is

99.91% and 99.20% lower than at inlet for the 930 and 3720 element grids, respectively! This clearly indicates the inadequacy of the equal order bilinear element for this formulation. To estimate the effect of grid size on the mass flux error, four uniform grids were tested for incompressible flow;

Grid	Δx	Δy	Mass Flux Error at Exit (%)
88*4	0.1250	0.1250	28.5
88*8	0.1250	0.0625	16.9
176*4	0.0625	0.1250	16.9
132*6	0.0833	0.0833	9.1

Table 6.2 Mass Flux Error

The mass flux error is approximately second order with respect to grid size in both directions. This observation cannot be extended to other geometries and other Reynolds numbers.

6.5 Test Case #4 : 3-D Driven Cavity

The three-dimensional driven cavity problem is analyzed at a Reynolds number of 100. This is carried out for incompressible flow and for lid Mach numbers of 0.2, 0.5 and 0.8. This problem is also analyzed at a Reynolds number of 400 for incompressible flow.

Figure 6.12 shows the geometry of the problem, with one side wall removed for visualization purposes, and the grid used for the Reynolds number 100 test cases. The top boundary is a moving lid with unity velocity from left ("back" wall) to right ("front" wall) while the back wall, front wall, two side walls and bottom wall are all stationary. The x-coordinate is in the direction

of motion of the lid, the y-coordinate is in the direction perpendicular to the lid, and the z-coordinate is in the direction normal to the symmetry plane. The pressure is specified at one corner point on the lid at the back wall.

For both the incompressible and subsonic cases, the initial iteration is for incompressible Stokes flow, while subsequent iterations are at the target Reynolds number of 100. Figure 6.13 compares the convergence history for the incompressible and compressible cases. For incompressible flow, quadratic convergence is attained and machine accuracy is reached in 6 iterations. For compressible flow, the pressure, density, temperature and viscosity are updated in a lagged manner from the velocity-vorticity system and linear convergence ensues. It must be remarked, however, that the convergence history is still impressive.

In Figure 6.14, the convergence history is compared for two grids, with the finer one containing eight times the number of elements of the coarse grid. The convergence rate is affected by grid refinement, requiring three additional iterations to reach machine accuracy.

Figure 6.15 shows the cavity centerline velocities on the symmetry plane for the two- and three-dimensional incompressible cases and compares the 3-D results to Ku et al. [79]. The effect of the third dimension is evident but is relatively weak at the Reynolds number of 100. The vortex is located higher in the cavity plane of symmetry than in two dimensions. Figure 6.16 shows the effect of compressibility on the cavity centerline velocities on the symmetry plane. For the compressible three-dimensional case, the velocity vectors are shown in Figure 6.12 and the density contours in Figure 6.17. The

trends in the velocity vectors are similar to those presented for incompressible flows. The centerline velocities show the trend of decreasing velocities with increasing compressibility, which is opposite of the usual behavior. The density contours of Figure 6.17 indicate, however, that the density is higher than unity for almost the entire domain. This is a result of specifying the reference pressure at the corner point of the back wall on the lid, at which the density will be unity. Since the pressure will be highest near the upper part of the front wall, towards which the lid moves, this will also be the region of highest density, as shown in Figure 6.17. Since the density is actually higher than unity, the velocities will be lower rather than higher as is usually the case. Figure 6.18 shows the normal vorticity contours for the three mid-planes in the incompressible three-dimensional case. These compare very well with the results presented by Osswald et al. [39], who used a velocity-vorticity finite difference fully implicit algorithm on a 17*17*17 uniformly distributed staggered grid. The vorticity contours in the streamwise plane indicate a small vortex at the bottom corners of the front and back walls. As in two dimensions, there is a discontinuity in velocity and thus a vorticity singularity at the upper corners. The velocity along the intersection of the lid with the stationary walls is arbitrarily set to unity. The vorticity contours in the spanwise plane indicate vortices have formed in the third dimension. The energy required for these secondary vortices reduce the strength of the primary vortex.

The compressible three-dimensional cases were carried out again using the energy equation instead of the constant total enthalpy assumption. A constant temperature is specified on the moving lid and zero heat flux is imposed on the stationary walls. A Prandtl number of 0.72 is used for all

cases. The convergence history is shown in Figure 6.19. Compared to the constant total enthalpy cases (see Figure 6.13), convergence is slower and less affected by compressibility. The slower convergence is due mostly to solving a differential equation that not only couples all the temperatures in the field, but also contains the velocity, density, pressure and viscosity. The constant enthalpy relation, on the other hand, is an explicit algebraic relation that only relies on the nodal temperature and velocity. Figure 6.20 shows the effect of compressibility on the cavity centerline velocities on the symmetry plane. The trends in the centerline velocities are similar to those for the constant total enthalpy cases (see Figure 6.16). Temperature contours in the symmetry plane are compared to those of the constant total enthalpy cases in Figure 6.21. The temperature contours in Figure 6.21 indicate a more complex distribution of temperature than for the constant enthalpy case, which may also contribute to the slower convergence. The temperature contours for the total enthalpy case indicate that the temperature has the same value in most of the cavity as a result of the low absolute velocity in most of the flow. The energy equation, however, contains a diffusion term which can create temperature gradients in regions of low velocity. Figure 6.21a shows that the temperature contours are normal to the three stationary walls, consistent with the zero heat flux boundary condition. The same physical reasoning that applied to the constant enthalpy case still applies for the energy equation case to explain the reduction of the centerline velocities for compressible flows. The temperature distribution has changed using the energy equation, but only by a few percent on the centerline of the symmetry plane. The density is influenced more by the pressure than by the temperature for this test case and is therefore, as with the constant enthalpy cases, greater than unity in most of the domain.

For the three-dimensional driven cavity problem for incompressible flow at a Reynolds number of 400, a finer grid is required. For comparison, this problem is solved using three different grids comprised of 8*8*4, 14*14*7 and 30*30*15 elements. For higher wall vorticity accuracy, the 14*14*7 element grid has a geometric expansion in each of the three directions with an element size of 0.0552 at walls to 0.09 at the center of the cavity. The 30*30*15 element grid has a geometric expansion from 0.0206 at walls to 0.05 at the center.

For the two finer grids, the memory required for the direct solver is listed in Table 6.3. Due to this high memory requirement, an iterative solver is used. There is no direct interaction between the iterative solver and the governing non-linear equations. The iterative solver was directly used as developed in [80] for the solution of the Euler and Navier-Stokes equations. The solver is based on Arnoldi's method, a Krylov subspace method for large non-symmetric linear algebraic systems of equations. It uses the Gram-Schmidt procedure, rather than the modified Gram-Schmidt procedure, to construct the required orthonormal basis of the Krylov subspace, relying on two applications of reorthogonalization to ensure the accuracy and stability of the orthogonalization process. For this particular iterative solver, only the non-zero entries are stored and the reduction in required memory is quite substantial as shown in Table 6.3:

Grid	Number of Unknowns	Half Bandwidth	Matrix Solver	Required Memory	CPU Time for 1 Matrix Soln. (1 Processor)
14*14*7	19 159	1 500	direct	51 138 845	279 sec
14*14*7	19 159	1 500	iterative	2 338 179	479 sec
30*30*15	195 615	6 796	direct	2 659 000 000	n/a
30*30*15	195 615	6 796	iterative	26 159 923	5 740 sec

Table 6.3 Required Memory and CPU Time on CRAY-YMP

It must be noted, however, that three arrays of this size are required; the matrix must be stored twice and the matrix column indices must be stored once.

The two finer grids were run on a CRAY-YMP/8-128 (8 processors and 128 MegaWords of memory). The memory on this machine was enough for the direct solver to be used on the 14*14*7 element grid but clearly not enough for the 30*30*15 element grid. The iterative solver was also used for one iteration on the 14*14*7 element grid to compare CPU times. From Table 6.3, it is seen that the iterative solver takes almost twice the CPU time as the direct solver. The direct solver, developed by V-N. Nguyen, is highly optimized for use on the CRAY-YMP in terms of both vectorization and parallelization [81]. All CPU times listed in Table 6.3 are for 1 processor. For these particular runs, it was rare that more than one processor was accessed at once. For the finer 30*30*15 element grid, the direct solver cannot even be attempted on this or any other machine today. The CPU time required for this case with the direct solver, if it were possible, can be estimated using;

$$\frac{t}{t_o} = \frac{N}{N_o}\left(\frac{b}{b_o}\right)^n \tag{6.4}$$

where

- N is the number of unknowns in the matrix system
- b is the matrix bandwidth
- t is the CPU time for one matrix solution
- n is the exponent with which the CPU time increases with respect to the matrix bandwidth (usually $1 < n < 2$)
- o reference values

In the usual range of the exponent n, the CPU time would be from 13 000 to 58 500 seconds, or from twice to ten times the CPU time of the iterative solver.

The two coarser grids (8*8*4 and 14*14*7 elements) are solved using the direct solver and the finer grid (30*30*15 elements) using the iterative solver. The convergence history for all three grids is shown in Figure 6.22. Since the iterative solver is not made to converge completely at each Newton iteration, the overall stability of the method changes. For this particular case, obtaining solutions at intermediary Reynolds numbers of 100 and 200 were required before starting at the final Reynolds number of 400.

Figure 6.23 shows the cavity centerline velocities on the symmetry plane for the three grids and clearly indicates the inadequacy of the two coarser ones. Figure 6.24 compares the centerline velocities of the finest grid to the two-dimensional case and to the 3-D results of Ku et al. [79] and Agarwal [34]. The centerline velocities are much lower in three dimensions than in two dimensions, indicating significant transverse flow in the third dimension. Comparing the centerline velocities to the two other sets of numerical

results, there is a discrepancy from the point of minimum velocity to the point of zero velocity. Judging by the significant changes in solution from the two coarser grids to the finer grid in Figure 6.23 and the differences with respect to other numerical results in Figure 6.24, the adequacy of the finest grid (30*30*15 elements) using the present formulation is still in question. Figure 6.25 shows the normal vorticity contours for the three mid-planes. The vorticity contours in the streamwise plane are very similar to those in two dimensions (see Figure 6.3a), except that the vortex strength is slightly weaker. This as shown in Figures 6.25b and 6.25c, is caused by the formation of vortices in the third dimension that draw away energy from the primary vortex.

The continuity equation is not solved for explicitly, as shown in section 3.1. To assess the error in mass conservation for each element in the domain the following measure was evaluated;

$$E^{e}_{mass} = \oint_{S'} [\vec{V} \cdot \vec{n}] \, dS \tag{6.5}$$

The maximum absolute error from all the elements is tabulated for each test case;

Re	M	Grid	Energy	Max. Mass Error	Location
100	incomp.	8*8*4		0.274E-03	.96 , .86 , .42
100	0.2	8*8*4	H=constant	0.296E-03	.96 , .86 , .42
100	0.5	8*8*4	H=constant	0.408E-03	.96 , .86 , .42
100	0.8	8*8*4	H=constant	0.594E-03	.96 , .86 , .42
100	0.2	8*8*4	Energy equation	0.283E-03	.96 , .86 , .42
100	0.5	8*8*4	Energy equation	0.392E-03	.96 , .86 , .42
100	0.8	8*8*4	Energy equation	0.576E-03	.96 , .86 , .42
400	incomp.	8*8*4		0.288E-03	.96 , .86 , .42
400	incomp.	14*14*7		0.962E-04	.03 , .97 , .03
400	incomp.	30*30*15		0.144E-04	.01 , .99 , .48

Table 6.4 Maximum Absolute Mass Error

The trends show that the mass conservation error increases with Mach number, increases slightly with Reynolds number, decreases with grid size and is slightly lower for the energy equation than for the constant total enthalpy assumption.

For the 3-D lid driven cavity, experimental laminar results are available at a Reynolds number of 3200 [82]. The experimental results clearly show that the flow in the symmetric plane is three-dimensional and cannot be accurately predicted with 2-D numerical methods. Experimental results are also available for flow through a 90 degree bend with a square cross-section [83] at a Reynolds number of 790. Secondary flow effects are present in the bend that prevent an accurate comparison to two-dimensional analysis. The goal of testing the three dimensional formulation against one of these two test cases was not achieved. Higher Reynolds numbers were not attempted since access to the CRAY-YMP was ended upon completion of the Reynolds number 400 test case. It is doubtful, however, that the 30*30*15 element grid

would have been fine enough to obtain an accurate solution at a Reynolds number of 3200. Since the present velocity-vorticity formulation cannot solve a finer grid on the CRAY-YMP, a change in iterative strategy, namely solving all six variables simultaneously in the entire field, would be necessary. A similar conclusion is reached for the above through-flow test case. Only coarse grids were attempted (e.g. 43*12*6 elements) for a Reynolds number of 100, resulting in unacceptable levels of mass loss of as much as 18%.

7. Discussion

7.1 Conclusions

Finite element vorticity-based methods have been shown to be suited to the formulation of the Navier-Stokes equations. The natural boundary conditions of the finite element method eliminate the need for explicit wall vorticity formulae in the stream function-vorticity formulation and for pressure extrapolation to the walls. The accuracy of imposition of boundary conditions and geometry approximation is improved through the use of quadratic elements.

The stream function-vorticity method is extended first to compressible subsonic symmetric external flows and then to lifting flows. Convergence for laminar flow at a Reynolds number of 10 000 was achieved without any upwinding or artificiai viscosity. The chosen solution procedure of solving the stream function and vorticity simultaneously by a Newton method and lagging the pressure, density, temperature and viscosity leads to a fast convergence rate for the test cases shown. It should be noted that extending this procedure to transonic flow would most likely result in very slow convergence due to the expected high coupling of the density and the flow (stream function and vorticity).

A velocity-vorticity approach using Poisson equations for velocity is developed for incompressible and compressible subsonic flows. A new finite element implementation of the wall vorticity boundary condition has been

demonstrated. The element discretizations for velocity and vorticity are set up to maximize the accuracy of the wall vorticity boundary condition. The method was first applied in two-dimensions and showed good accuracy for the driven cavity, good stability for the trough at high laminar Reynolds number and a fast linear convergence for subsonic nozzle flow. For the 3-D cavity at a Reynolds number of 100, the formulation compared well to other numerical methods for incompressible flows and exhibited a fast linear convergence for high subsonic flows. For the 3-D cavity at a Reynolds number of 400, a much finer grid was required and an iterative solver was used. The convergence rate was linear and fast but required Reynolds number stepping for stability. In all the test cases attempted in both two- and three-dimensions, no artificial viscosity was required to stabilize the iterative process or to smooth the solution.

The formulation and the boundary conditions of this velocity-vorticity method make it simpler to apply to three-dimensional flows than stream function methods. For two-dimensional flows, the relative advantages and disadvantages of the stream function-vorticity and velocity-vorticity formulations are;

1) The mass is conserved exactly, locally and globally, for stream function-vorticity formulations. For velocity-vorticity this has proven to be a source of difficulty. For example, for enclosed flows mass is conserved globally, but the scheme cannot guarantee local mass conservation. For through-flows the scheme has shown difficulties at the local and global levels.
2) There are two variables for stream function-vorticity, compared to three for velocity-vorticity, to solve for.

3) Since vorticity is defined in terms of gradients of velocity or alternatively in terms of the second derivatives of stream function, it is clear that the use of elements having only one order interpolation difference between the variables, is more appropriate for the velocity-vorticity formulation.

Overall, it is preferable to use the stream function-vorticity method for two-dimensional flows.

7.2 Recommendations for Extending the Current Work

Current work concerns extending the stream function-vorticity formulation to transonic external flow. It has already been attempted to solve the inviscid equations by lagging the density, pressure and temperature. Artificial compressibility and upwinding on the operator matrix have been introduced for transonic flow. The convergence, however, is very slow. The recommended strategy that is presently being implemented is to solve the pressure simultaneously with the stream function and vorticity. The density and temperature could be eliminated through the equation of state and assuming a constant total enthalpy, respectively.

When solving the velocity-vorticity system using the second order Poisson equations for velocity, the first order continuity equation and definition of vorticity are assumed to be satisfied to within a reasonable error. On coarse grids, this error will be quite large and the grid must be refined until these errors are judged reasonable. In this formulation, reducing these errors to reasonable levels relies solely on grid refinement. It must be noted that even if the continuity equation and the definition of vorticity are solved for

directly, there will still be a discretization error present. Any error analysis done with the present formulation must separate the errors due to solving the second order Poisson equation and the discretization errors that would be present if solving the first order equations. The question is whether these errors are reasonable for realistic grids. The answer depends on the definition of reasonable, which is subjective in nature, and may also depend on the geometry and flow conditions. Apart from grid refinement, there are presently two options that address the mass conservation problem; 1) solving the continuity equation directly instead of the Poisson velocity equations, and 2) using a staggered finite difference discretization. If the answer to the above question is that unreasonably fine grids are required for the present formulation, it is recommended for finite element formulations to solve the continuity equation directly. As for obtaining a solenoidal vorticity, there are two methods available in the literature for incompressible flow; 1) using the conservative form of the vorticity transport equation with an initial solenoidal vorticity field, and 2) introducing a potential to project the vorticity on to a solenoidal field. The second method, unlike the first, can be extended to subsonic flow but has the disadvantage of introducing an extra unknown into the system. Before introducing this inconvenience, it must be clearly established that the error is unreasonable for realistic grids, which is not an easy task.

Current work also concerns extending the 3-D velocity-vorticity formulation to higher Reynolds number inflow-outflow problems. The grids necessary for these types of flows will be larger than the grids used for the driven cavity. The memory limit of the CRAY-YMP/8-128 was nearly reached for the driven cavity at Re=400 using an iterative solver in which only the non-

zeroes were stored. Since this is the lower limit for memory use solving the velocity and vorticity simultaneously for the entire domain, another strategy will have to be selected to solve these problems on today's computers. Domain decomposition methods, on parallel computers, are being studied. Another possible reduction of the required computer memory is to solve only a selected number of variables simultaneously, say one velocity and one vorticity in a block. The selection would be made with both the non-linear convective terms and the vorticity wall boundary condition as the major considerations. For either strategy, since the coupling of the entire velocity-vorticity system is reduced, convergence is expected to be slower.

References

1. Sani, R.L., Gresho, P.M., Lee, R.L. and Griffiths, D.F., "The Cause and Cure (?) of the Spurious Pressures Generated by Certain FEM Solutions of the Incompressible Navier-Stokes Equations: Part 1", *International Journal for Numerical Methods in Fluids*, Vol. 1, pp. 17-43, 1981.

2. Harlow, F.H. and Welch, J.E., "Numerical Calculation of Time-Dependent Viscous Incompressible Flow of Fluid with Free Surface", *Physics of Fluids*, Vol. 8, pp. 2182-2189, 1965.

3. Chorin, A.J., "A Numerical Method for Solving Incompressible Viscous Flow Problems", *Journal of Computational Physics*, Vol. 2, pp. 12-26, 1967.

4. R. Peyret and T.D. Taylor, *Computational Methods for Fluid Flow*, Springer-Verlag, 1983.

5. Hood, P. and Taylor, C., "Navier-Stokes Equations Using Mixed Interpolation", *Finite Element Methods in Flow Problems: International Symposium on Finite Element Methods in Flow Problems*, Swansea, (Eds. Oden, J.T., Zienkiewicz, O.C., Gallagher, R.H. and Taylor, C.), UAH Press, Huntsville, Alabama, pp. 121-132, 1974.

6. Campion-Renson, A. and Crochet, M.J., "On the Stream Function Vorticity Finite Element Solutions of Navier-Stokes Equations", *International Journal for Numerical Methods in Engineering*, Vol. 12, pp. 1809-1818, 1978.

7. Dhatt, G., Fomo, B.K. and Bourque, C.A., "A ψ-ω Finite Element Formulation for the Navier-Stokes Equations", *International Journal for Numerical Methods in Engineering*, Vol. 17, pp. 199-212, 1981.

8. Peeters, M.F., Habashi, W.G. and Dueck, E.G., "Finite Element Stream Function-Vorticity Solutions of the Incompressible Navier-Stokes Equations", *International Journal for Numerical Methods in Fluids*, Vol. 7, pp. 17-27, 1987.

9. Aziz, K. and Hellums, J.D., "Numerical Solution of the Three-Dimensional Equations of Motion for Laminar Natural Convection", *Physics of Fluids*, Vol. 10, pp. 314-324, 1967.

10. Hirasaki, G.J. and Hellums, J.D., "A General Formulation of the Boundary Conditions on the Vector Potential in Three-Dimensional Hydrodynamics", *Quarterly of Applied Mathematics*, Vol. 26, No. 3, pp. 331-342, 1968.

11. Hirasaki, G.J. and Hellums, J.D., "Boundary Conditions on the Vector and Scalar Potentials in Viscous Three-Dimensional Hydrodynamics", *Quarterly of Applied Mathematics*, Vol. 28, No. 2, pp. 293-296, 1970.

12. Richardson, S.M. and Cornish, A.R.H., "Solution of Three-Dimensional Incompressible Flow Problems", *Journal of Fluid Mechanics*, Vol. 82, pp. 309-319, 1977.

13. Aregbesola, Y.A.S. and Burley, D.M., "The Vector and Scalar Potential Method for the Numerical Solution of Two- and Three-Dimensional Navier-Stokes Equations", *Journal of Computational Physics*, Vol. 24, pp. 398-415, 1977.

14. Sherif, A. and Hafez, M.M., "Computation of Three-Dimensional Flows Using Two Stream Functions", AIAA Paper 83-1948-CP, 1983.

15. Davis, R.L., Carter, J.E. and Hafez, M.M., "3-D Viscous Flow Solutions with a Vorticity-Stream Function Formulation", AIAA-Paper-87-0601, 1987.

16. Wong, A.K. and Reizes, J.A., "An Effective Vorticity-Vector Potential Formulation for the Numerical Solution of Three-Dimensional Duct Flow Problems", *Journal of Computational Physics*, Vol. 55, pp. 98-114, 1984.

17. Lin, A., de Vahl Davis, G., Leonardi, E. and Reizes, J.A., "Numerical Study of the Three-Dimensional Incompressible Flow Between Closed Rotating Cyiinders", *Lecture Notes in Physics no. 218 : 9th International Conference on Numerical Methods in Fluid Dynamics*, Saclay, France, pp. 380-387, 1984.

18. Yang, H. and Camarero, R., "An Improved Vorticity-Potential Method for Three-Dimensional Duct Flow Simulations", *International Journal for Numerical Methods in Fluids*, Vol. 6, pp. 35-45, 1986.

19. Hamed, A. and Abdallah, S., "Internal Three-Dimensional Viscous Flow Solution Using the Streamlike Function", *Journal of Fluids Engineering, Transactions of the ASME*, Vol. 108, No. 3, pp. 348-353, 1986.

20. Agarwal, R.K., "A Fourth-Order-Accurate Compact Differencing Scheme for Steady Navier-Stokes Equations", AIAA Paper 82-0977, 1982.

21. Habashi, W.G., Peeters, M.F., Guevremont, G. and Hafez, M.M., "Finite Element Solutions of the Compressible Navier-Stokes Equations", *AIAA Journal*, Vol. 25, No. 7, pp. 944-948, 1987.

22. Habashi, W.G. and Hafez, M.M., "Finite Element Stream Function Solutions of Transonic Rotational Internal and External Flows", *Journal of Numerical Methods for Partial Differential Equations*, Vol. 1, pp. 127-144, 1985.

23. P.J. Roache, *Computational Fluid Dynamics*, Hermosa Publishers, 1976.

24. Luchini, P., "An Adaptive-Mesh Finite-Difference Solution Method for the Navier-Stokes Equations", *Journal of Computational Physics*, Vol. 68, pp. 283-306, 1987.

25. Strikwerda, J. C., "Upwind Differencing, False Scaling, and Nonphysical Solutions to the Driven Cavity Problem", *Journal of Computational Physics*, Vol. 47, pp. 303-307, 1982.

26. Ghia, K.N., Osswald, G.A. and Ghia, U., "Analysis of Two-Dimensional Incompressible Flow Past Airfoils Using Unsteady Navier-Stokes Equations", *Numerical and Physical Aspects of Aerodynamic Flows*, Vol. III, (Ed. Cebeci, T.), Springer-Verlag, pp. 318-338, 1986.

27. Gresho, P.M., "Incompressible Fluid Dynamics: Some Fundamental Formulation Issues", *Annual Review of Fluid Mechanics*, Vol. 23, pp. 413-453, 1991.

28. Rubin, S.G. and Khosla, P.K., "Navier-Stokes Calculations with a Coupled Strongly Implicit Method-I", *Computers and Fluids*, Vol. 9, pp. 163-180, 1981.

29. Markham, D.M. and Lewis, C.H., "A Numerical Model for a Turbulent Buoyant Jet in a Shallow Open Channel", *Progress in Astronautics and Aeronautics, vol. 36 : Thermal Pollution Analysis*, pp. 203-218, 1975.

30. Fasel, H., "Investigation of the Stability of Boundary Layers by a Finite-Difference Model of the Navier-Stokes Equations", *Journal of Fluid Mechanics*, Vol. 78, pp. 355-383, 1976.

31. Cook, R.N., "Numerical Solutions of the Navier-Stokes Equations in 3 Dimensions", *Ph.D. Thesis*, University of Western Ontario, 1976.

32. Dennis, S.C.R., Ingham, D.B. and Cook, R.N., "Finite-Difference Methods for Calculating Steady Incompressible Flows in Three Dimensions", *Journal of Computational Physics*, Vol. 33, pp. 325-339, 1979.

33. Speziale, C.G., "On the Advantages of the Vorticity-Velocity Formulation of the Equations of Fluid Dynamics", *Journal of Computational Physics*, Vol. 73, pp. 476-480, 1987.

34. Agarwal, R.K., "Third-Order-Accurate Upwind Scheme for Navier-Stokes Solutions in Three Dimensions", *Computers in Flow Predictions and Fluid Dynamics Experiments*, (Eds. Ghia, K.N., Mueller, T.J. and Patel, B.R.), ASME, New York, pp. 73-82, 1981.

35. Gatski, T.B., Grosch, C.E. and Rose, M.E., "A Numerical Study of the Two-Dimensional Navier-Stokes Equations in Vorticity-Velocity Variables", *Journal of Computational Physics*, Vol. 48, pp. 1-22, 1982.

36. Gatski, T.B., Grosch, C.E. and Rose, M.E., "The Numerical Solution of the Navier-Stokes Equations for 3-Dimensional, Unsteady, Incompressible Flows by Compact Schemes", *Journal of Computational Physics*, Vol. 82, pp. 298-329, 1989.

37. Farouk, B. and Fusegi, T., "A Coupled Solution of the Vorticity-Velocity Formulation of the Incompressible Navier-Stokes Equations", *International Journal for Numerical Methods in Fluids*, Vol. 5, pp. 1017-1034, 1985.

38. Orlandi, P., "Vorticity-Velocity Formulation for High Re Flows", *Computers and Fluids*, Vol. 15, No. 2, pp. 137-149, 1987.

39. Osswald, G.A., Ghia, K.N. and Ghia, U., "A Direct Algorithm for Solution of Incompressible Three-Dimensional Unsteady Navier-Stokes Equations", *Proceedings of the AIAA 8th Computational Fluid Dynamics Conference*, Honolulu, pp. 408-421, 1987.

40. Huang, Y., Ghia, U., Osswald, G.A. and Ghia, K.N., "Unsteady Three-Dimensional Flow Simulation Using Vorticity-Velocity Form of Navier-Stokes Equations and ADI+MG-DGS Method", *Proceedings of the AIAA 10th Computational Fluid Dynamics Conference*, Honolulu, AIAA Paper 91-1562-CP, pp. 380-392, 1991.

41. Toumi, A. and Ta Phuoc Loc, "Numerical Study of Three-Dimensional Viscous Incompressible Flow by Vorticity and Velocity Formulation", *Numerical Methods in Laminar and Turbulent Flow, Vol. V*, (Eds. Taylor, C., Habashi, W.G. and Hafez, M.M.), Pineridge Press, pp. 595-606, 1987.

42. Guj, G. and Stella, F., "Numerical Solutions of High-Re Recirculating Flows in Vorticity-Velocity Form", *International Journal for Numerical Methods in Fluids*, Vol. 8, pp. 405-416, 1988.

43. Stella, F. and Guj, G., "Vorticity-Velocity Formulation in the Computation of Flows in Multiconnected Domains", *International Journal for Numerical Methods in Fluids*, Vol. 9, pp. 1285-1298, 1989.

44. Napolitano, M. and Pascazio, G., "A Numerical Method for the Vorticity-Velocity Navier-Stokes Equations in Two and Three Dimensions", *International Symposium on Computational Fluid Dynamics*, Nagoya, Japan, pp. 590-595, 1989.

45. Napolitano, M. and Catalano, L.A., "A Multi-Grid Solver for the Velocity-Vorticity Navier-Stokes Equations", *International Journal for Numerical Methods in Fluids*, Vol. 13, pp. 49-59, 1991.

46. Dacles, J. and Hafez, M.M, "Numerical Methods For 3-D Viscous Incompressible Flows Using Velocity / Vorticity Formulation", AIAA-Paper-90-0237, 1990.

47. Stremel, P.M., "Calculation of Flow About Two-Dimensional Bodies by Means of the Velocity-Vorticity Formulation on a Staggered Grid", AIAA-Paper-91-0600, 1991.

48. Murata S., Satofuka, N. and Kushiyama, T., "Parabolic Multi-Grid Method for Incompressible Viscous Flows Using a Group Explicit Relaxation Scheme", *Computers and Fluids*, Vol. 19, No. 1, pp. 33-41, 1991.

49. Hansen, M.O.L., Sorensen, J.N. and Barker, V.A., "A Numerical Investigation of 3-D Flow Past an Infinite Cylinder", *Proceedings of the First European Computational Fluid Dynamics Conference*, Brussels, (Eds. Hirsch, C., Periaux, J. and Kordulla, W.), Elsevier Science Publishers, pp. 375-381, 1992.

50. Daube, O., "Resolution of the 2-D Navier-Stokes Equations in Velocity-Vorticity Form by Means of an Influence Matrix Technique", *Journal of Computational Physics*, Vol. 103, pp. 402-414, 1992.

51. Gunzburger, M.D. and Peterson, J.S., "Finite Element Methods for Vorticity Formulations of Incompressible Viscous Flow", *Numerical Methods in Laminar and Turbulent Flow, Vol. V*, (Eds. Taylor, C., Habashi, W.G. and Hafez, M.M.), Pineridge Press, pp. 170-181, 1987.

52. Gunzburger, M.D. and Peterson, J.S., "On Finite Element Approximations of the Streamfunction-Vorticity and Velocity-Vorticity Equations", *International Journal for Numerical Methods in Fluids*, Vol. 8, pp. 1229-1240, 1988.

53. Gunzburger, M., Mundt, M. and Peterson, J., "Experiences with Finite Element Methods for the Velocity-Vorticity Formulation of Three-Dimensional Viscous Incompressible Flows", *Computational Methods in Viscous Aerodynamics*, (Ed. Brebbia, C.A.), Springer-Verlag, 1990.

54. Du, Q., Gunzburger, M.D. and Meir, A.J., "Vorticity Constraints in Velocity-Vorticity Formulations of Steady, Viscous, Incompressible Flow", *Numerical Methods in Laminar and Turbulent Flow, Vol. VII*, (Eds. Taylor, C., Chin, J.H. and Homsy, G.M.), Pineridge Press, pp. 774-781, 1991.

55. Hafez, M.M., Dacles, J. and Soliman, M., "A Velocity/Vorticity Method for Viscous Incompressible Flow Calculations", *Lecture Notes in Physics no. 323 : 11th International Conference on Numerical Methods in Fluid Dynamics*, Williamsburg, VA., pp. 288-296, 1988.

56. Nicolaides, R.A., "Triangular Discretization for the Vorticity-Velocity Equations", *Finite Element Analysis in Fluids : Proceedings of the Seventh International Conference on Finite Element Methods in Flow Problems*, (Eds. Chung, T.J. and Karr, G.R.), UAH Press, Huntsville, Alabama, pp. 824-829, 1989.

57. Choudhury, S. and Nicolaides, R.A., "Discretization of Incompressible Vorticity-Velocity Equations on Triangular Meshes", *International Journal for Numerical Methods in Fluids*, Vol. 11, pp. 823-833, 1990.

58. Brebbia, C.A. and Wrobel, L.C., "Viscous Flow Problems by the Boundary Element Method", *Recent Advances in Numerical Methods in Fluids*, Vol. 5, pp. 1-21, 1986.

59. Wang, C.M. and Wu, J.C., "A Numerical Method for Three-Dimensional Viscous Flows", AIAA-Paper-90-0236, 1990.

60. Stremel, P.M., "Aerodynamic Interaction Between Vortical Wakes and the Viscous Flow about a Circular Cylinder", AIAA-Paper-85-4063, 1985.

61. Stremel, P.M., "The Calculation of Rotor/Fuselage Interaction for Two-Dimensional Bodies", *16th European Rotorcraft Forum*, Glasgow, Scotland, pp. II.11.3.1-II.11.3.32, 1990.

62. Ku, H.-C. and Hatziavramidis, D., "Solutions of the Two-Dimensional Navier-Stokes Equations by Chebyshev Expansion Methods", *Computers and Fluids*, Vol. 13, pp. 99-113, 1985.

63. Mizukami, A., "A Stream Function-Vorticity Finite Element Formulation for Navier-Stokes Equations in Multi-Connected Domain", *International Journal for Numerical Methods in Engineering*, Vol. 19, pp. 1403-1420, 1983.

64. Gunzburger, M.D. and Peterson, J.S., "On the Finite Element Approximation of the Streamfunction-Vorticity Equations", *5th IMACS International Symposium on Computer Methods for Partial Differential Equations*, pp. 47-56, 1984.

65. Tezduyar, T.E., Glowinski, R. and Liou, J., "Petrov-Galerkin Methods on Multiply Connected Domains for the Vorticity-Stream Function Formulation of the Incompressible Navier-Stokes Equations", *International Journal for Numerical Methods in Fluids*, Vol. 8, pp. 1269-1290, 1988.

66. Guevremont, G., Habashi, W.G., Hafez, M.M. and Peeters, M.F., "A Velocity-Vorticity Finite Element Formulation of the Compressible Navier-Stokes Equations", *Proceedings of the 4th International Conference on Computational Engineering Science*, Atlanta, (Eds. Atluri, S.N. and Yagawa, G.), Springer-Verlag, pp. 51.x.1-51.x.4, 1988.

67. Habashi, W.G., Guevremont, G. and Hafez, M.M., "Finite Element Solution of the Navier-Stokes Equations by a Velocity-Vorticity Method", *First International Conference on Computational Methods in Flow Analysis*, Okayama, Japan, (Eds. Kawahara, M. and Niki, H.), pp. 312-319, 1988.

68. Habashi, W.G., Guevremont, G., Peeters, M.F., Przybytkowski, S.M. and Hafez, M.M., "Finite Element Vorticity-Based Methods for the Solution of the Compressible Navier-Stokes Equations", *Computational Methods in Viscous Aerodynamics*, (Ed. Brebbia, C.A.), Springer-Verlag, 1990.

69. Guevremont, G., Habashi, W.G. and Hafez, M.M., "Finite Element Solution of the Navier-Stokes Equations by a Velocity-Vorticity Method", *International Journal for Numerical Methods in Fluids*, Vol. 10, pp. 461-475, 1990.

70. Guevremont, G., Habashi, W.G., Kotiuga, P.L. and Hafez, M.M., "Finite Element Solution of the 3-D Compressible Navier-Stokes Equations by a Velocity-Vorticity Method", AIAA-Paper-90-0404, 1990.

71. Guevremont, G., Habashi, W.G., Kotiuga, P.L. and Hafez, M.M., "Finite Element Solution of the 3-D Compressible Navier-Stokes Equations by a Velocity-Vorticity Method", *Journal of Computational Physics*, Vol. 107, pp. 176-187, 1993.

72. H. Schlichting, *Boundary Layer Theory*, McGraw-Hill, 7th Edition, p. 328, 1979.

73. R.H.F. Pao, *Fluid Dynamics*, Charles E. Merrill Books, Columbus, Ohio, p. 280, 1967.

74. Hinton, E., Scott, F.C. and Ricketts, R.E., "Local Least Squares Stress Smoothing for Parabolic Isoparametric Elements", *International Journal for Numerical Methods in Engineering*, Vol. 9, pp. 235-256, 1975.

75. Rizzi, A., "Computational Mesh for Transonic Airfoils", *Numerical Methods for the Computation of Inviscid Transonic Flows*, (Eds. Rizzi, A. and Viviand, H.), Vieweg and Sohn, 1981.

76. Steger, J.L., "Implicit Finite-Difference Simulation of Flow about Arbitrary Two-Dimensional Geometries", *AIAA Journal*, Vol. 16, No. 7, pp. 679-686, 1978.

77. Venkatakrishnan, V., "Preconditioned Conjugate Gradient Methods for the Compressible Navier-Stokes Equations", AIAA-Paper-90-0586, 1990.

78. Ghia, U., Ghia, K.N. and Shin, C.T., "High-Re Solutions for Incompressible Flow Using the Navier-Stokes Equations and a Multigrid Method", *Journal of Computational Physics*, Vol. 48, pp. 387-411, 1982.

79. Ku, H.C., Hirsh, R.S. and Taylor, T.D., "A Pseudospectral Method for Solution of the Three-Dimensional Incompressible Navier-Stokes Equations", *Journal of Computational Physics*, Vol. 70, pp. 439-462, 1987.

80. Strigberger, J., Baruzzi, G., Habashi, W.G. and Fortin, M., "Some Special Purpose Preconditioners for Conjugate Gradient-Like Methods Applied to CFD", *International Journal for Numerical Methods in Fluids*, Vol. 16, pp. 581-596, 1993.

81. Habashi, W.G., Nguyen, V-N. and Bhat, M.V., "Efficient Direct Solvers for Large-Scale Computational Fluid Dynamics Problems", *Computer Methods in Applied Mechanics and Engineering*, Vol. 87, pp. 253-265, 1991.

82. Koseff, J.R. and Street, R.L., "The Lid-Driven Cavity Flow: A Synthesis of Qualitative and Quantitative Observations", *Journal of Fluids Engineering, Transactions of the ASME*, Vol. 106, pp. 390-398, 1984.

83. Humphrey, J.A.C., Taylor, A.M.K. and Whitelaw, J.H., "Laminar Flow in a Square Duct of Strong Curvature", *Journal of Fluid Mechanics*, Vol. 83, pp. 509-527, 1977.

Appendix A

Derivation of the 2-D Subsonic Vorticity Transport Equation in Stream Function-Vorticity Variables

1) Conventions

   a. subscripts x and y refer to partial derivatives

2) Definitions of Stream Function, Vorticity and Inverse Density

$$\Psi_y \equiv \rho u \qquad \Psi_x \equiv -\rho v \qquad \text{(A.1a,b)}$$

$$\omega \equiv v_x - u_y \qquad \bar{\rho} \equiv \frac{1}{\rho} \qquad \text{(A.2a,b)}$$

therefore

$$u = \bar{\rho}\,\Psi_y \qquad v = -\bar{\rho}\,\Psi_x \qquad \text{(A.3a,b)}$$

3) Governing Equations

x-Momentum Equation

$$\rho u u_x + \rho v u_y = -p_x + \left[\mu\left(2u_x - \frac{2}{3}(u_x + v_y)\right)\right]_x + \left[\mu(u_y + v_x)\right]_y \qquad \text{(A.4a)}$$

y-Momentum Equation

$$\rho u v_x + \rho v v_y = -p_y + \left[\mu\left(2v_y - \frac{2}{3}(u_x + v_y)\right)\right]_y + \left[\mu(u_y + v_x)\right]_x \qquad \text{(A.4b)}$$

Vorticity Transport Equation

$$\frac{\partial}{\partial x}(\text{y-momentum}) - \frac{\partial}{\partial y}(\text{x-momentum})$$

4) Convective Terms

replacing the definition of the stream function (equations A.1) into the convective terms of the vorticity transport equation (LHS):

$$\begin{aligned} LHS &= \left(\Psi_y v_x - \Psi_x v_y\right)_x - \left(\Psi_y u_x - \Psi_x u_y\right)_y \\ &= \Psi_x(u_{yy} - v_{yx}) + \Psi_y(v_{xx} - u_{xy}) - \Psi_{xx} v_y - \Psi_{yy} u_x \\ &\quad + \Psi_{xy}(v_x + u_y) \end{aligned} \tag{A.5}$$

replacing the velocities using the inverse density (equations A.3):

$$\begin{aligned} LHS &= \Psi_y(v_x - u_y)_x - \Psi_x(v_x - u_y)_y - \Psi_{xx}(-\bar{\rho}\Psi_x)_y \\ &\quad - \Psi_{yy}(\bar{\rho}\Psi_y)_x + \Psi_{xy}\left[(-\bar{\rho}\Psi_x)_x + (\bar{\rho}\Psi_y)_y\right] \end{aligned} \tag{A.6}$$

replacing the definition of vorticity (equation A.2a) and expanding:

$$\begin{aligned} LHS &= \Psi_y\omega_x - \Psi_x\omega_y + \bar{\rho}\Psi_{xy}\left(\Psi_{xx} - \Psi_{yy} - \Psi_{xx} + \Psi_{yy}\right) \\ &\quad - \bar{\rho}_x\left(\Psi_y\Psi_{yy} + \Psi_x\Psi_{xy}\right) + \bar{\rho}_y\left(\Psi_x\Psi_{xx} + \Psi_y\Psi_{xy}\right) \\ &= \Psi_y\omega_x - \Psi_x\omega_y - \frac{1}{2}\bar{\rho}_x\left(\Psi_x^2 + \Psi_y^2\right)_y + \frac{1}{2}\bar{\rho}_y\left(\Psi_x^2 + \Psi_y^2\right)_x \end{aligned} \tag{A.7}$$

5) Viscous Terms

taking the curl of the viscous terms of the momentum equations to form the right hand side of the vorticity transport equation (RHS):

$$\begin{aligned} RHS &= [2\mu v_y]_{yx} - \left[\frac{2}{3}\mu\left(u_x + v_y\right)\right]_{yx} + [\mu(u_y + v_x)]_{xx} \\ &\quad - [2\mu u_x]_{xy} + \left[\frac{2}{3}\mu\left(u_x + v_y\right)\right]_{xy} - [\mu(u_y + v_x)]_{yy} \end{aligned} \tag{A.8}$$

replacing the definition of vorticity (equation A.2a) and rearranging:

$$\begin{aligned} RHS &= [2\mu v_y]_{yx} + [\mu(2u_y + \omega)]_{xx} - [2\mu u_x]_{xy} - [\mu(-\omega + 2v_x)]_{yy} \\ &= \nabla^2(\mu\omega) + [(2\mu u_y)_x - (2\mu u_x)_y]_x + [(2\mu v_y)_x - (2\mu v_x)_y]_y \\ &= \nabla^2(\mu\omega) + 2[\mu_x u_y - \mu_y u_x]_x + 2[\mu_x v_y - \mu_y v_x]_y \end{aligned} \tag{A.9}$$

6) Vorticity Transport Equation

equating the right and left hand sides (equations A.7 and A.9):

$$\mathrm{Re}\left\{\Psi_y\omega_x - \Psi_x\omega_y - \frac{1}{2}\bar{\rho}_x\left(\Psi_x^2 + \Psi_y^2\right)_y + \frac{1}{2}\bar{\rho}_y\left(\Psi_x^2 + \Psi_y^2\right)_x\right\}$$

$$= \nabla^2(\mu\omega) + 2\left[\mu_x u_y - \mu_y u_x\right]_x + 2\left[\mu_x v_y - \mu_y v_x\right]_y \qquad \text{(A.10)}$$

Appendix B

Integration by Parts of the Compressibility Source Term of the 2-D Subsonic Vorticity Transport Equation in Stream Function-Vorticity Variables

1) Conventions

   a. subscripts x, y, and s refer to partial derivatives

2) Definitions

$$q^2 \equiv u^2 + v^2 \qquad f \equiv \frac{1}{2}(\rho q)^2 \qquad W \equiv - W_i^{\omega} \, Re \tag{B.1a,b,c}$$

3) Galerkin Weighted Residual Form : Compressibility Source Term

$$\int_A W_i^{\omega} \left[- Re \left\{ \frac{1}{2} \bar{\rho}_y [(\rho q)^2]_x - \frac{1}{2} \bar{\rho}_x [(\rho q)^2]_y \right\} \right] dA$$

4) Integration by Parts

$$\int_A W \left[f_x \bar{\rho}_y - f_y \bar{\rho}_x \right] dA$$

$$= \int_A \left[(W f \bar{\rho}_y)_x - W_x f \bar{\rho}_y - W f \bar{\rho}_{yx} - (W f \bar{\rho}_x)_y + W_y f \bar{\rho}_x + W f \bar{\rho}_{xy} \right] dA$$

$$= \int_A \left[- W_x f \bar{\rho}_y + W_y f \bar{\rho}_x \right] dA + \int_C \left[W f \bar{\rho}_y dy + W f \bar{\rho}_x dx \right]$$

$$= \int_A \left[f \left(W_y \bar{\rho}_x - W_x \bar{\rho}_y \right) \right] dA + \int_C \left[W f \bar{\rho}_s ds \right] \tag{B.2}$$

Appendix C

Transformation of the Viscosity Source Term in the Contour Integral of the 2-D Subsonic Vorticity Transport Equation in Stream Function-Vorticity Variables

1) Conventions

   a. subscripts x, y, s, and n refer to partial derivatives

2) Definitions

   s represents the tangential direction along the boundary

   n represents the normal direction to the boundary

   α represents the angle between the n and x axes

3) Viscosity Source Term in the Contour Integral in Cartesian Coordinates

$$-\int_C W_i^{\omega}\left[2\left(\mu_x u_y - \mu_y u_x\right)dy - 2\left(\mu_x v_y - \mu_y v_x\right)dx\right]$$

4) Transformation to s-n Coordinates

$$u_x = u_s s_x + u_n n_x = -u_s \sin\alpha + u_n \cos\alpha \qquad \text{(C.1a)}$$

$$u_y = u_s s_y + u_n n_y = u_s \cos\alpha + u_n \sin\alpha \qquad \text{(C.1b)}$$

replacing equations (C.1) into the first viscosity source term:

$$\mu_x u_y - \mu_y u_x = \left(\mu_s s_x + \mu_n n_x\right)\left(u_s s_y + u_n n_y\right) - \left(\mu_s s_y + \mu_n n_y\right)\left(u_s s_x + u_n n_x\right)$$

$$= (\mu_s u_s - \mu_s u_s) s_x s_y + (\mu_s u_n - \mu_n u_s) s_x n_y$$
$$+ (\mu_n u_s - \mu_s u_n) s_y n_x + (\mu_n u_n - \mu_n u_n) n_x n_y$$
$$= (\mu_n u_s - \mu_s u_n)(s_y n_x - s_x n_y)$$
$$= (\mu_n u_s - \mu_s u_n)(\cos^2\alpha + \sin^2\alpha)$$
$$= \mu_n u_s - \mu_s u_n \qquad \text{(C.2)}$$

similarly for the second viscosity term:

$$\mu_x v_y - \mu_y v_x = \mu_n v_s - \mu_s v_n \qquad \text{(C.3)}$$

replacing equations (C.2,C.3) back into the contour integral:

$$-\int_C W_i^{\omega}[2(\mu_n u_s - \mu_s u_n)\,dy - 2(\mu_n v_s - \mu_s v_n)\,dx]$$

Thus at exit planes where zero normal derivatives are zero, this entire term is equal to zero.

Appendix D

Derivation of the 3-D Subsonic Vorticity Transport Equation in Velocity-Vorticity Variables

1) Conventions

a. subscripts x, y, and z refer to partial derivatives

2) Definition of Vorticity

$$\vec{\Omega} \equiv \nabla \times \vec{V} \qquad \text{and therefore} \qquad \nabla \cdot \vec{\Omega} = 0 \tag{D.1a,b}$$

3) Governing Equations

Continuity Equation

$$\nabla \cdot (\rho \vec{V}) = 0 \tag{D.2}$$

Momentum Equation

$$(\rho \vec{V} \cdot \nabla)\vec{V} = -\nabla p + \frac{1}{Re}\left\{\nabla\left[\frac{4}{3}\mu(\nabla \cdot \vec{V}) + \vec{V} \cdot \nabla\mu\right] - \vec{V}\left[\nabla^2\mu\right] - \left[\nabla \cdot \vec{V}\right]\nabla\mu + \nabla\mu \times \left[\nabla \times \vec{V}\right] - \nabla \times \left[\nabla \times (\mu\vec{V})\right]\right\} \tag{D.3}$$

Vorticity Transport Equation

$\nabla \times$(Momentum)

4) Convective Terms

modifying the convective terms of the momentum equations:

$$(\rho \vec{V} \cdot \nabla)\vec{V} = \frac{1}{2}\rho\,\nabla(\vec{V} \cdot \vec{V}) - \rho\vec{V} \times (\nabla \times \vec{V}) \tag{D.4}$$

taking the curl of the convective terms to form the left hand side of the vorticity transport equation (LHS):

$$\text{LHS} = \nabla \times \left[\frac{1}{2} \rho \, \nabla(\vec{V} \cdot \vec{V}) \right] - \nabla \times \left[\rho \vec{V} \times (\nabla \times \vec{V}) \right] \tag{D.5}$$

expanding each term and using the definition of vorticity (equations D.1) and the continuity equation (equation D.2):

$$\begin{aligned} \nabla \times \left[\rho \, \nabla(\vec{V} \cdot \vec{V}) \right] &= \nabla\rho \times \nabla(\vec{V} \cdot \vec{V}) + \rho \left[\nabla \times \nabla(\vec{V} \cdot \vec{V}) \right] \\ &= \nabla\rho \times \nabla(\vec{V} \cdot \vec{V}) + 0 \end{aligned} \tag{D.6}$$

$$\begin{aligned} -\nabla \times \left[\rho \vec{V} \times \vec{\Omega} \right] &= -(\vec{\Omega} \cdot \nabla) \rho \vec{V} + \vec{\Omega} \left[\nabla \cdot (\rho \vec{V}) \right] + (\rho \vec{V} \cdot \nabla) \vec{\Omega} - \rho \vec{V} \left[\nabla \cdot \vec{\Omega} \right] \\ &= -(\vec{\Omega} \cdot \nabla) \rho \vec{V} + \vec{\Omega}[0] + (\rho \vec{V} \cdot \nabla) \vec{\Omega} - \rho \vec{V}[0] \end{aligned} \tag{D.7}$$

replacing equations (D.6,D.7) back into equation (D.5):

$$\text{LHS} = \frac{1}{2} \nabla\rho \times \nabla(\vec{V} \cdot \vec{V}) - (\vec{\Omega} \cdot \nabla) \rho \vec{V} + (\rho \vec{V} \cdot \nabla) \vec{\Omega} \tag{D.8}$$

5) Viscous Terms

take the viscous terms of the momentum equations (VTERM):

$$\begin{aligned} \text{VTERM} \equiv \nabla \left[\frac{4}{3} \mu (\nabla \cdot \vec{V}) + \vec{V} \cdot \nabla\mu \right] - \vec{V} \left[\nabla^2 \mu \right] - \left[\nabla \cdot \vec{V} \right] \nabla\mu \\ + \nabla\mu \times \left[\nabla \times \vec{V} \right] - \nabla \times \left[\nabla \times (\mu \vec{V}) \right] \end{aligned} \tag{D.9}$$

expanding the last term:

$$-\nabla \times \left[\nabla \times (\mu \vec{V}) \right] = -\nabla \times \left[\nabla\mu \times \vec{V} + \mu (\nabla \times \vec{V}) \right] \tag{D.10}$$

replacing equation (D.10) back into equation (D.9) using the definition of vorticity (equation D.1a):

$$\begin{aligned} \text{VTERM} = \nabla \left[\frac{4}{3} \mu (\nabla \cdot \vec{V}) + \vec{V} \cdot \nabla\mu \right] - \vec{V} \left[\nabla^2 \mu \right] - \left[\nabla \cdot \vec{V} \right] \nabla\mu \\ + \nabla\mu \times \left[\nabla \times \vec{V} \right] - \nabla \times \left[\nabla\mu \times \vec{V} \right] - \nabla \times \left[\mu \vec{\Omega} \right] \end{aligned} \tag{D.11}$$

combining terms and modifying:

$$\nabla\mu\times\left[\nabla\times\vec{V}\right] - \nabla\times\left[\nabla\mu\times\vec{V}\right] = \nabla\left[\nabla\mu\bullet\vec{V}\right] - 2\left[\vec{V}\bullet\nabla\right]\nabla\mu + \vec{V}\left[\nabla^2\mu\right] - \nabla\mu\left[\nabla\bullet\vec{V}\right] - \vec{V}\times\left[\nabla\times\nabla\mu\right] \quad (D.12)$$

replacing equation (D.12) back into equation (D.11):

$$VTERM = \nabla\left[\frac{4}{3}\mu\left(\nabla\bullet\vec{V}\right) + 2\vec{V}\bullet\nabla\mu\right] - 2\left[\nabla\bullet\vec{V}\right]\nabla\mu - 2\left[\vec{V}\bullet\nabla\right]\nabla\mu - \nabla\times\left[\mu\vec{\Omega}\right] \quad (D.13)$$

taking the curl of the viscous terms (equation D.13) to form the right hand side of the vorticity transport equation (RHS):

$$RHS = 0 - 2\nabla\times\left\{\left[\nabla\bullet\vec{V}\right]\nabla\mu + \left[\vec{V}\bullet\nabla\right]\nabla\mu\right\} - \nabla\times\left\{\nabla\times\left[\mu\vec{\Omega}\right]\right\} \quad (D.14)$$

expanding the last term:

$$\begin{aligned} -\nabla\times\left[\nabla\times\left(\mu\vec{\Omega}\right)\right] &= -\nabla\left[\nabla\bullet\left(\mu\vec{\Omega}\right)\right] + \nabla^2\left[\mu\vec{\Omega}\right] \\ &= -\nabla\left[\nabla\mu\bullet\vec{\Omega} + \mu\left(\nabla\bullet\vec{\Omega}\right)\right] + \nabla^2\left[\mu\vec{\Omega}\right] \\ &= -\nabla\left[\nabla\mu\bullet\vec{\Omega}\right] + \nabla^2\left[\mu\vec{\Omega}\right] \end{aligned} \quad (D.15)$$

replacing equation (D.15) back into equation (D.14):

$$RHS = -2\nabla\times\left[\left(\nabla\bullet\vec{V}\right)\nabla\mu + \left(\vec{V}\bullet\nabla\right)\nabla\mu\right] - \nabla\left[\nabla\mu\bullet\vec{\Omega}\right] + \nabla^2\left[\mu\vec{\Omega}\right] \quad (D.16)$$

6) Vorticity Transport Equation

equating the right and left hand sides (equations D.8 and D.16):

$$Re\left\{\left(\rho\vec{V}\bullet\nabla\right)\vec{\Omega} - \left(\vec{\Omega}\bullet\nabla\right)\rho\vec{V} + \frac{1}{2}\nabla\rho\times\nabla\left(\vec{V}\bullet\vec{V}\right)\right\} = \nabla^2\left[\mu\vec{\Omega}\right] - 2\nabla\times\left[\left(\nabla\bullet\vec{V}\right)\nabla\mu + \left(\vec{V}\bullet\nabla\right)\nabla\mu\right] - \nabla\left[\nabla\mu\bullet\vec{\Omega}\right] \quad (D.17)$$

7) Viscosity Source Term in Cartesian Coordinates

viscosity source term in vector form:

$$\vec{S}^{\mu} = -2\nabla\times\left[\left(\nabla\bullet\vec{V}\right)\nabla\mu + \left(\vec{V}\bullet\nabla\right)\nabla\mu\right] - \nabla\left[\nabla\mu\bullet\vec{\Omega}\right] \tag{D.18}$$

expressing the terms inside the curl in Cartesian coordinates:

$$\begin{aligned}\left(\nabla\bullet\vec{V}\right)\nabla\mu + \left(\vec{V}\bullet\nabla\right)\nabla\mu &= \left(u_x + v_y + w_z\right)\nabla\mu \\ &\quad + u\left(\nabla\mu\right)_x + v\left(\nabla\mu\right)_y + w\left(\nabla\mu\right)_z \\ &= \left(u\,\nabla\mu\right)_x + \left(v\,\nabla\mu\right)_y + \left(w\,\nabla\mu\right)_z\end{aligned} \tag{D.19}$$

expanding the curl term:

$$\begin{aligned}&-2\nabla\times\left[\left(\nabla\bullet\vec{V}\right)\nabla\mu + \left(\vec{V}\bullet\nabla\right)\nabla\mu\right] \\ &= -2\left\{\left(u\,\mu_z\right)_{xy} + \left(v\,\mu_z\right)_{yy} + \left(w\,\mu_z\right)_{zy} - \left(u\,\mu_y\right)_{xz} - \left(v\,\mu_y\right)_{yz} - \left(w\,\mu_y\right)_{zz}\right\}\hat{i} \\ &\quad - 2\left\{\left(u\,\mu_x\right)_{xz} + \left(v\,\mu_x\right)_{yz} + \left(w\,\mu_x\right)_{zz} - \left(u\,\mu_z\right)_{xx} - \left(v\,\mu_z\right)_{yx} - \left(w\,\mu_z\right)_{zx}\right\}\hat{j} \\ &\quad - 2\left\{\left(u\,\mu_y\right)_{xx} + \left(v\,\mu_y\right)_{yx} + \left(w\,\mu_y\right)_{zx} - \left(u\,\mu_x\right)_{xy} - \left(v\,\mu_x\right)_{yy} - \left(w\,\mu_x\right)_{zy}\right\}\hat{k} \\ &= -2\left\{\left[\left(u\,\mu_z\right)_y - \left(u\,\mu_y\right)_z\right]_x + \left[\left(v\,\mu_z\right)_y - \left(v\,\mu_y\right)_z\right]_y + \left[\left(w\,\mu_z\right)_y - \left(w\,\mu_y\right)_z\right]_z\right\}\hat{i} \\ &\quad - 2\left\{\left[\left(u\,\mu_x\right)_z - \left(u\,\mu_z\right)_x\right]_x + \left[\left(v\,\mu_x\right)_z - \left(v\,\mu_z\right)_x\right]_y + \left[\left(w\,\mu_x\right)_z - \left(w\,\mu_z\right)_x\right]_z\right\}\hat{j} \\ &\quad - 2\left\{\left[\left(u\,\mu_y\right)_x - \left(u\,\mu_x\right)_y\right]_x + \left[\left(v\,\mu_y\right)_x - \left(v\,\mu_x\right)_y\right]_y + \left[\left(w\,\mu_y\right)_x - \left(w\,\mu_x\right)_y\right]_z\right\}\hat{k} \\ &= -2\left\{\left[u_y\mu_z - u_z\mu_y\right]_x + \left[v_y\mu_z - v_z\mu_y\right]_y + \left[w_y\mu_z - w_z\mu_y\right]_z\right\}\hat{i} \\ &\quad - 2\left\{\left[u_z\mu_x - u_x\mu_z\right]_x + \left[v_z\mu_x - v_x\mu_z\right]_y + \left[w_z\mu_x - w_x\mu_z\right]_z\right\}\hat{j} \\ &\quad - 2\left\{\left[u_x\mu_y - u_y\mu_x\right]_x + \left[v_x\mu_y - v_y\mu_x\right]_y + \left[w_x\mu_y - w_y\mu_x\right]_z\right\}\hat{k}\end{aligned} \tag{D.20}$$

expressing the gradient term in Cartesian coordinates:

$$\begin{aligned}&-\nabla\left[\nabla\mu\bullet\vec{\Omega}\right] \\ &= -\left\{\left[\mu_x\Omega_1 + \mu_y\Omega_2 + \mu_z\Omega_3\right]_x\right\}\hat{i} - \left\{\left[\mu_x\Omega_1 + \mu_y\Omega_2 + \mu_z\Omega_3\right]_y\right\}\hat{j} \\ &\quad - \left\{\left[\mu_x\Omega_1 + \mu_y\Omega_2 + \mu_z\Omega_3\right]_z\right\}\hat{k}\end{aligned} \tag{D.21}$$

adding the curl and gradient terms (equations D.20 and D.21) to obtain the viscosity source term in Cartesian coordinates:

$$\begin{aligned}\vec{S}^{\mu} = &-\Big\{\big[2(u_y\mu_z - u_z\mu_y) + \Omega_1\mu_x + \Omega_2\mu_y + \Omega_3\mu_z\big]_x \\ &\quad + 2\big[v_y\mu_z - v_z\mu_y\big]_y + 2\big[w_y\mu_z - w_z\mu_y\big]_z\Big\}\hat{i} \\ &-\Big\{\big[2(v_z\mu_x - v_x\mu_z) + \Omega_1\mu_x + \Omega_2\mu_y + \Omega_3\mu_z\big]_y \\ &\quad + 2\big[u_z\mu_x - u_x\mu_z\big]_x + 2\big[w_z\mu_x - w_x\mu_z\big]_z\Big\}\hat{j} \\ &-\Big\{\big[2(w_x\mu_y - w_y\mu_x) + \Omega_1\mu_x + \Omega_2\mu_y + \Omega_3\mu_z\big]_z \\ &\quad + 2\big[u_x\mu_y - u_y\mu_x\big]_x + 2\big[v_x\mu_y - v_y\mu_x\big]_y\Big\}\hat{k}\end{aligned} \tag{D.22}$$

or

$$\vec{S}^{\mu} = \frac{\partial\vec{S}^{\mu 1}}{\partial x} + \frac{\partial\vec{S}^{\mu 2}}{\partial y} + \frac{\partial\vec{S}^{\mu 3}}{\partial z} \tag{D.23}$$

where

$$\begin{aligned}\vec{S}^{\mu 1} = &-\Big\{2(u_y\mu_z - u_z\mu_y) + \Omega_1\mu_x + \Omega_2\mu_y + \Omega_3\mu_z\Big\}\hat{i} \\ &-\Big\{2(u_z\mu_x - u_x\mu_z)\Big\}\hat{j} - \Big\{2(u_x\mu_y - u_y\mu_x)\Big\}\hat{k}\end{aligned} \tag{D.24a}$$

$$\begin{aligned}\vec{S}^{\mu 2} = &-\Big\{2(v_z\mu_x - v_x\mu_z) + \Omega_1\mu_x + \Omega_2\mu_y + \Omega_3\mu_z\Big\}\hat{j} \\ &-\Big\{2(v_y\mu_z - v_z\mu_y)\Big\}\hat{i} - \Big\{2(v_x\mu_y - v_y\mu_x)\Big\}\hat{k}\end{aligned} \tag{D.24b}$$

$$\begin{aligned}\vec{S}^{\mu 3} = &-\Big\{2(w_x\mu_y - w_y\mu_x) + \Omega_1\mu_x + \Omega_2\mu_y + \Omega_3\mu_z\Big\}\hat{k} \\ &-\Big\{2(w_y\mu_z - w_z\mu_y)\Big\}\hat{i} - \Big\{2(w_z\mu_x - w_x\mu_z)\Big\}\hat{j}\end{aligned} \tag{D.24c}$$

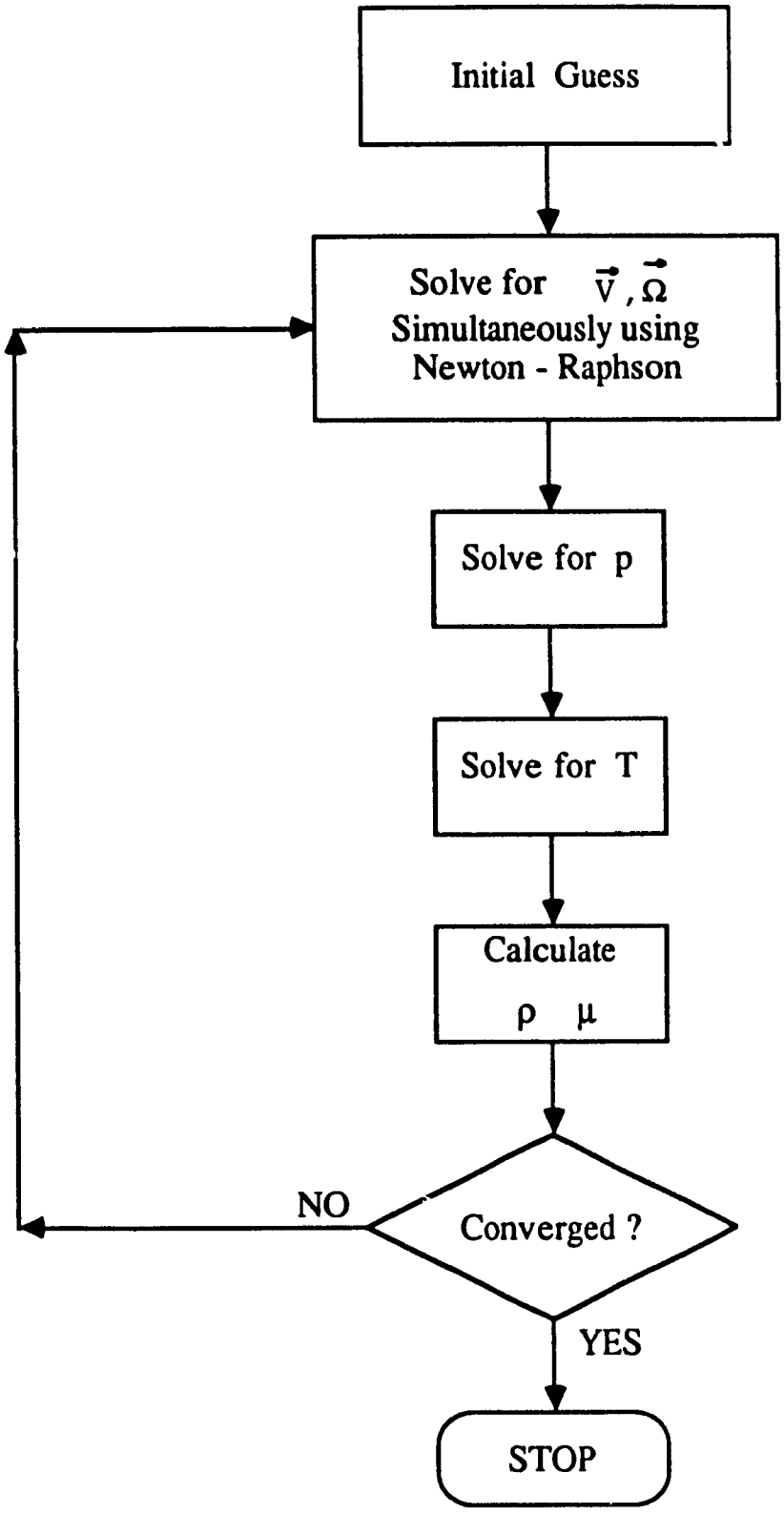

Figure 4.1 Flowchart of iterative procedure

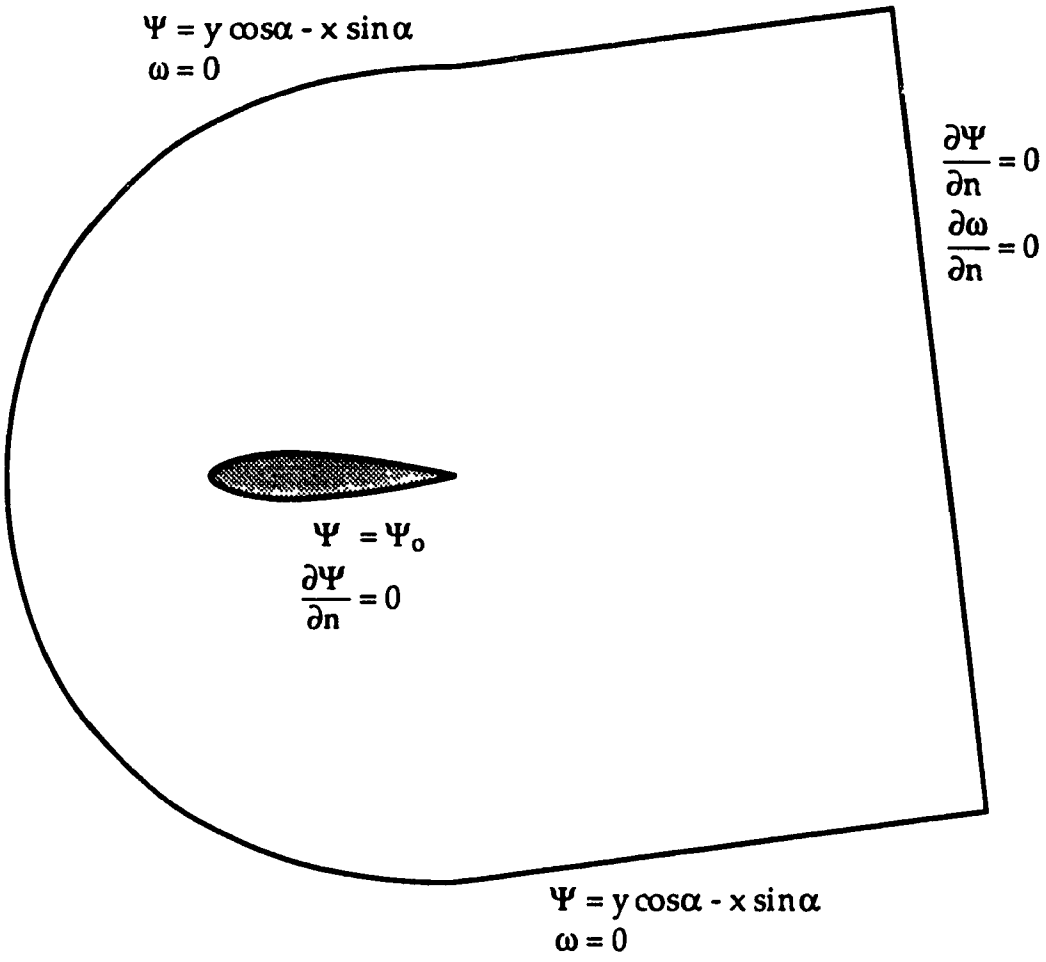

Figure 5.1 Geometry and boundary conditions for airfoil.

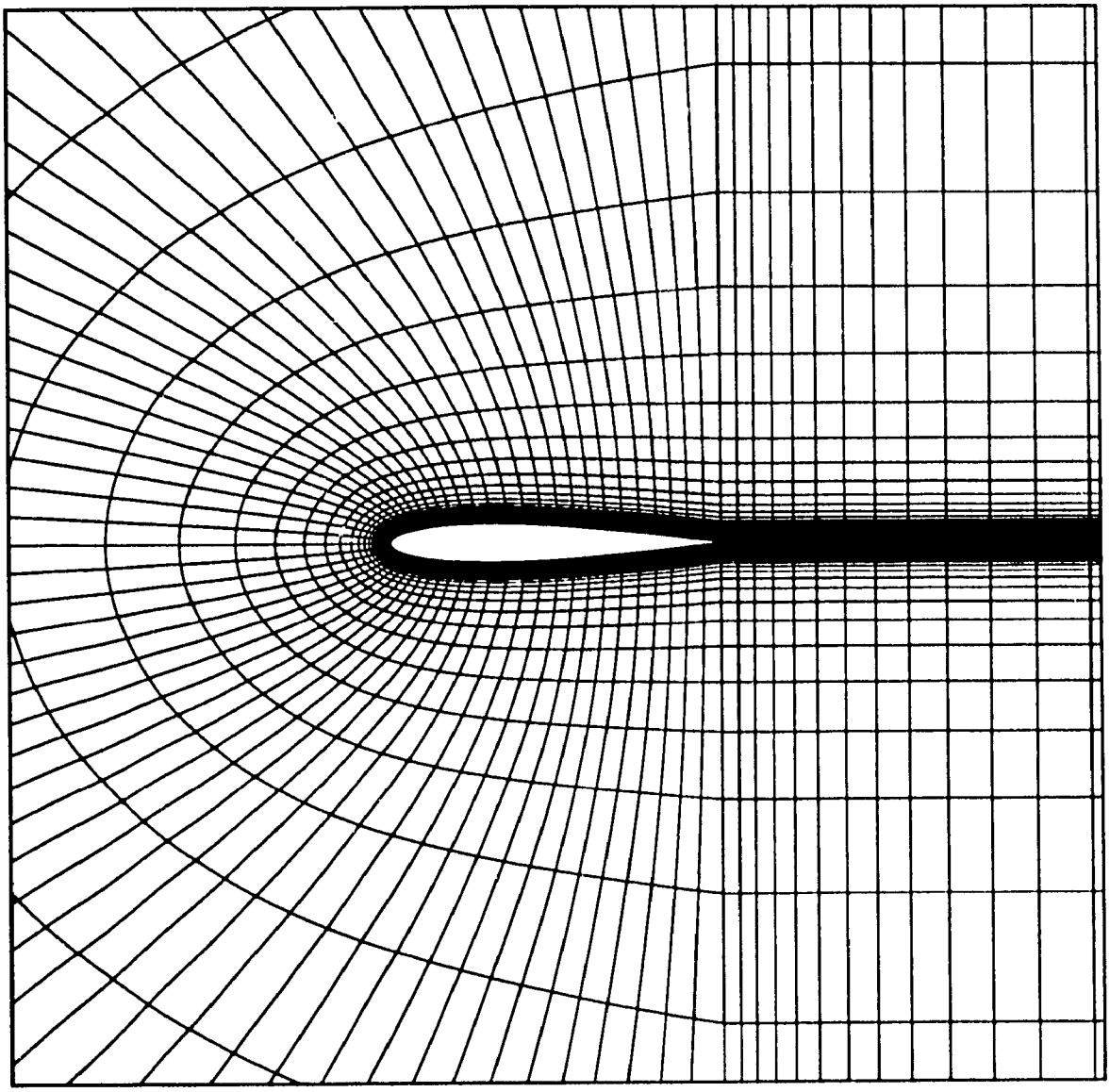

Figure 5.2 C-grid for NACA-0012 airfoil.

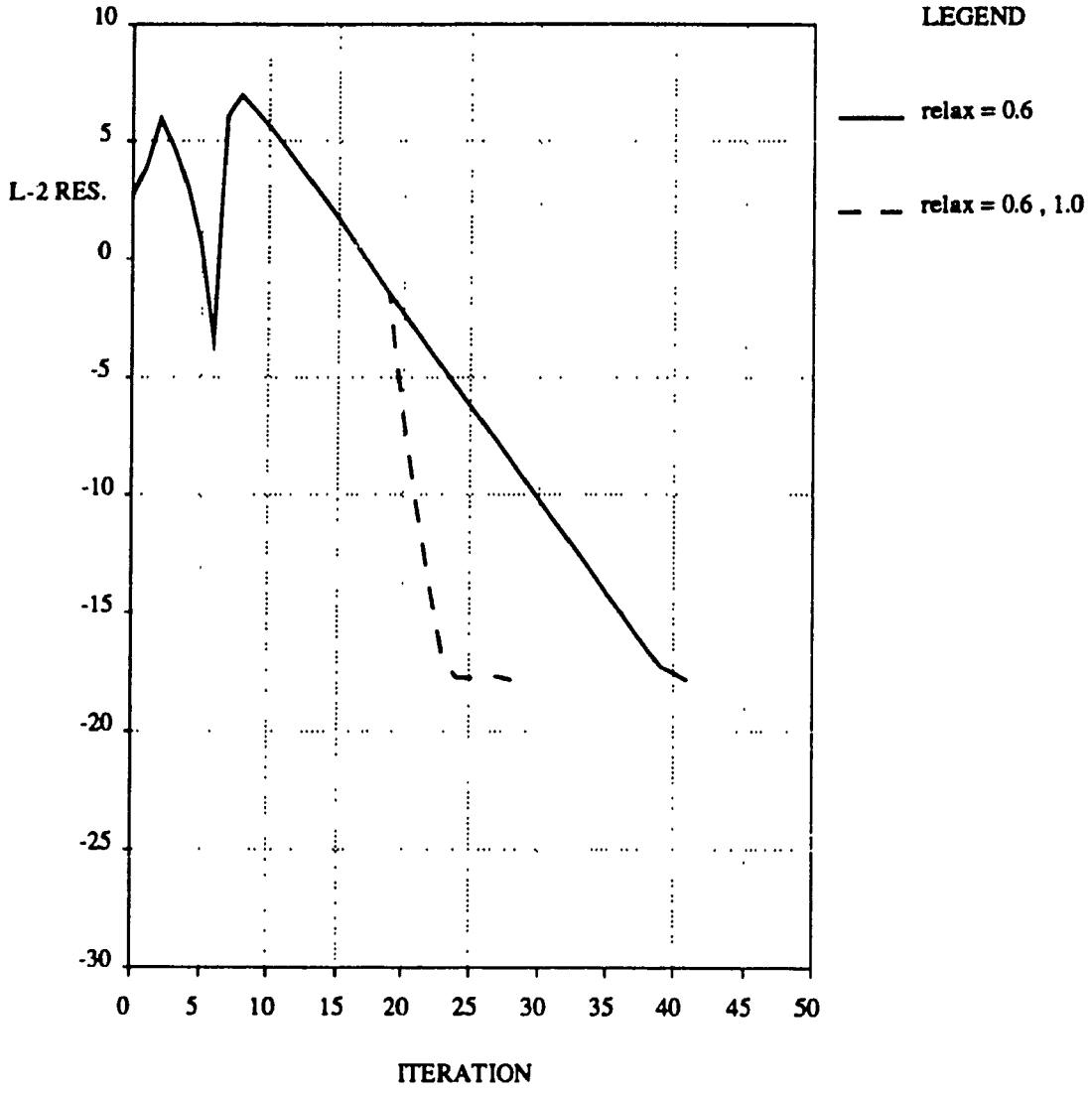

Figure 5.3 Convergence history for NACA-0012 airfoil, $Re = 10\,000$, $M = 0.2$, $\alpha = 0°$.

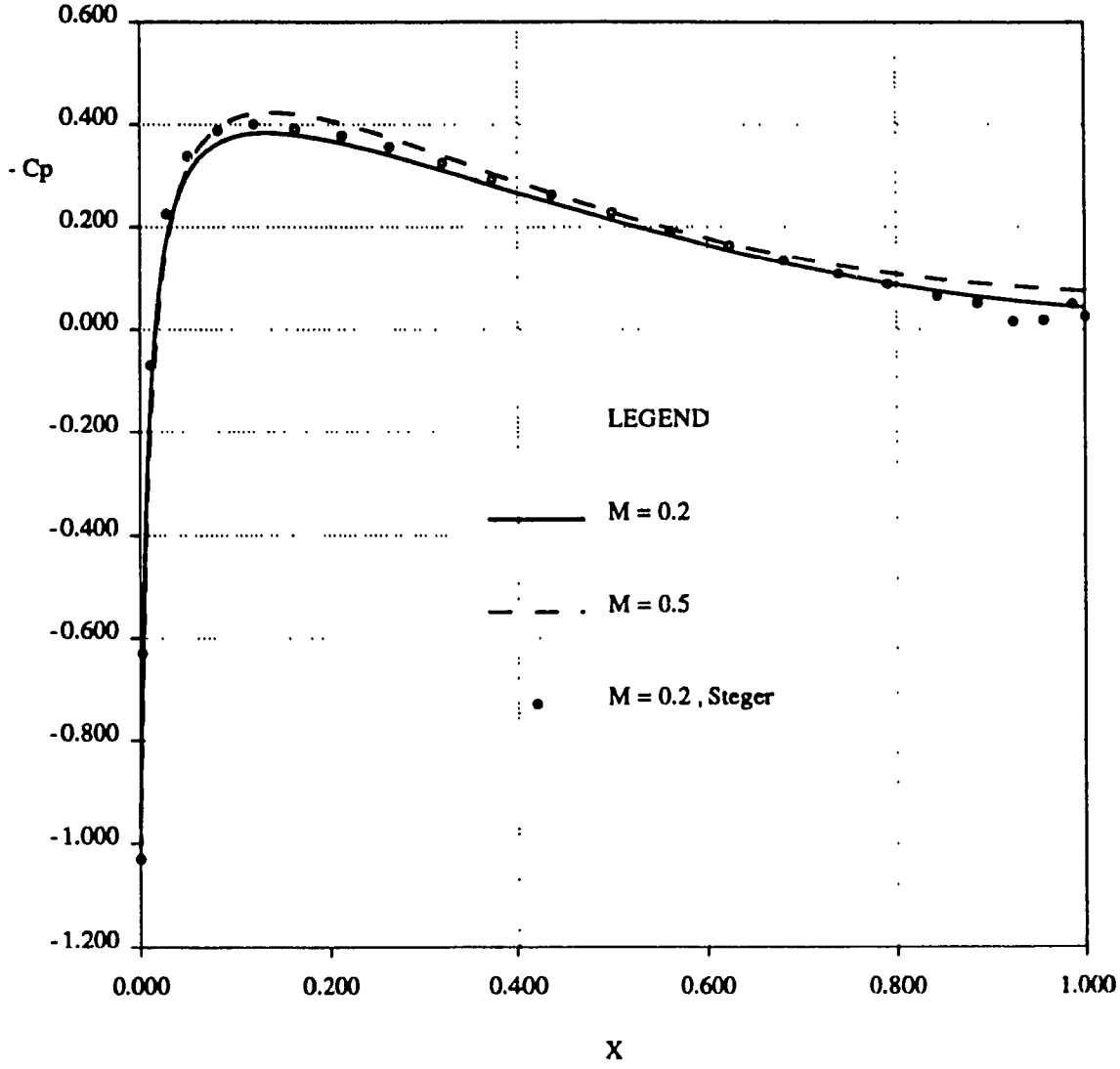

Figure 5.4 C_p distribution for NACA-0012 airfoil, Re = 10 000, $\alpha = 0°$.

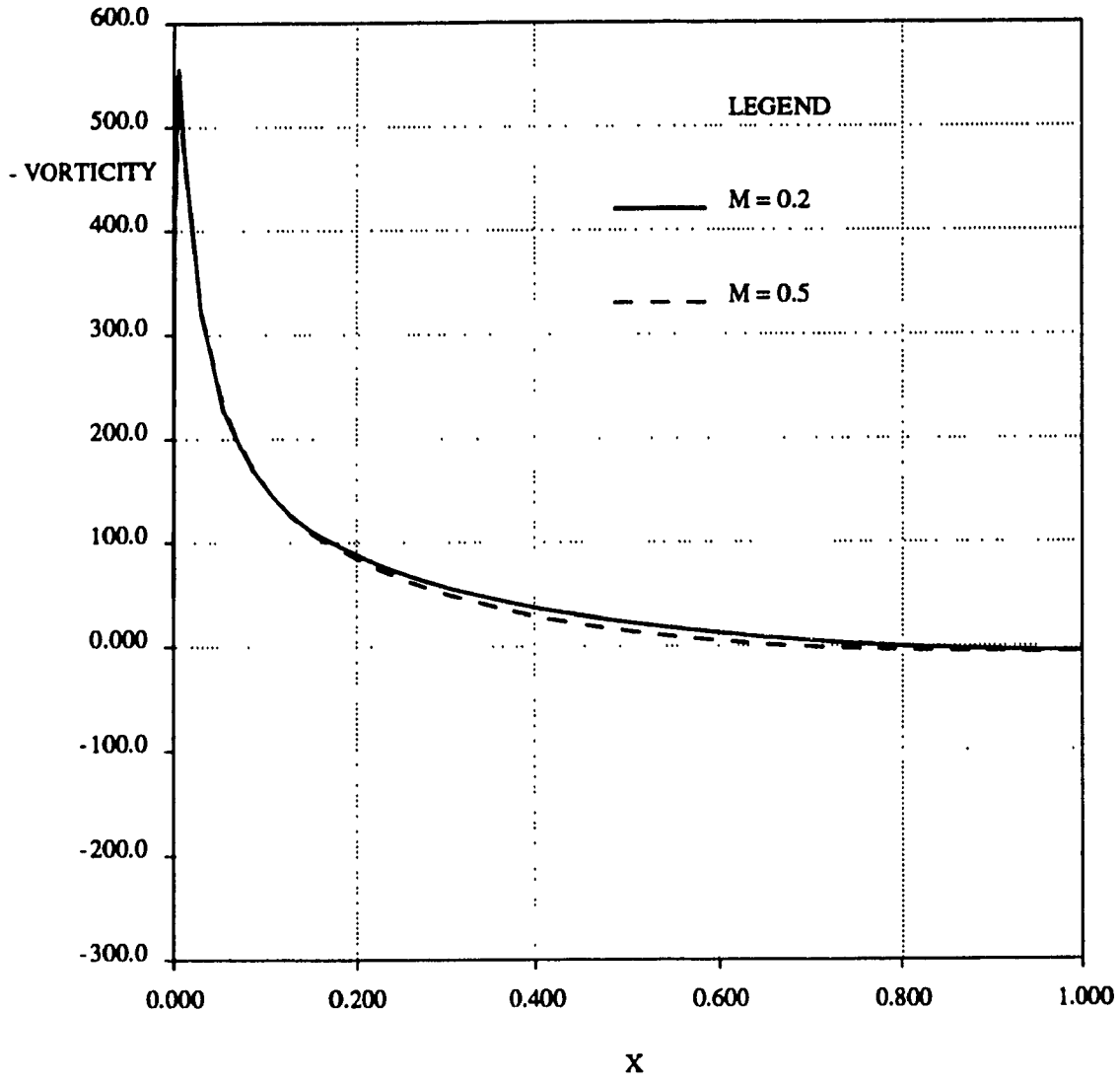

Figure 5.5 Surface Vorticity distribution for NACA-0012 airfoil, $Re = 10\,000$, $\alpha = 0°$.

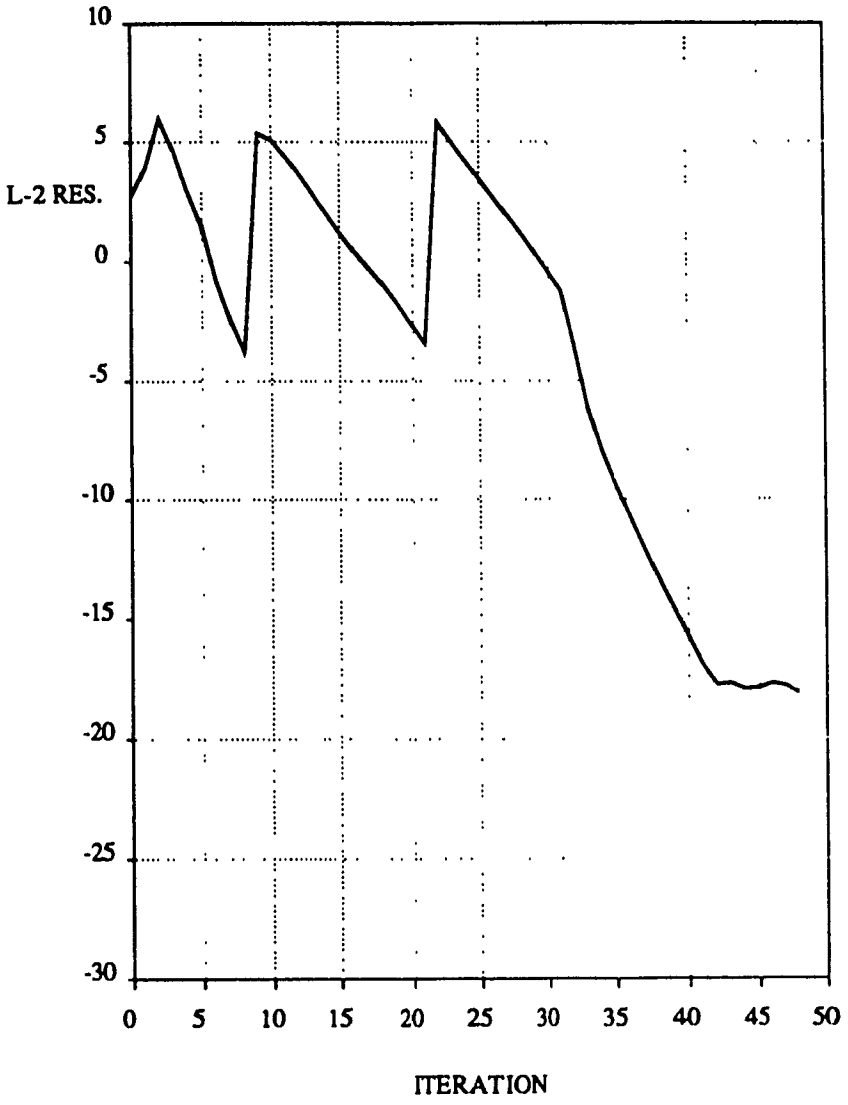

Figure 5.6 Convergence history for NACA-0012 airfoil, $Re = 10\,000$, $M = 0.5$, $\alpha = 0°$.

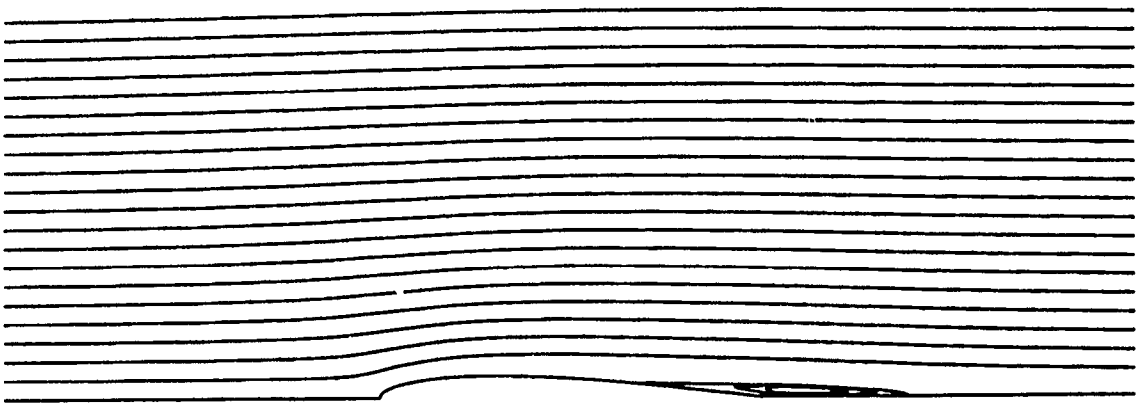

Figure 5.7 Streamline plots for NACA-0012 airfoil,
$Re = 10\,000$, $M = 0.5$, $\alpha = 0°$.

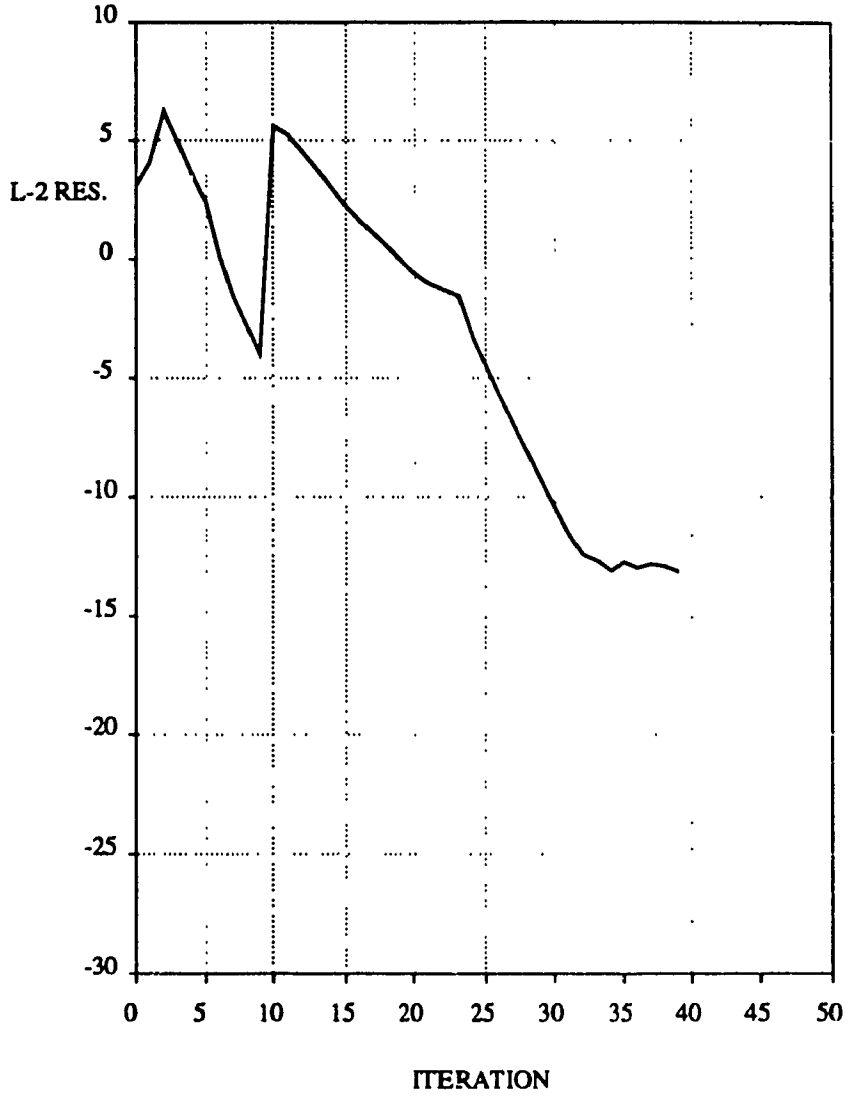

Figure 5.8 Convergence history for NACA-0012 airfoil, $Re = 5\,000$, $M = 0.5$, $\alpha = 3°$.

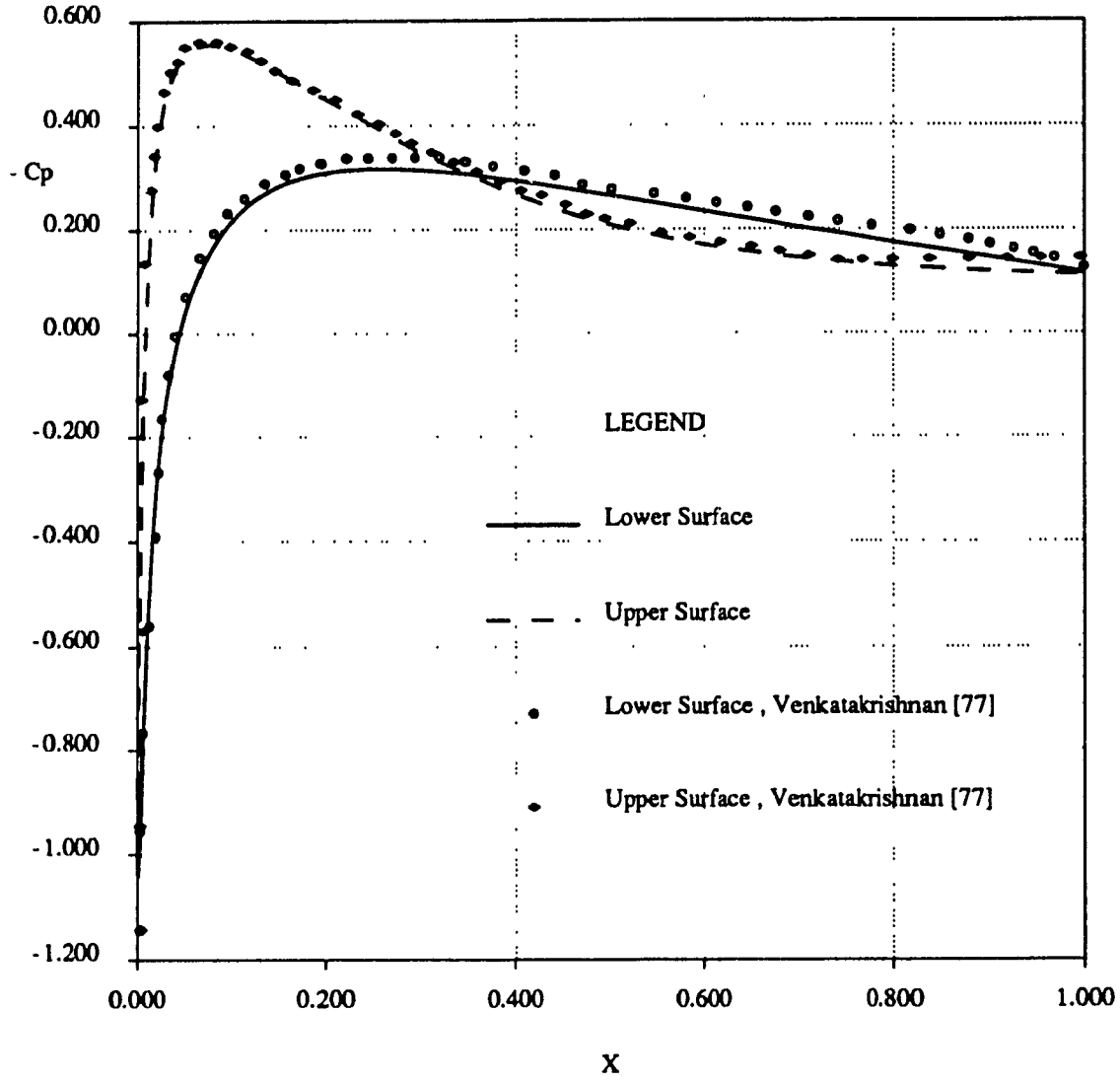

Figure 5.9 C_p distribution for NACA-0012 airfoil,

$Re = 5\,000$, $M = 0.5$, $\alpha = 3°$.

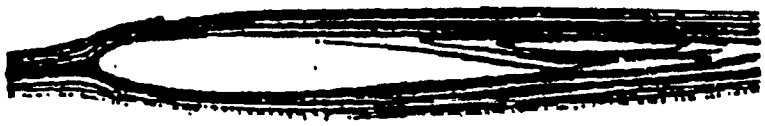

Venkatakrishnan [77]

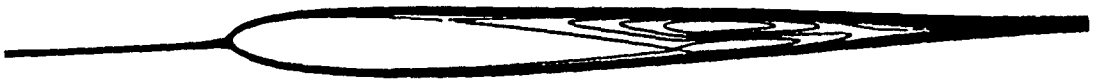

Present Method

Figure 5.10 Streamline plots for NACA-0012 airfoil, $Re = 5\,000$, $M = 0.5$, $\alpha = 3°$.

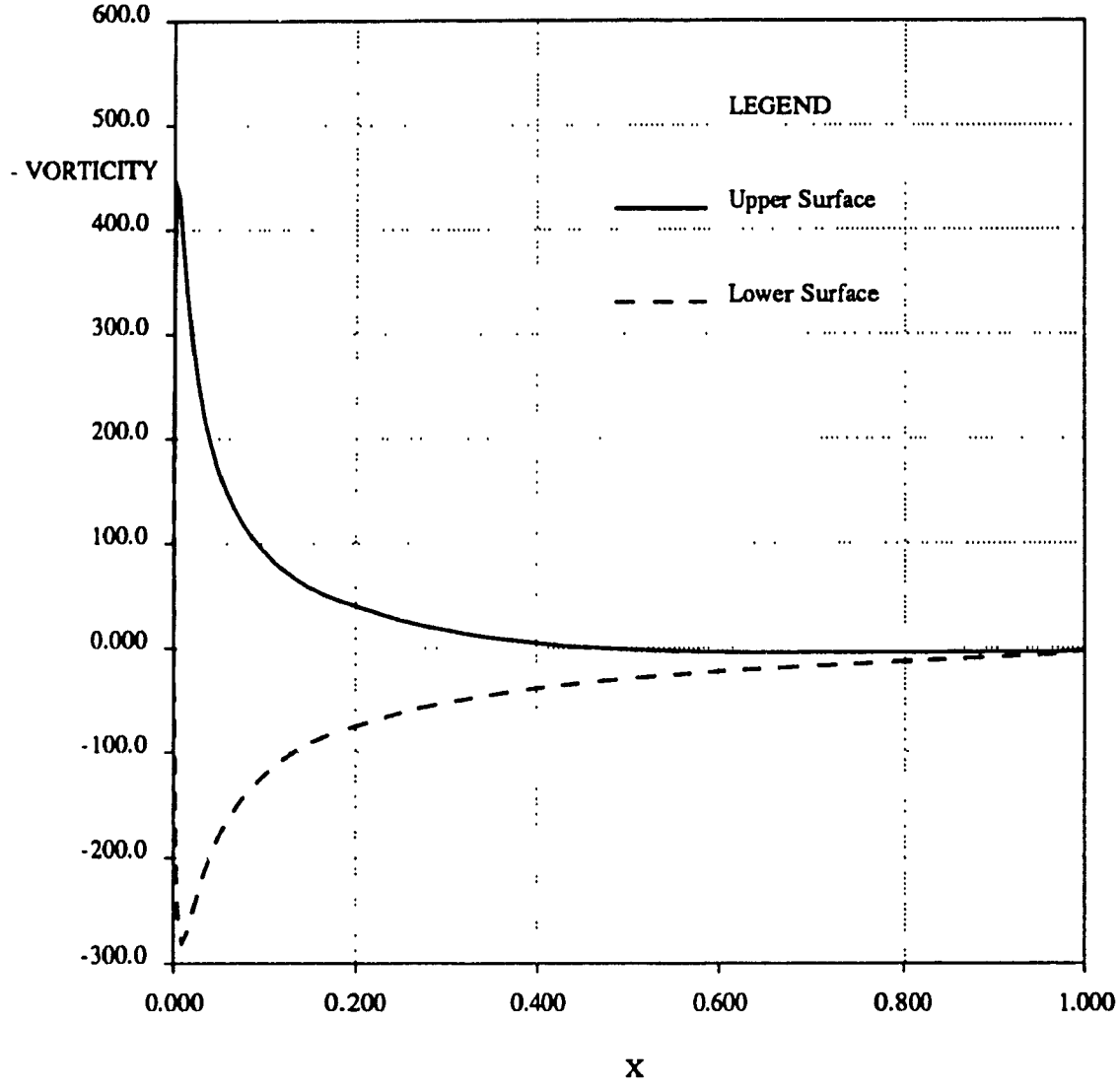

Figure 5.11 Surface vorticity distribution for NACA-0012 airfoil, $Re = 5\,000$, $M = 0.5$, $\alpha = 3°$.

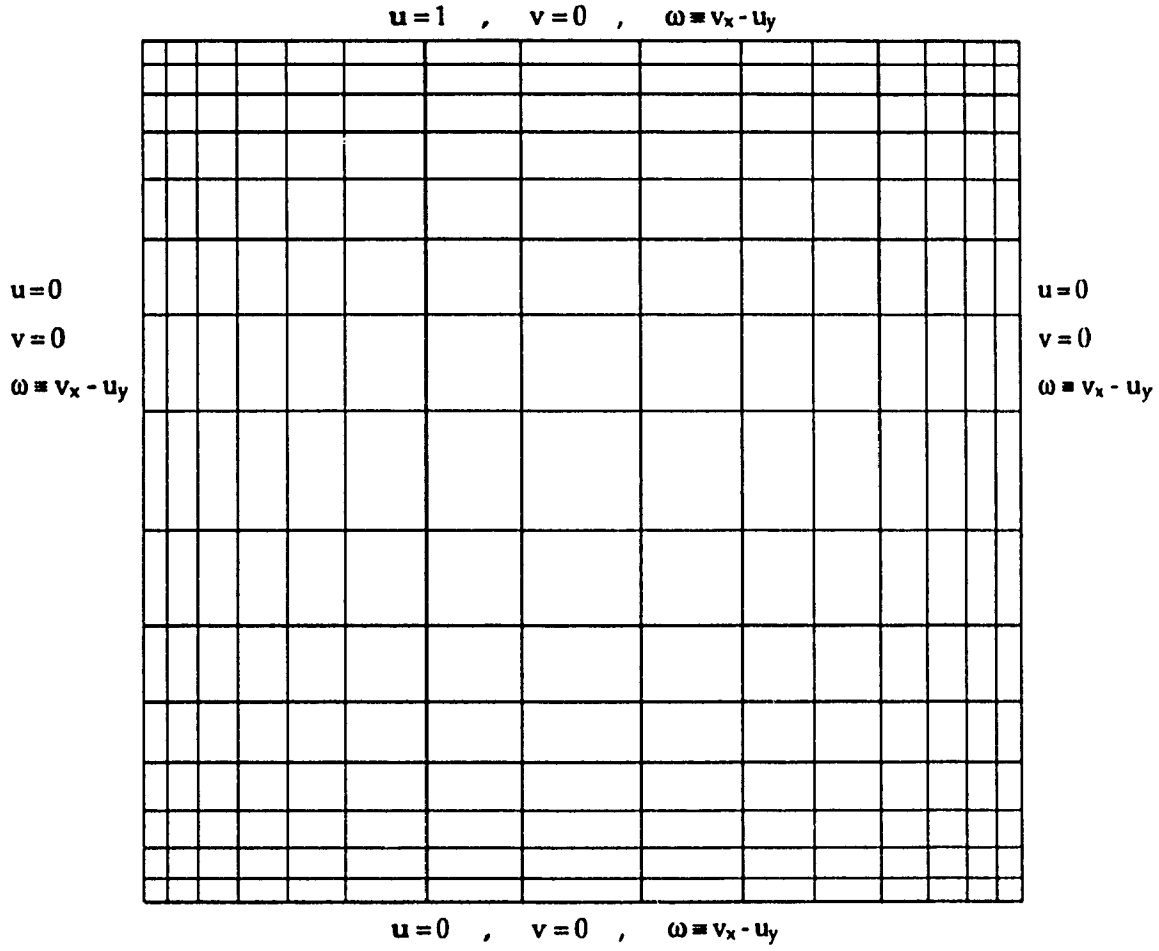

Figure 6.1 Geometry, grid and boundary conditions for the 2-D driven cavity.

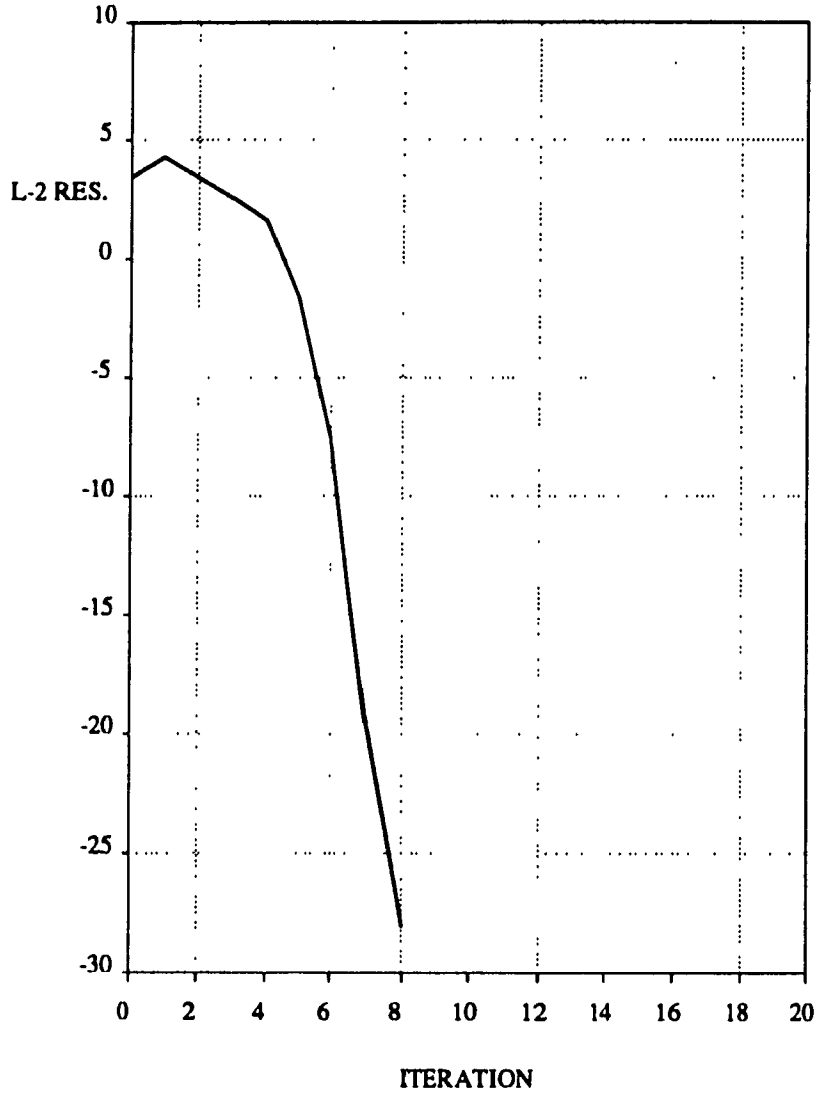

Figure 6.2 Convergence history for 2-D driven cavity, $Re = 400$.

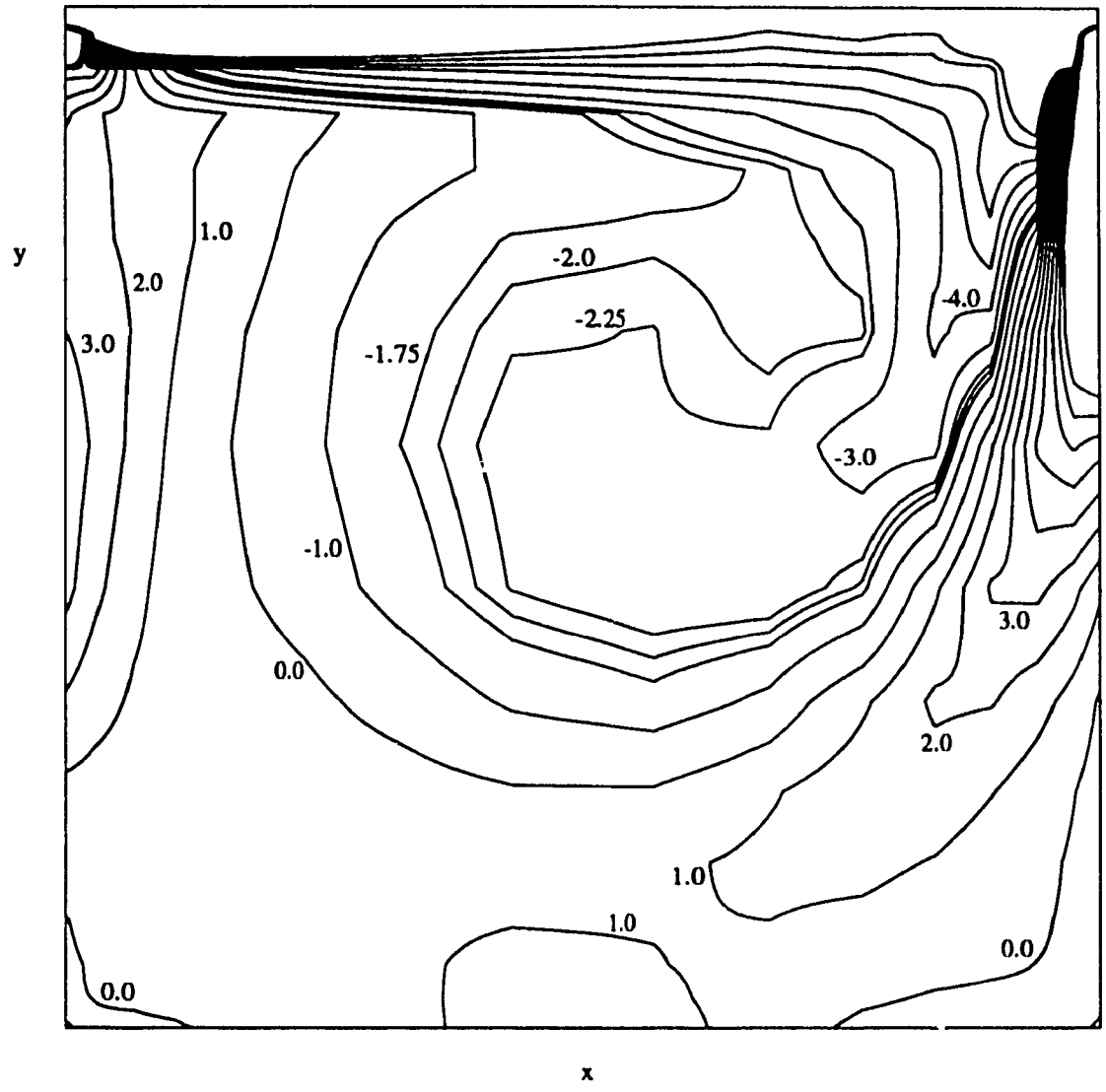

Figure 6.3a Equi-vorticity contours for 2-D driven cavity, velocity-vorticity, Re = 400.

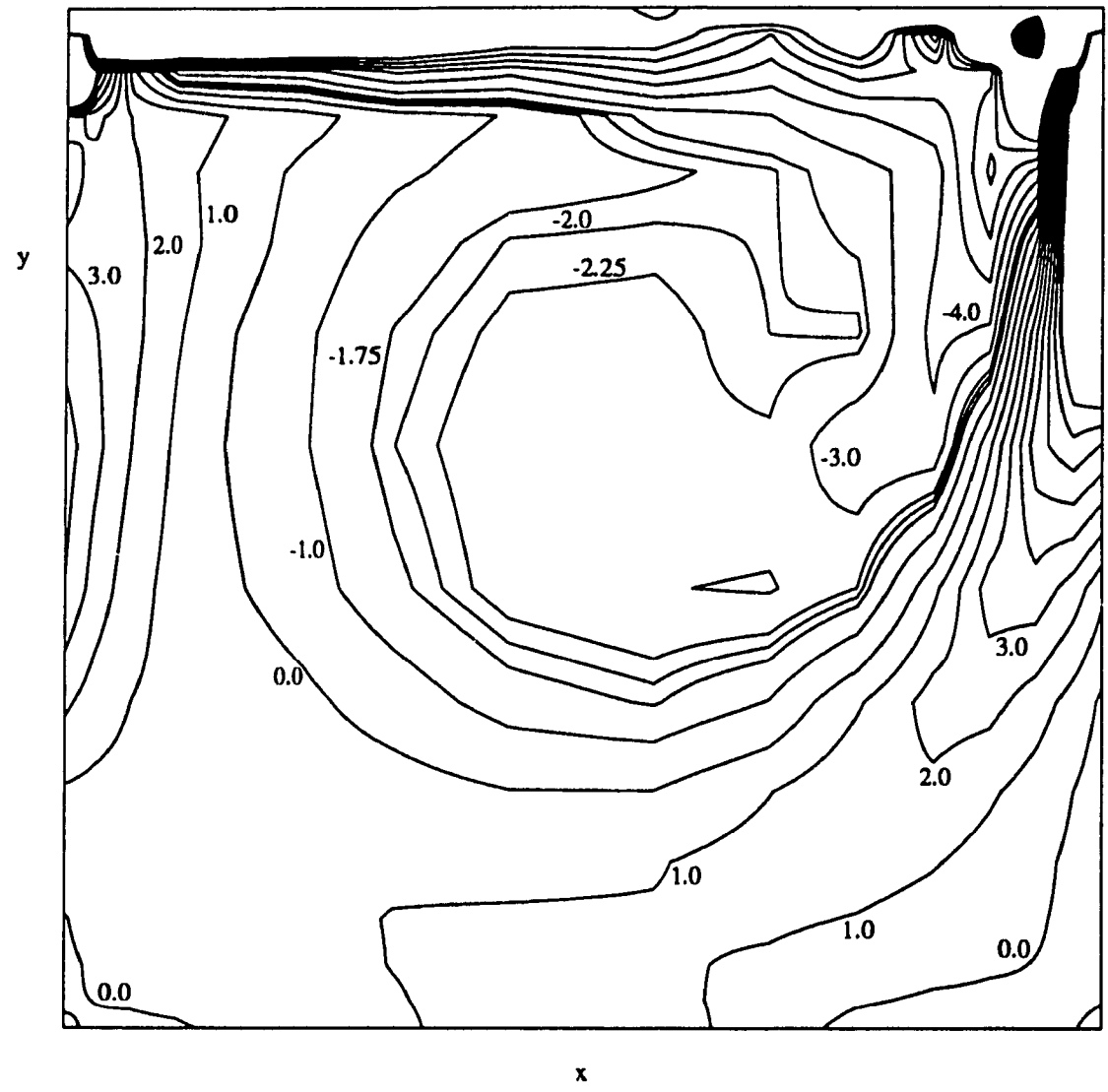

Figure 6.3b Equi-vorticity contours for 2-D driven cavity, stream function-vorticity, Re = 400.

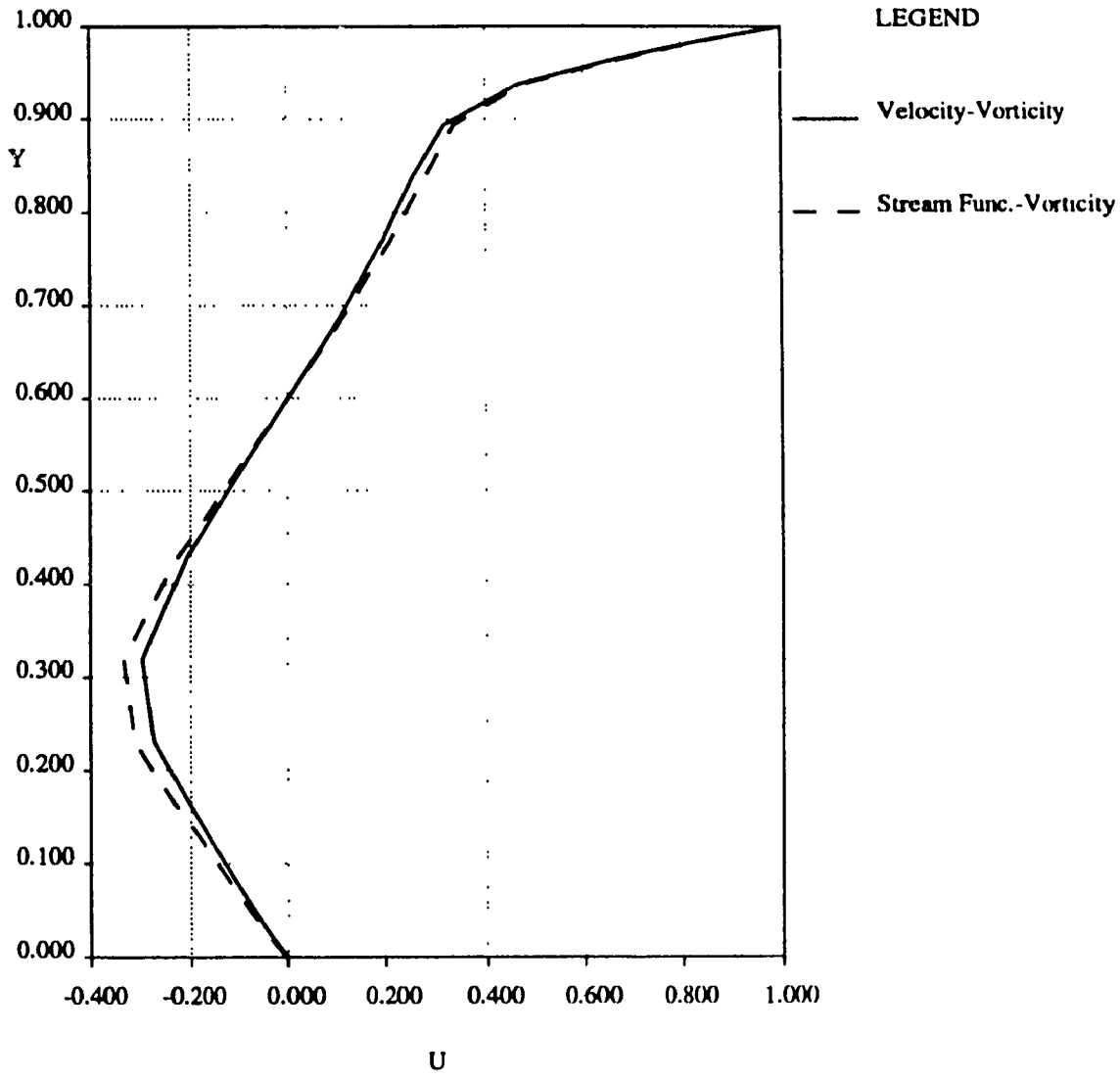

Figure 6.4 Centerline velocities for 2-D driven cavity, Re = 400.

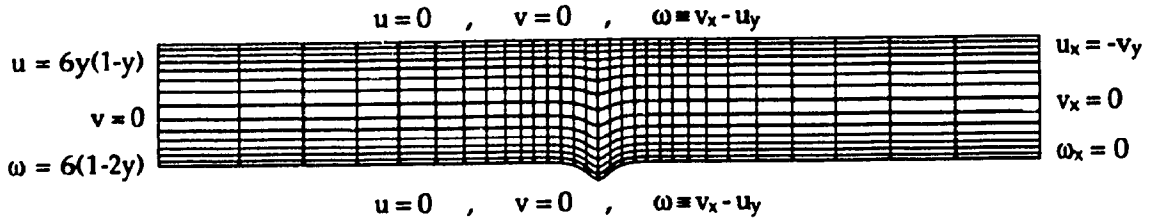

a) Geometry, grid and boundary conditions

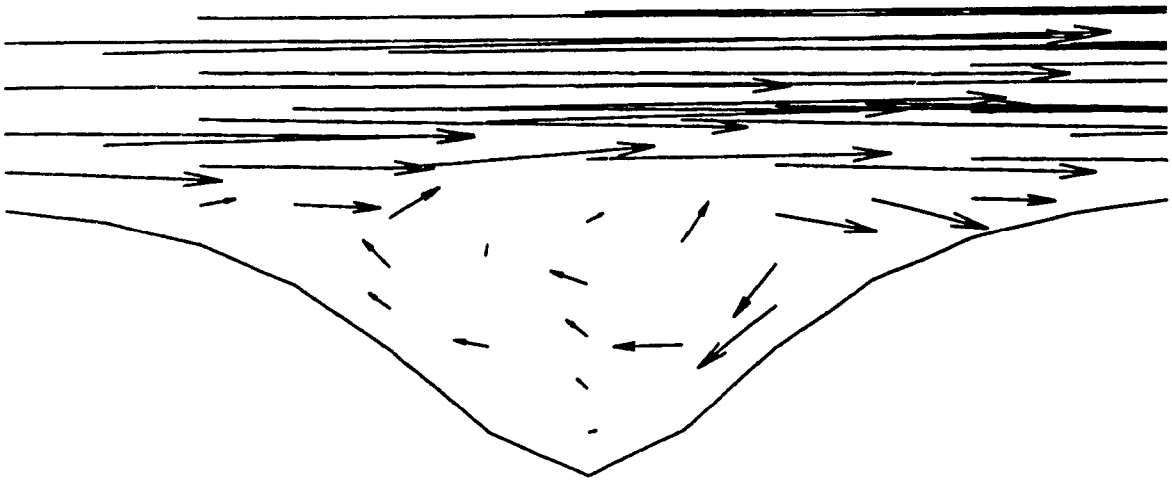

b) Velocity vectors in region of trough

Figure 6.5 2-D trough, *Re* = 10 000.

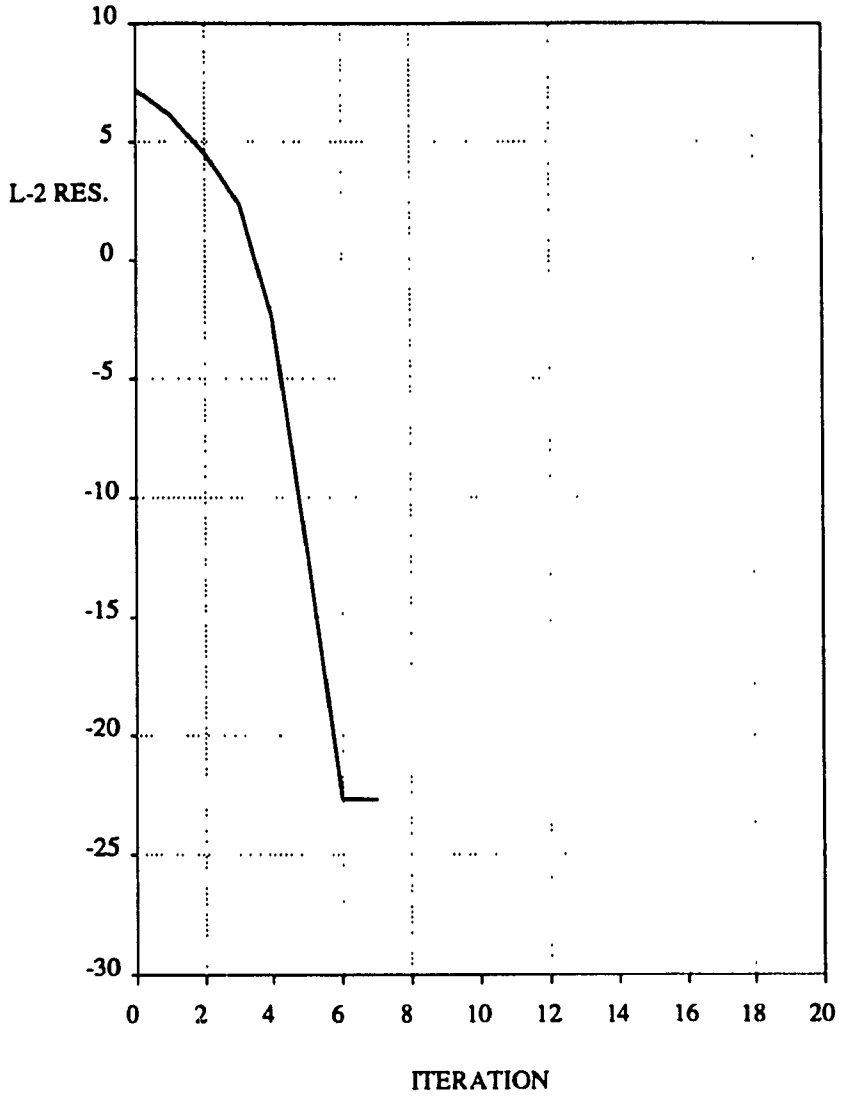

Figure 6.6 Convergence history for 2-D trough, Re = 10 000.

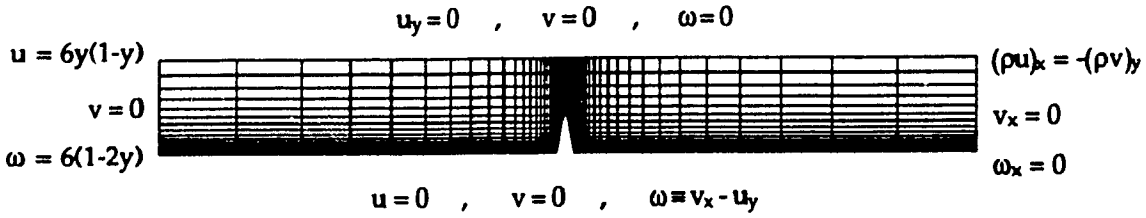

a) Geometry, grid and boundary conditions
(vertical scale magnified by a factor of 10)

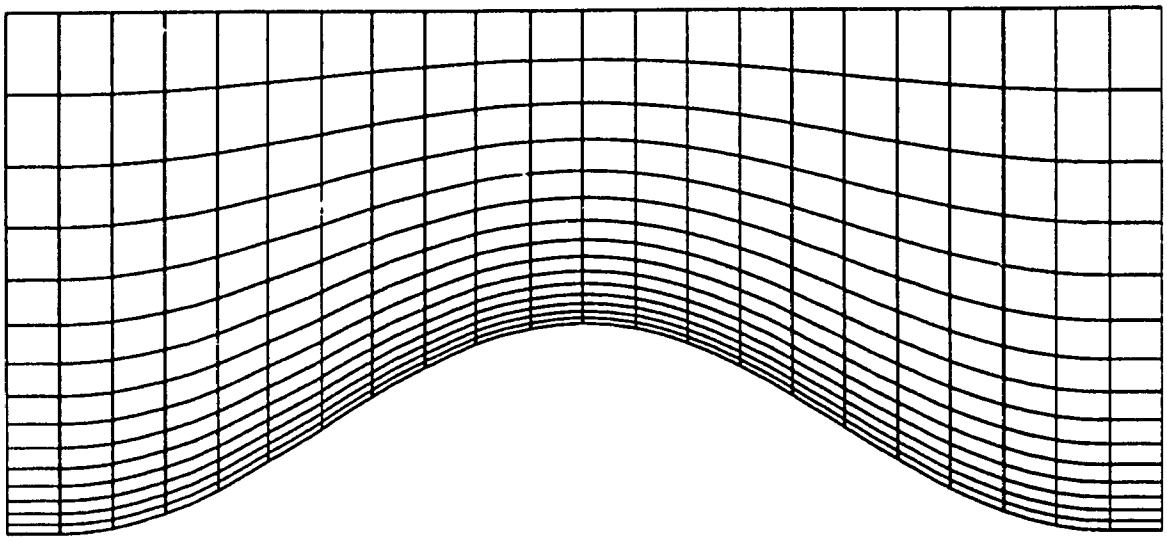

b) Geometry and grid in region of nozzle

Figure 6.7 2-D nozzle, Re = 100.

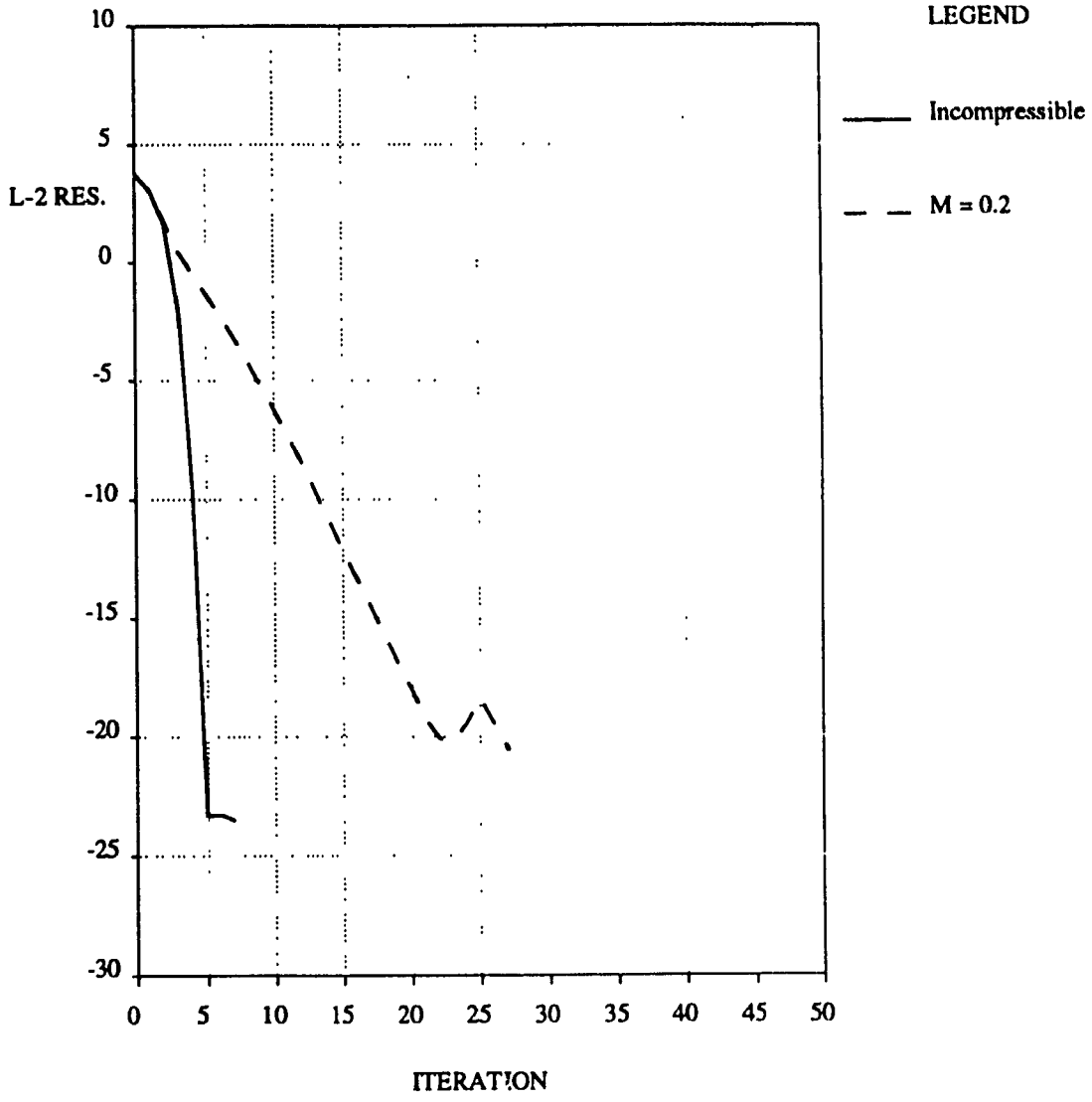

Figure 6.8 Convergence history for 2-D convergent-divergent nozzle, Re = 100.

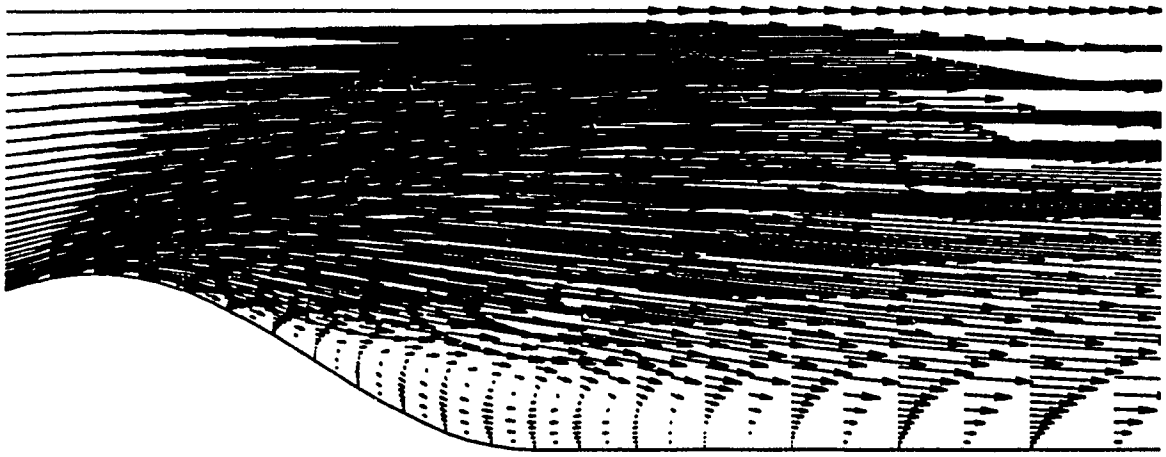

Figure 6.9 Velocity vectors for 2-D convergent-divergent nozzle, Re = 100.

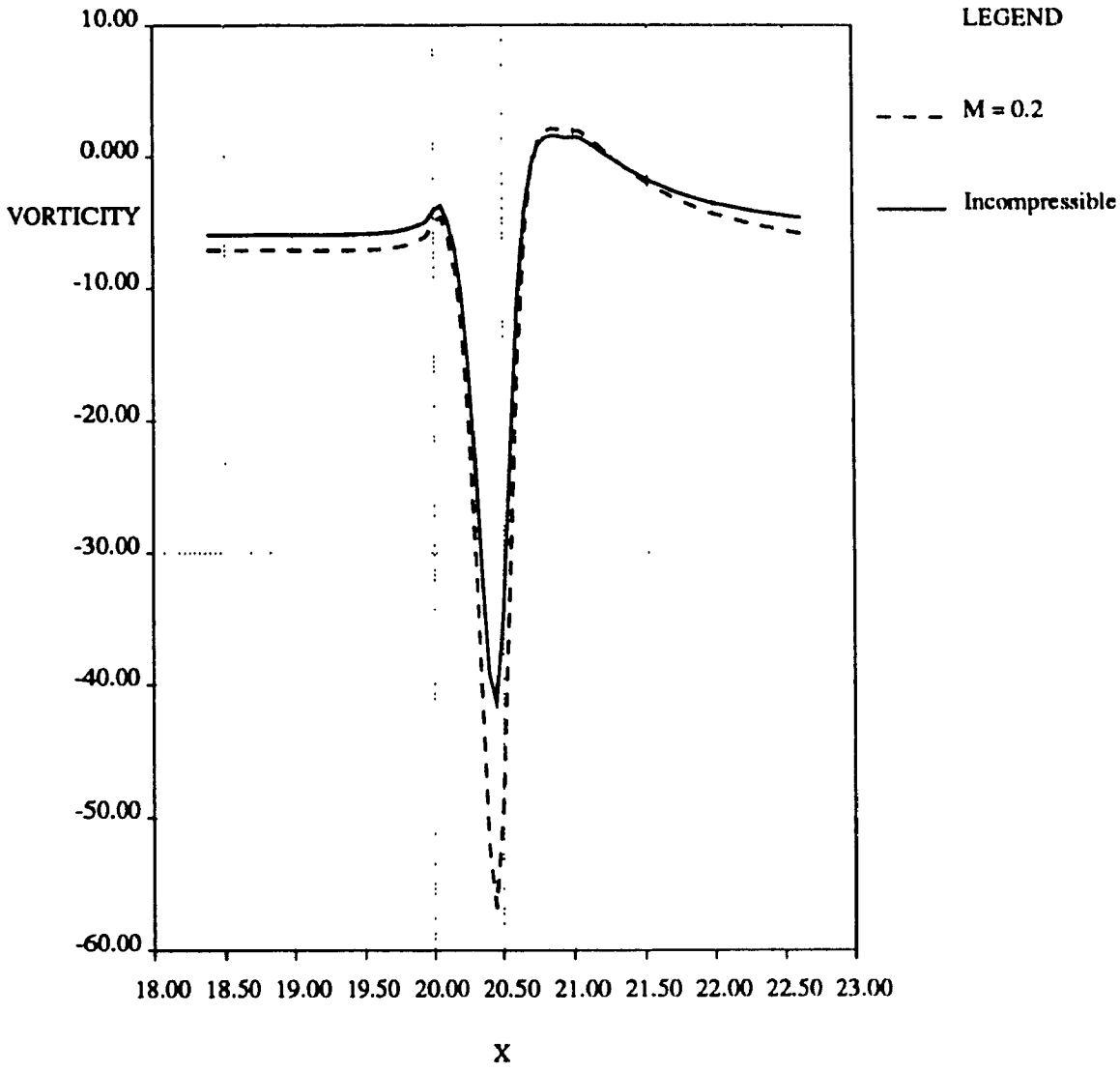

Figure 6.10 Vorticity profiles for 2-D convergent-divergent nozzle, Re = 100.

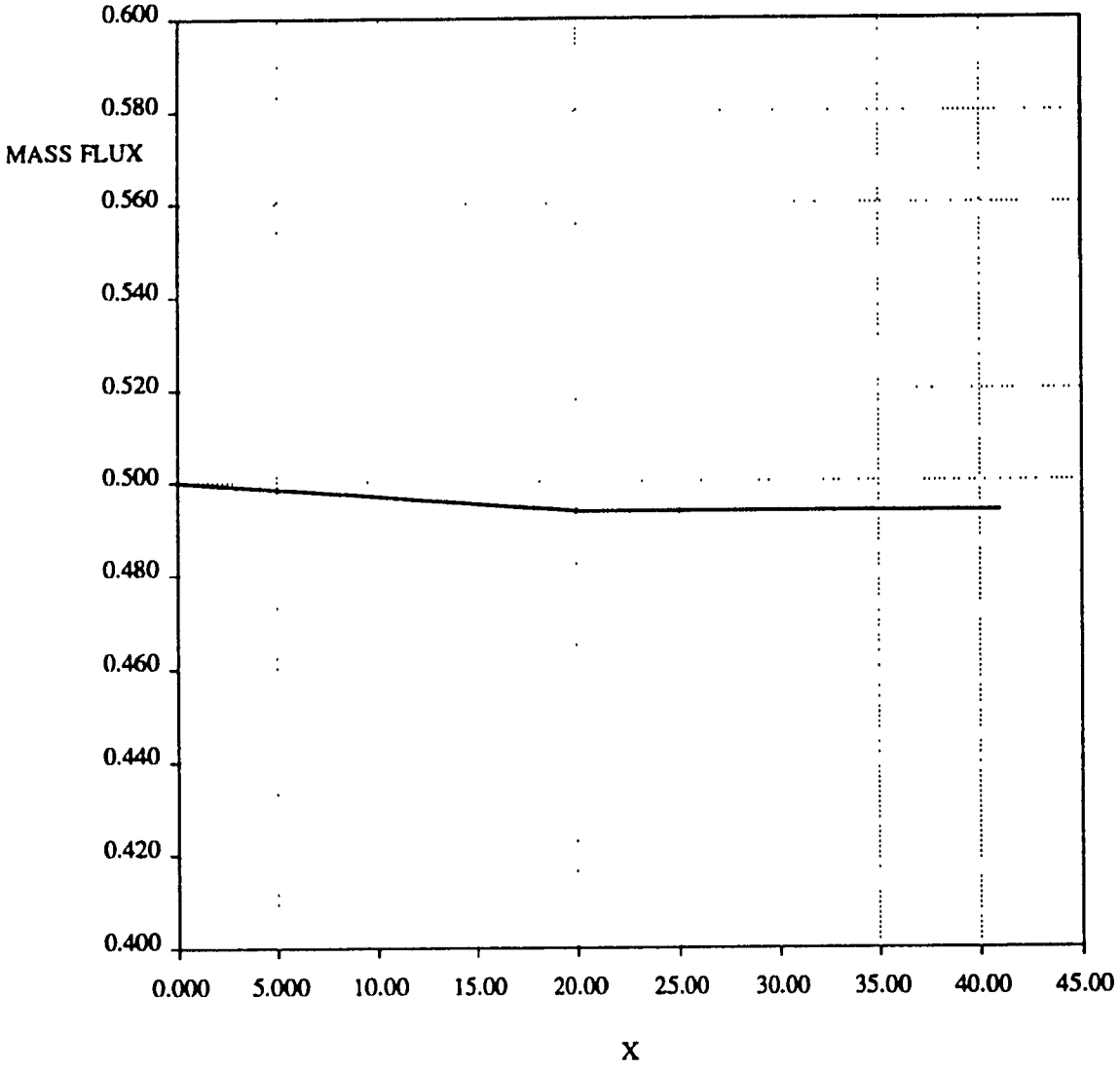

Figure 6.11 Mass Flux for 2-D convergent-divergent nozzle, Re = 100.

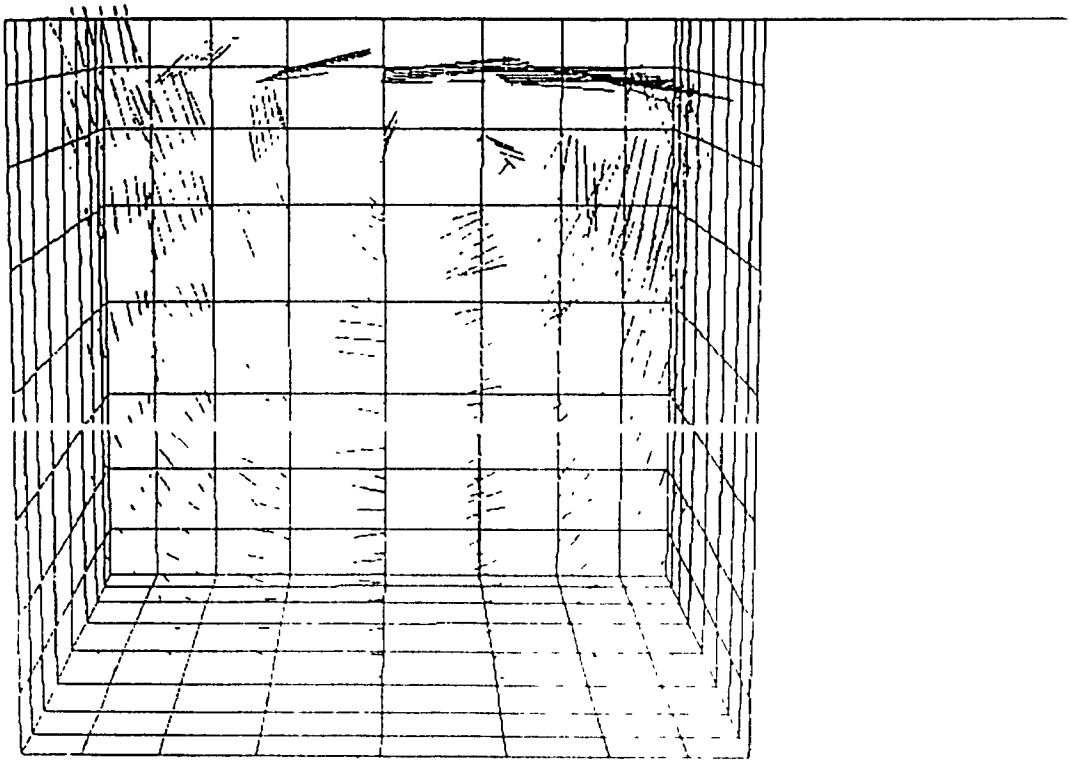

Figure 6.12 Geometry, grid and velocity vectors for 3-D driven cavity, $Re = 100$, $M = 0.5$.

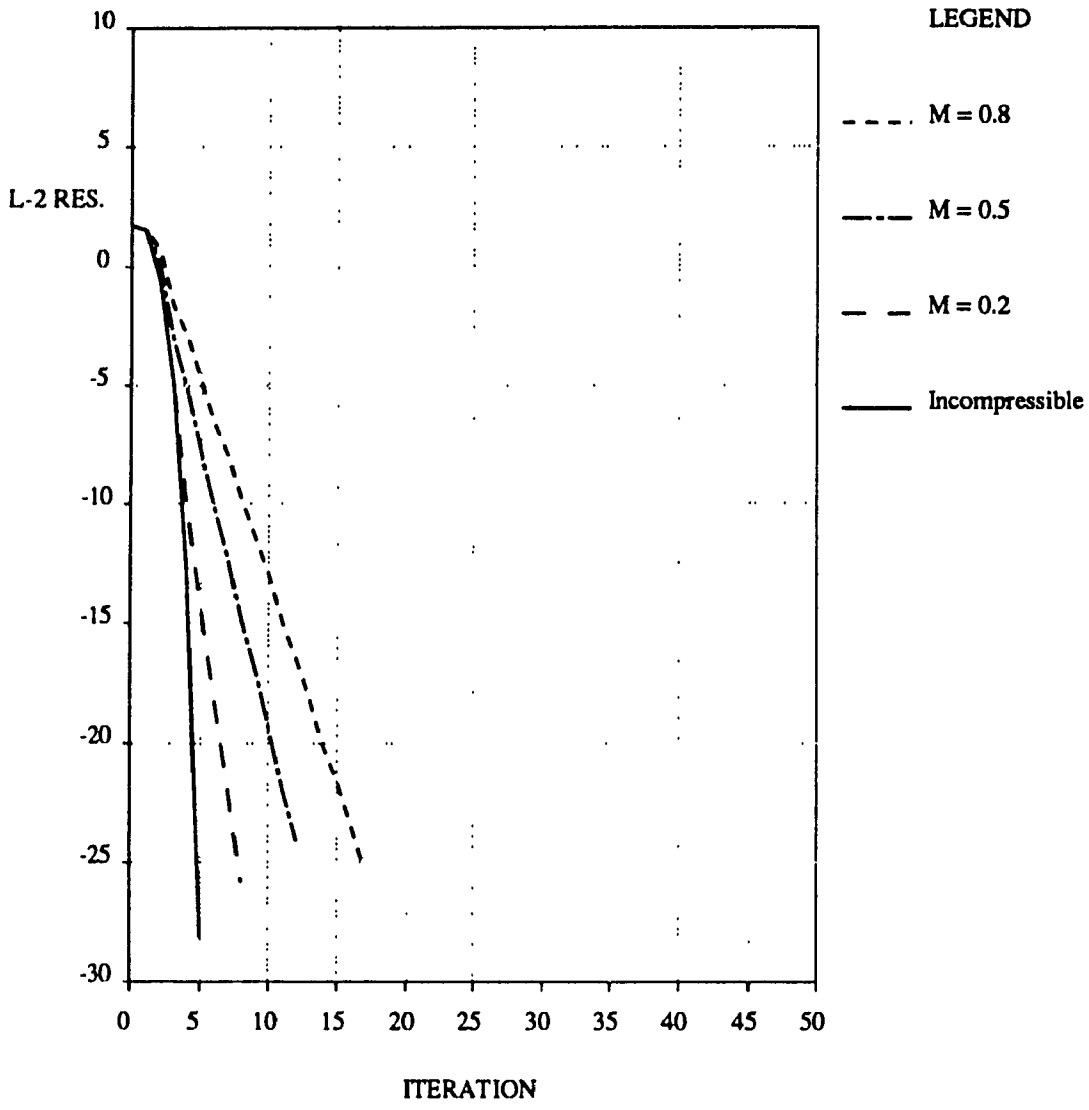

Figure 6.13 Convergence history for 3-D driven cavity, Re = 100.

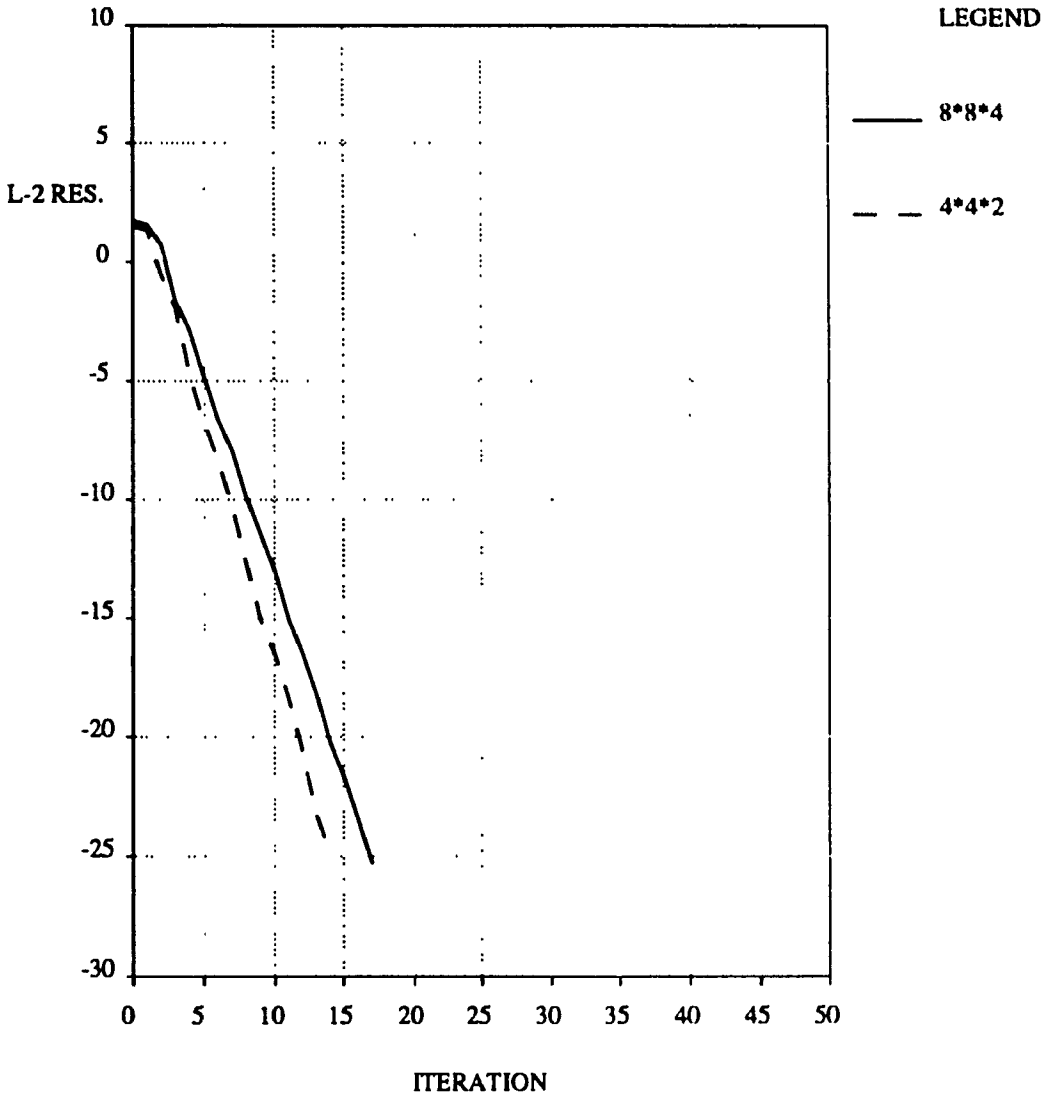

Figure 6.14 Convergence history for 3-D driven cavity, effect of grid size, Re = 100.

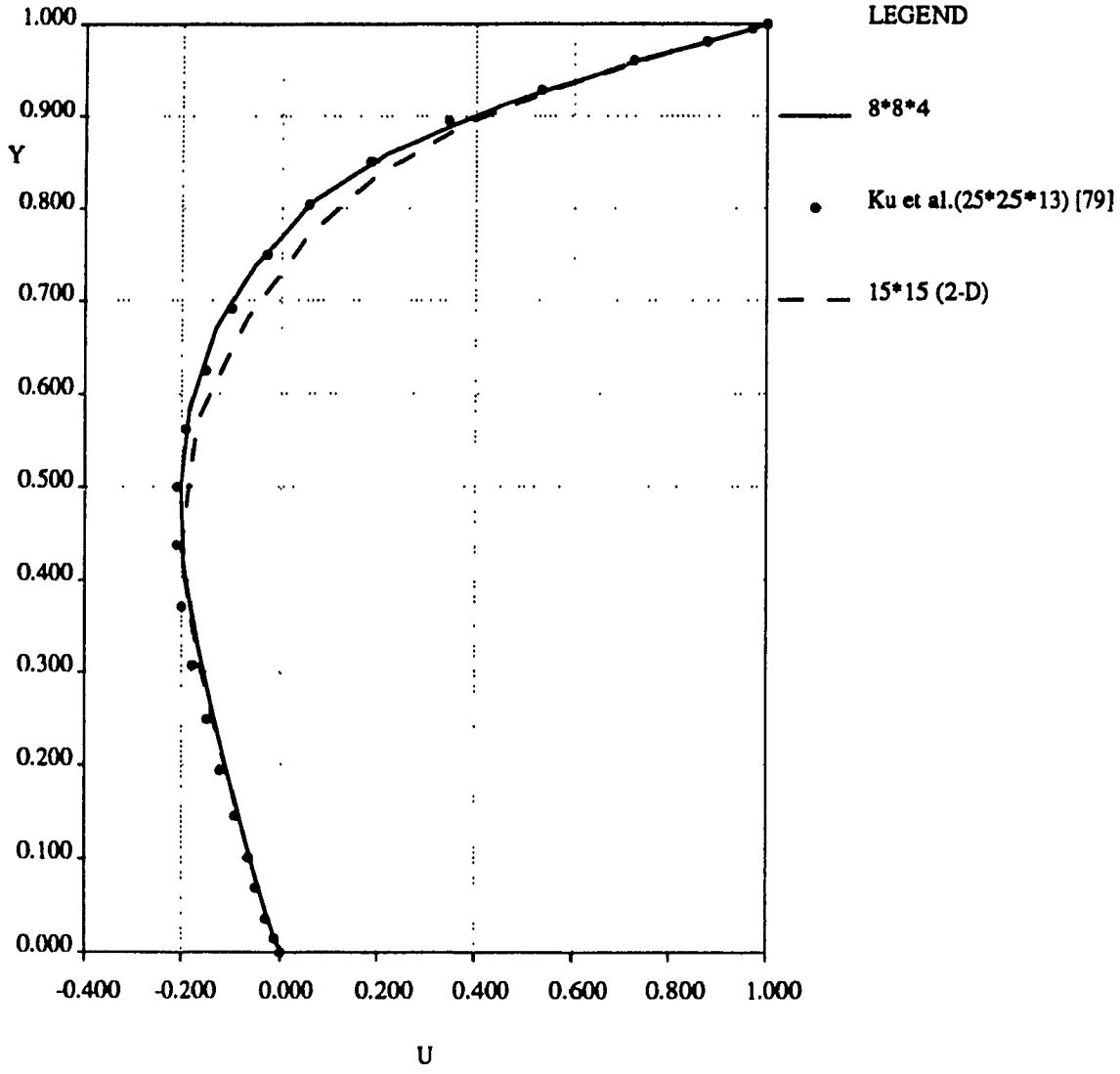

Figure 6.15 Centerline velocities for 3-D driven cavity, Re = 100.

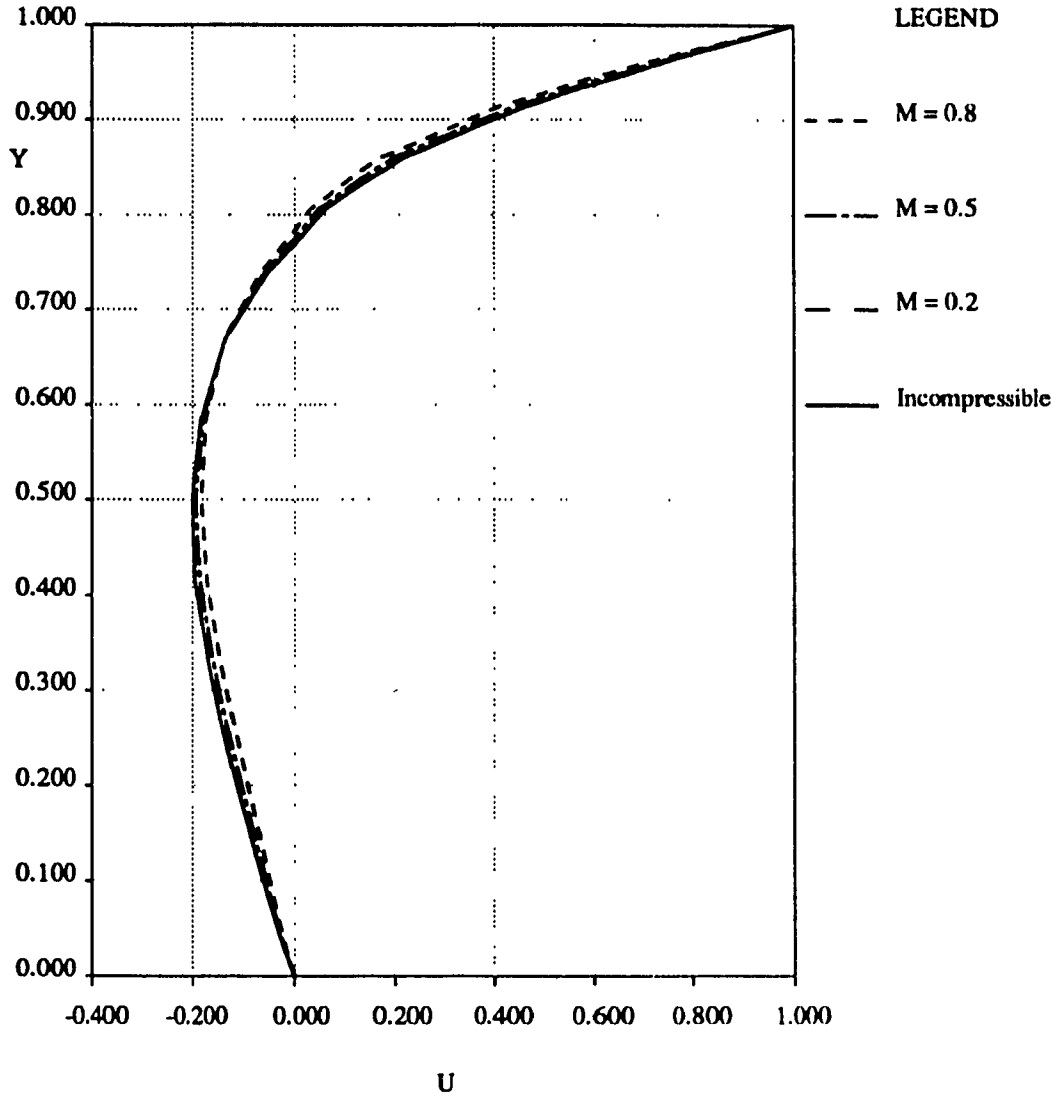

Figure 6.16 Centerline velocities for 3-D driven cavity, effect of compressibility, Re =100.

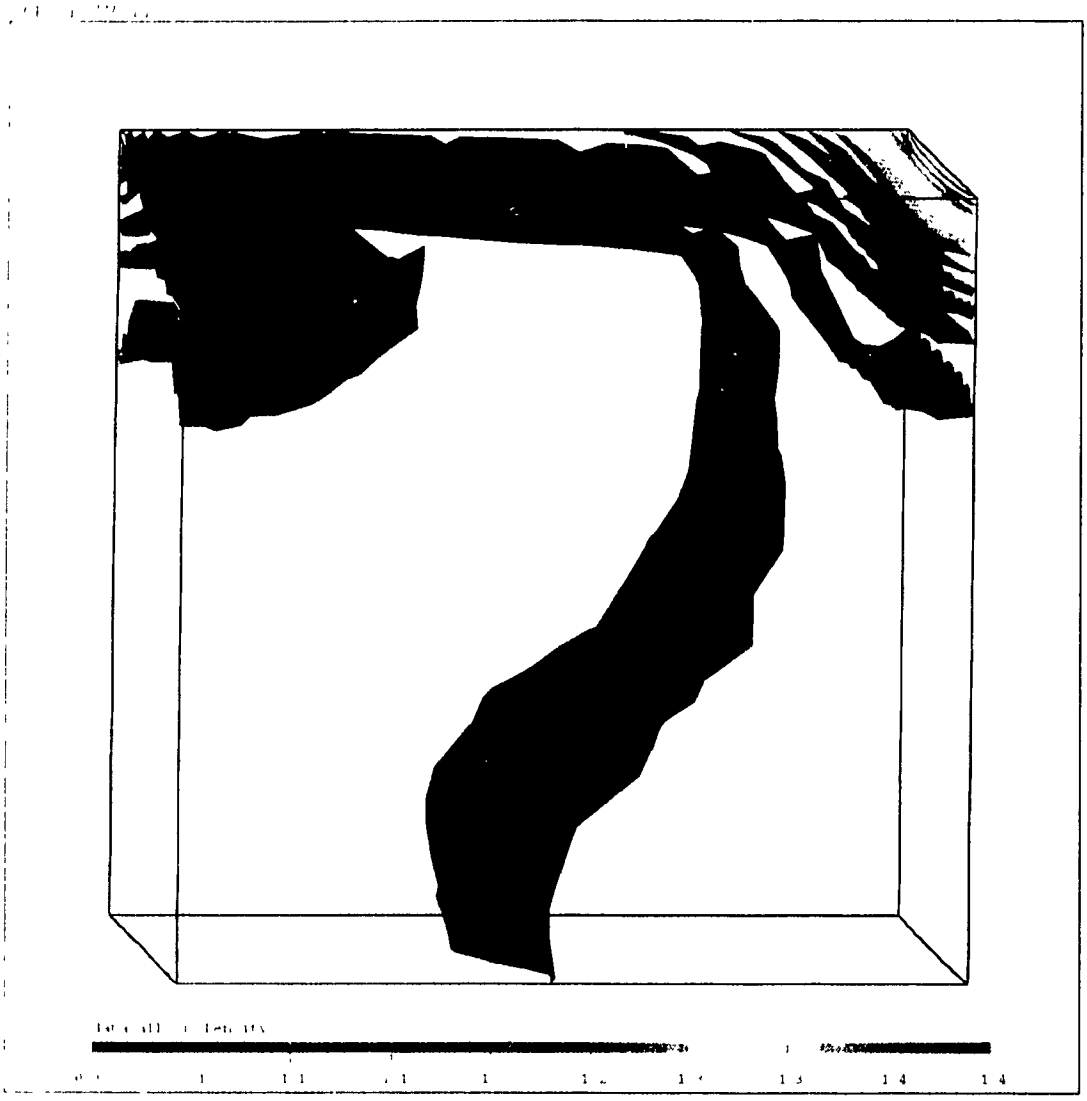

Figure 6.17 Density contours for 3-D driven cavity, Re = 100, M = 0.5.

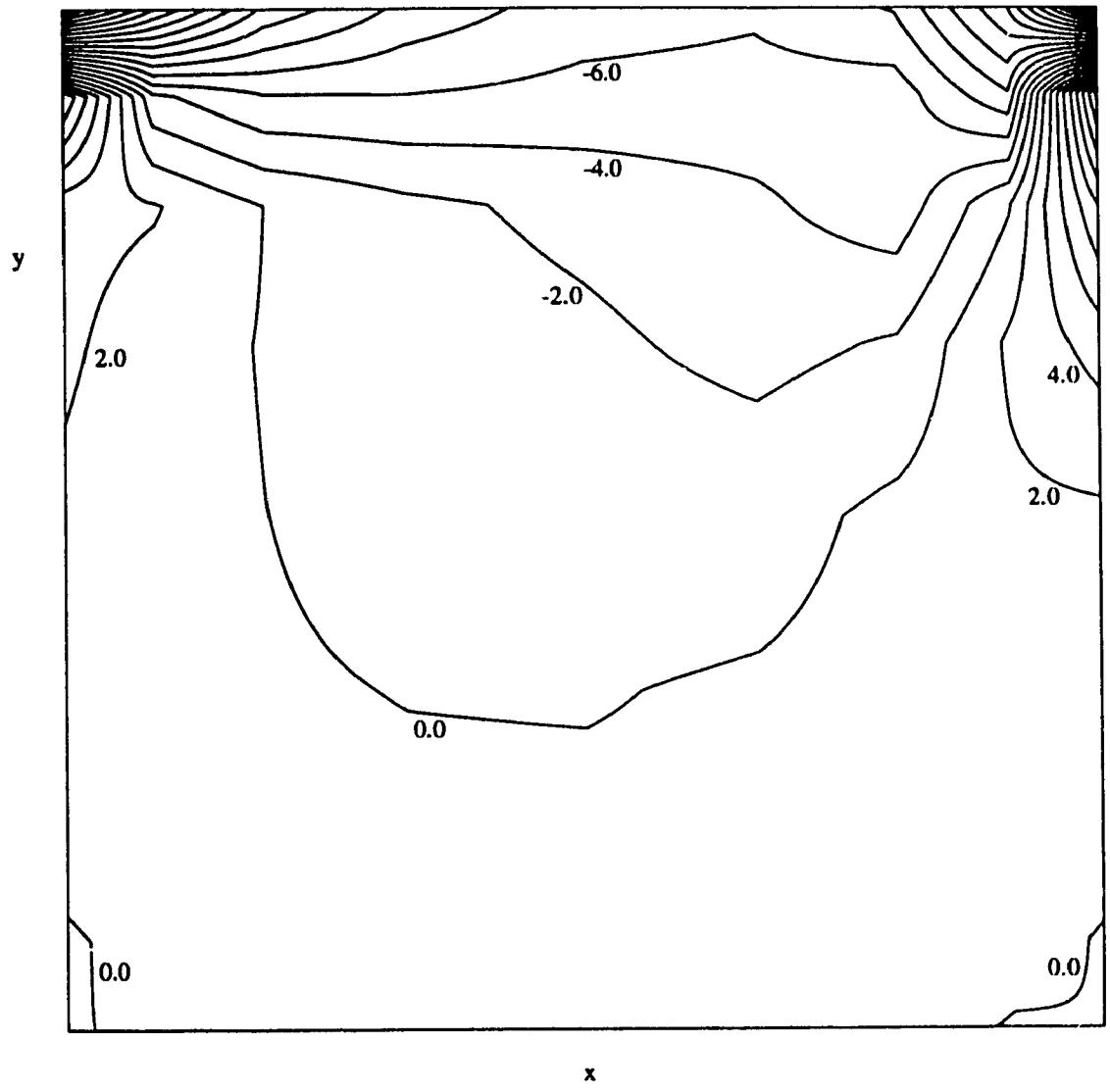

Figure 6.18a 3-D driven cavity, Re = 100,

Mid-plane normal vorticity lines, Streamwise.

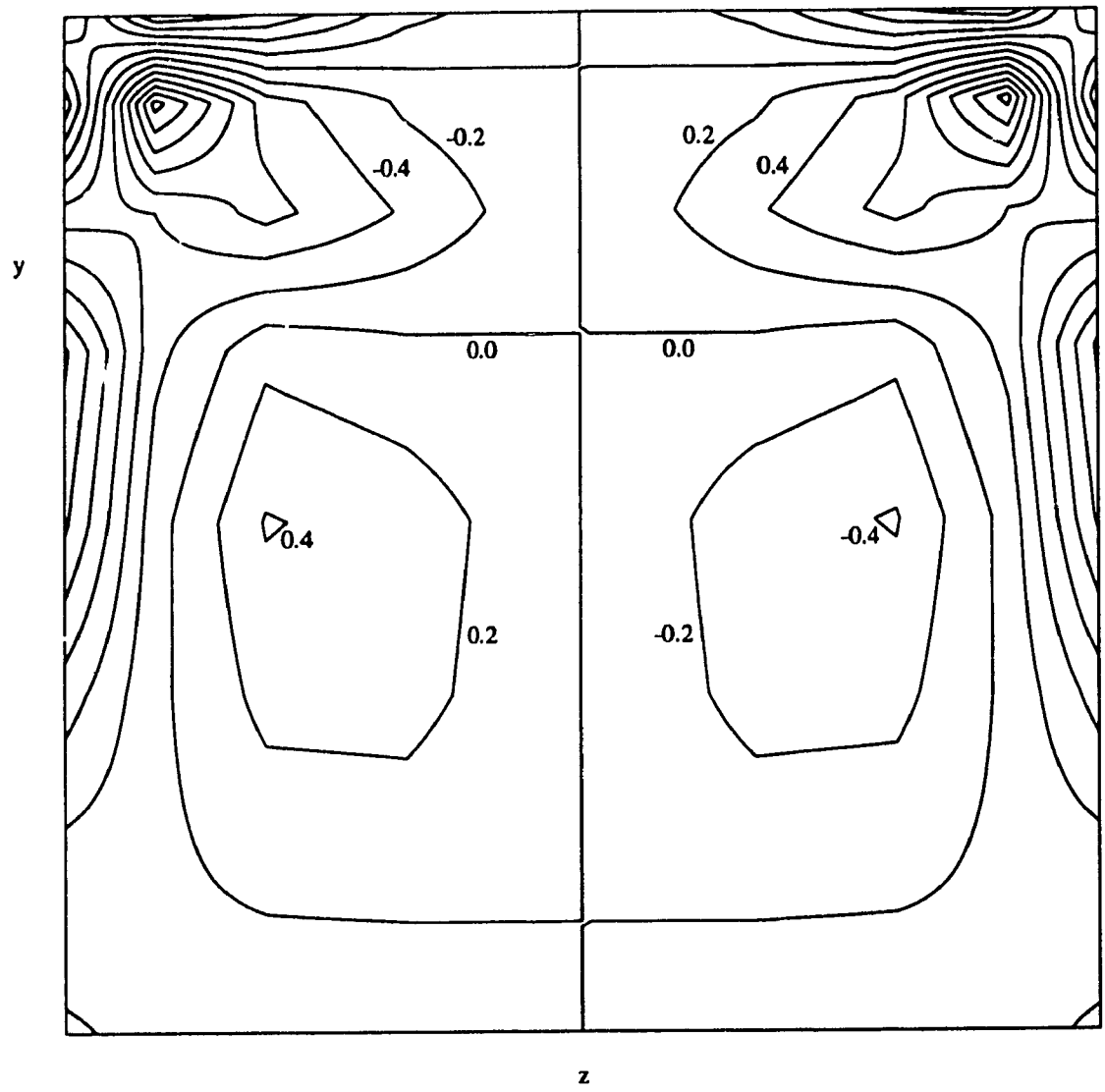

Figure 6.18b 3-D driven cavity, *Re* = 100,

Mid-plane normal vorticity lines, Spanwise.

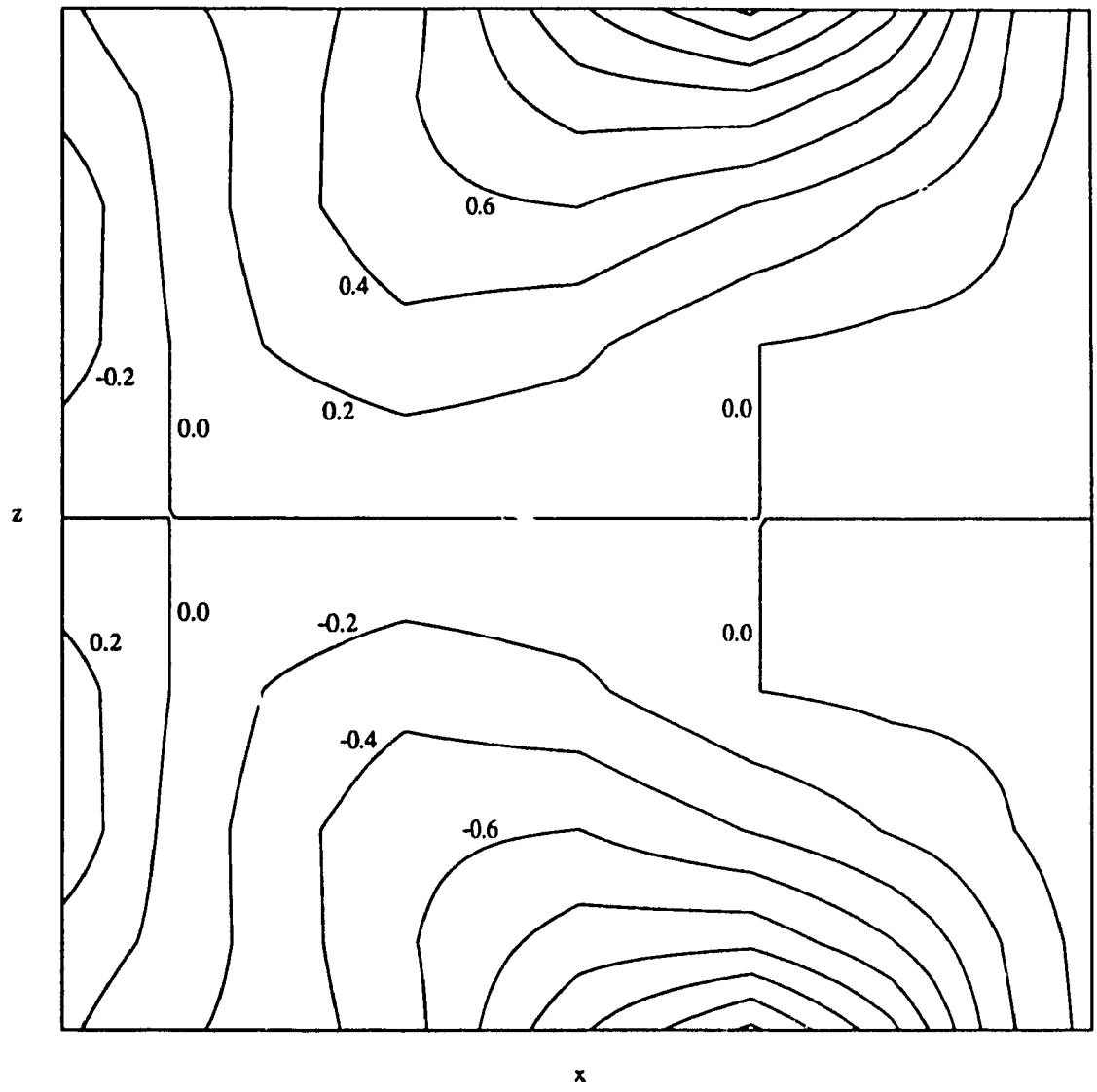

Figure 6.18c 3-D driven cavity, *Re* = 100,

Mid-plane normal vorticity lines, Horizontal.

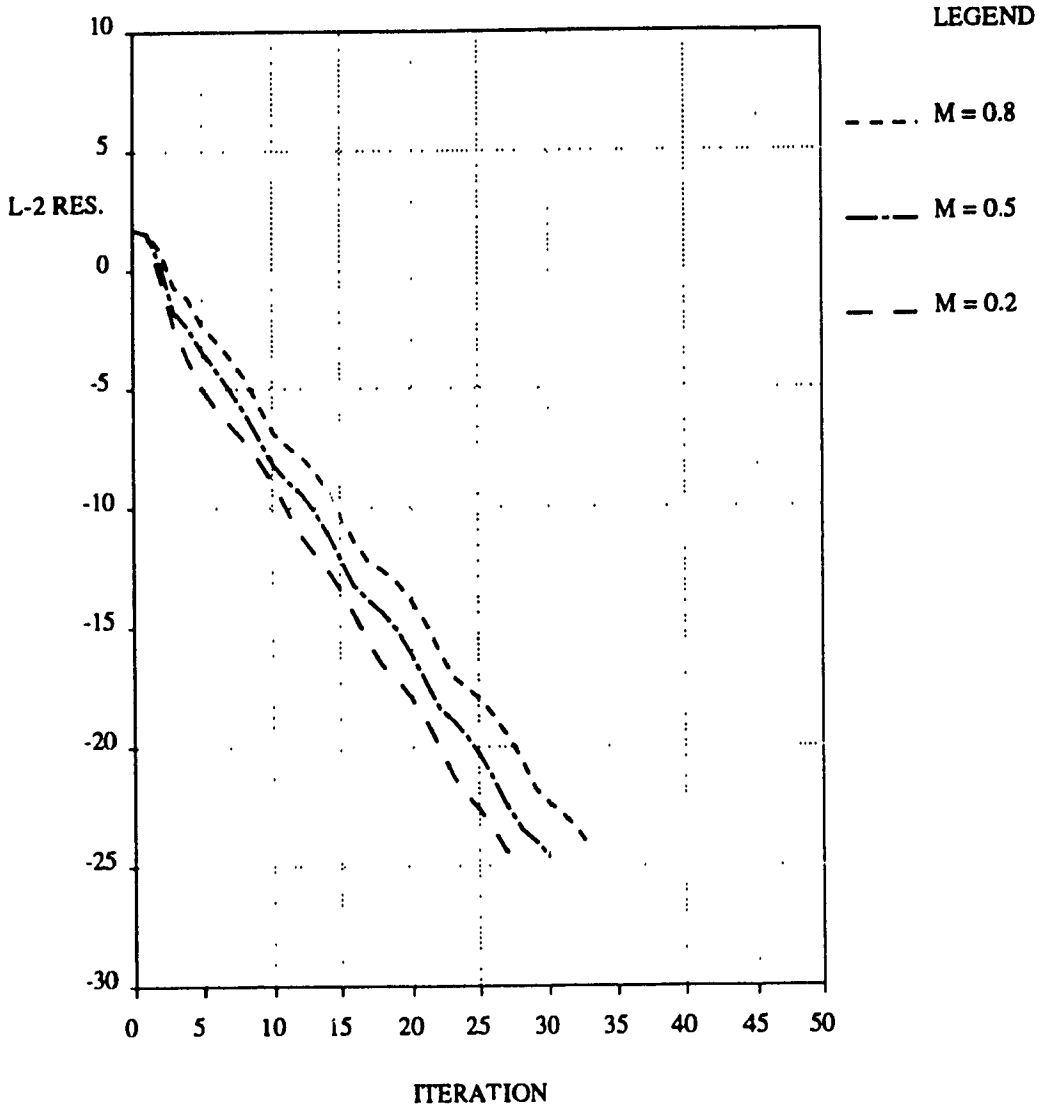

Figure 6.19 Convergence history for 3-D driven cavity, Energy equation, Re =100, Pr=0.72.

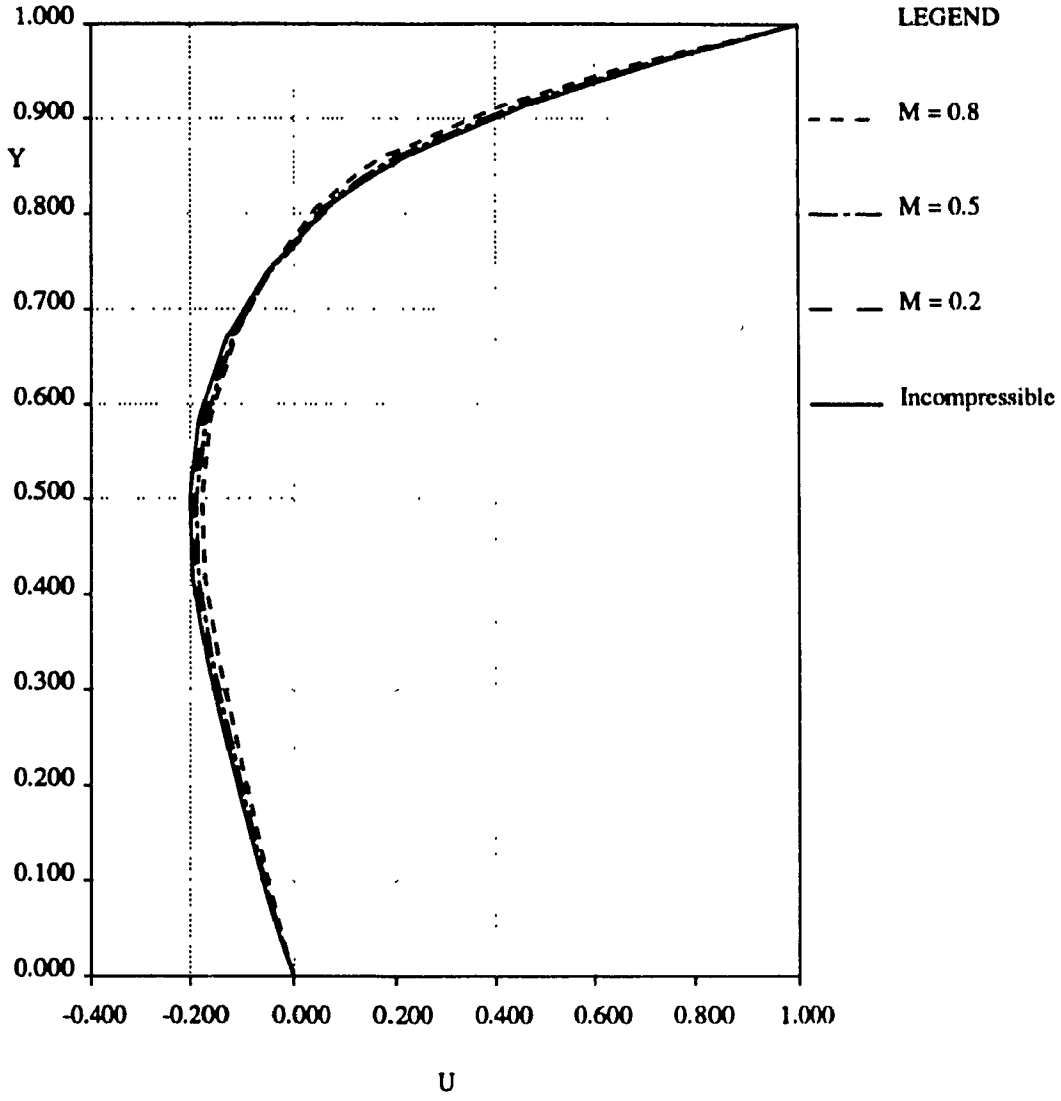

Figure 6.20 Centerline velocities for 3-D driven cavity, effect of compressibility, Energy equation, Re =100, Pr=0.72.

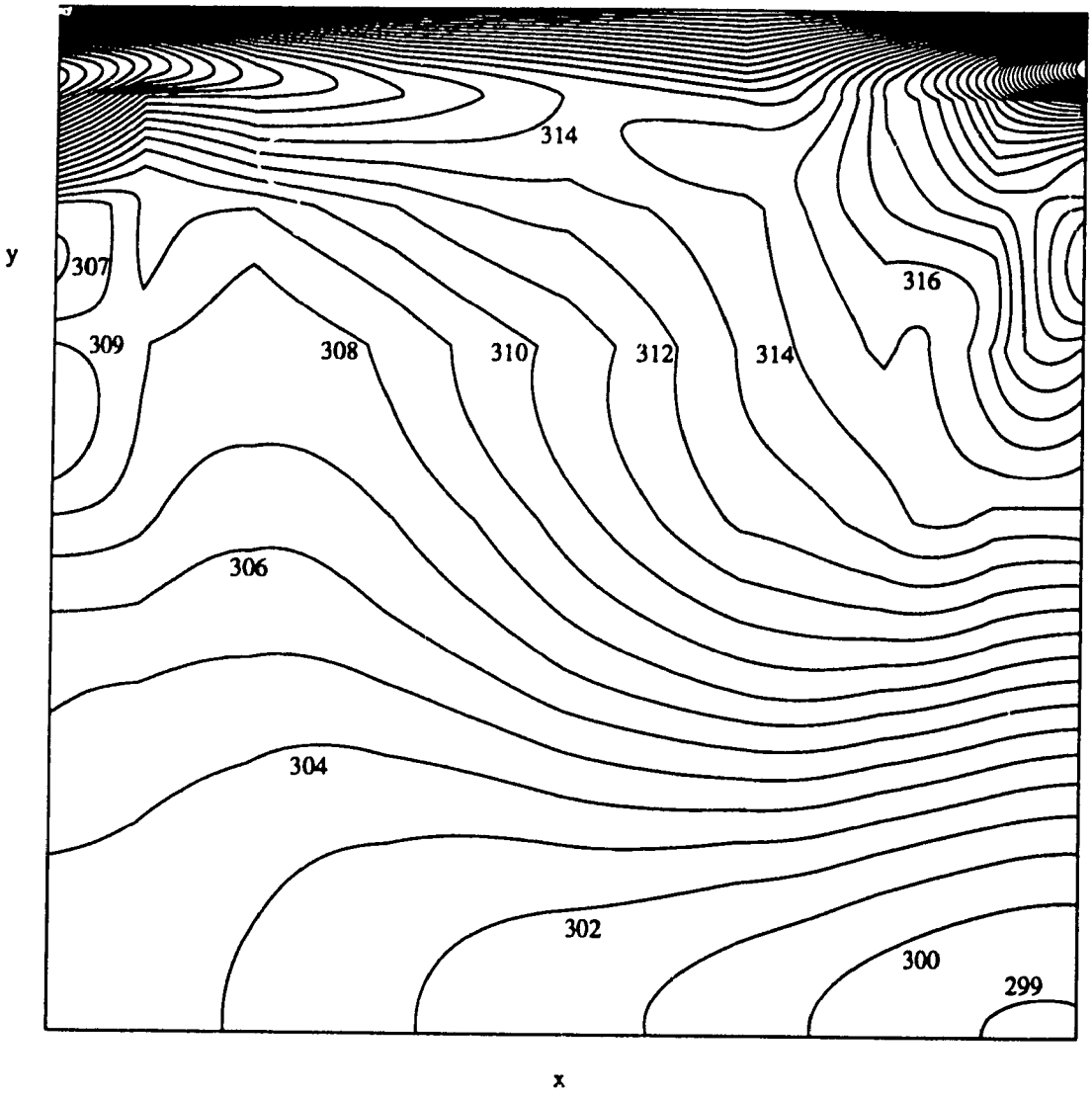

Figure 6.21a 3-D driven cavity, Energy equation, Re =100, Pr=0.72,

Constant temperature lines, Symmetry plane.

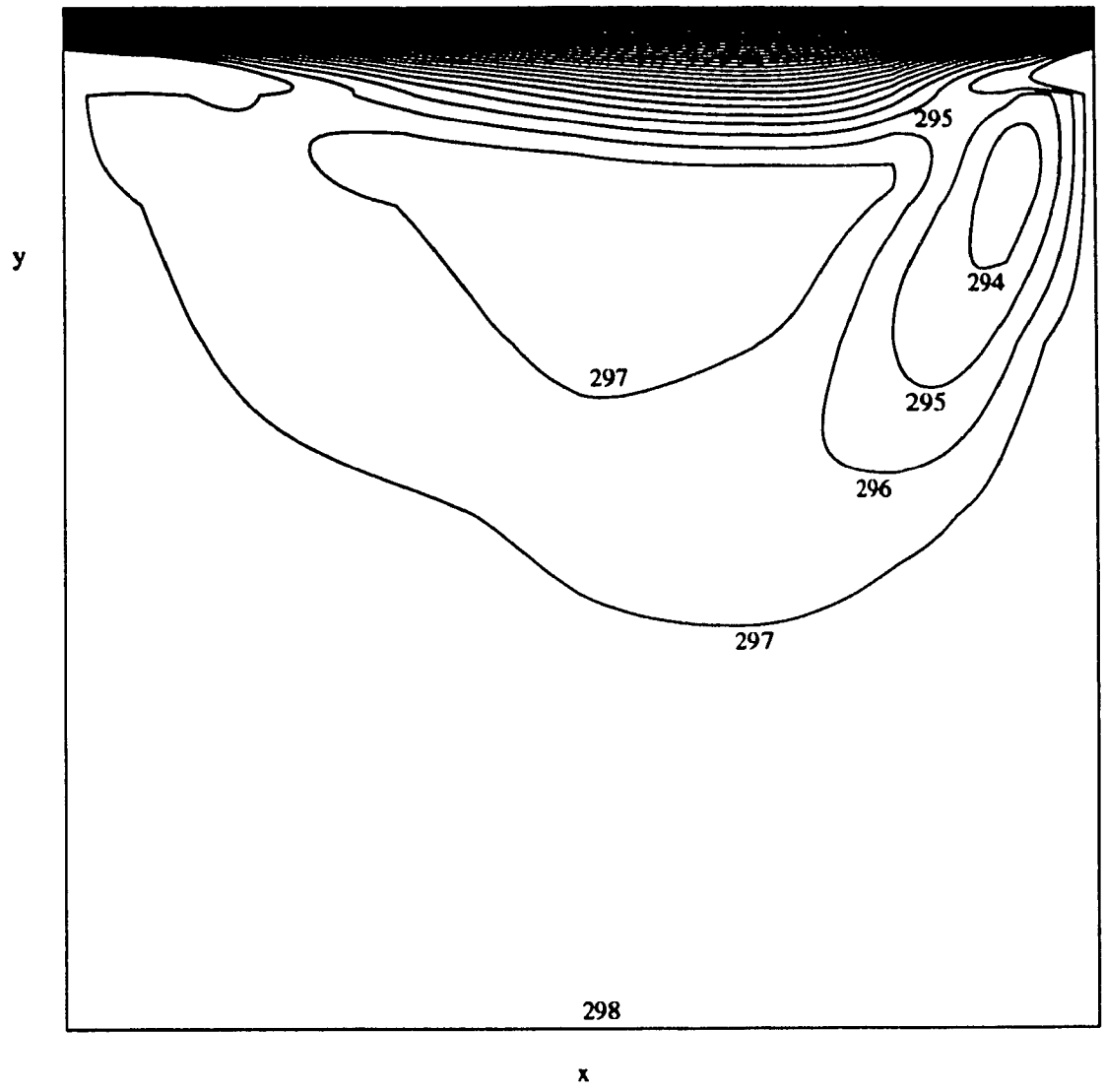

Figure 6.21b 3-D driven cavity, Constant total enthalpy, *Re* =100,
Constant temperature lines, Symmetry plane.

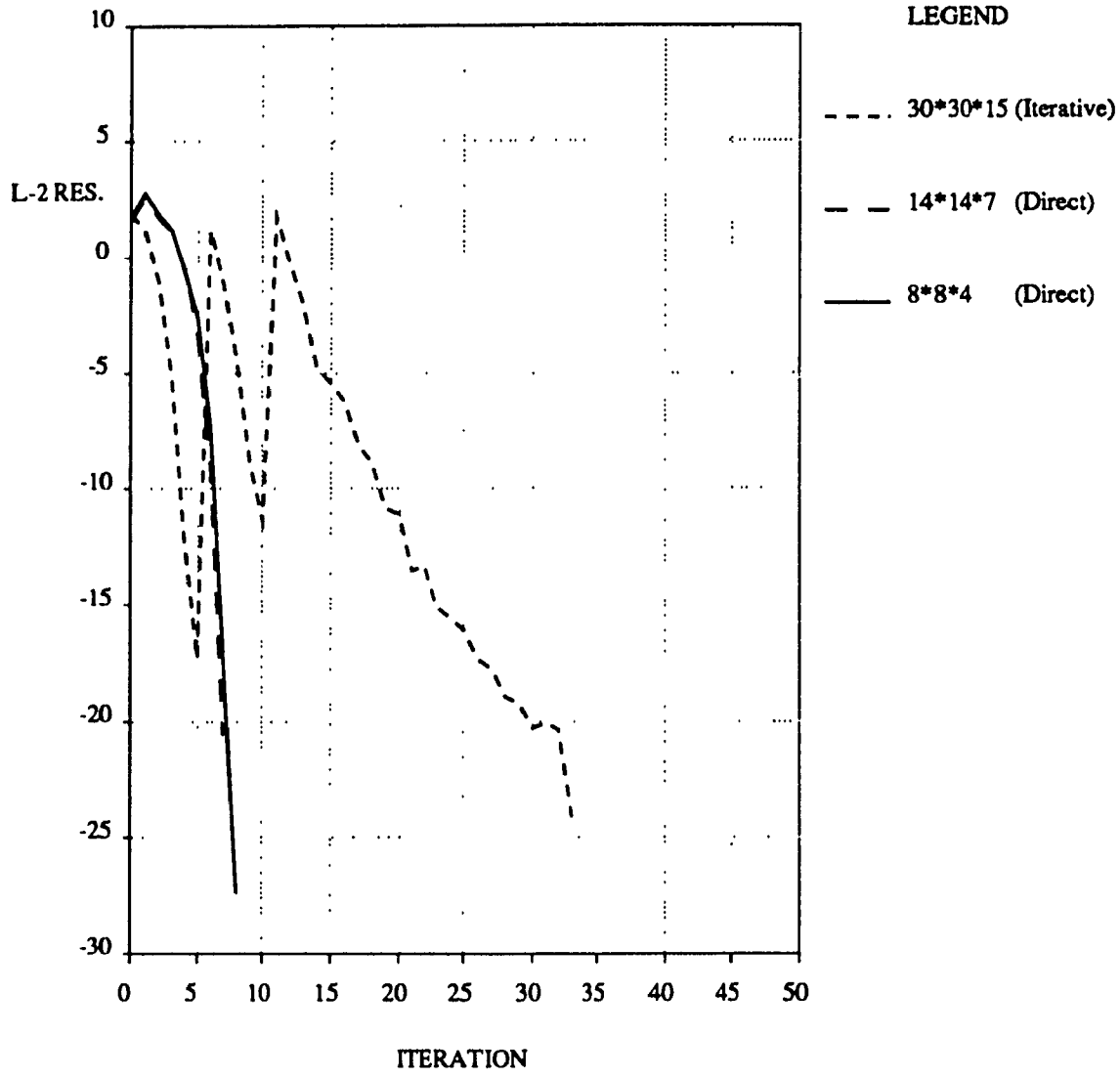

Figure 6.22 Convergence history for 3-D driven cavity, *Re* =400.

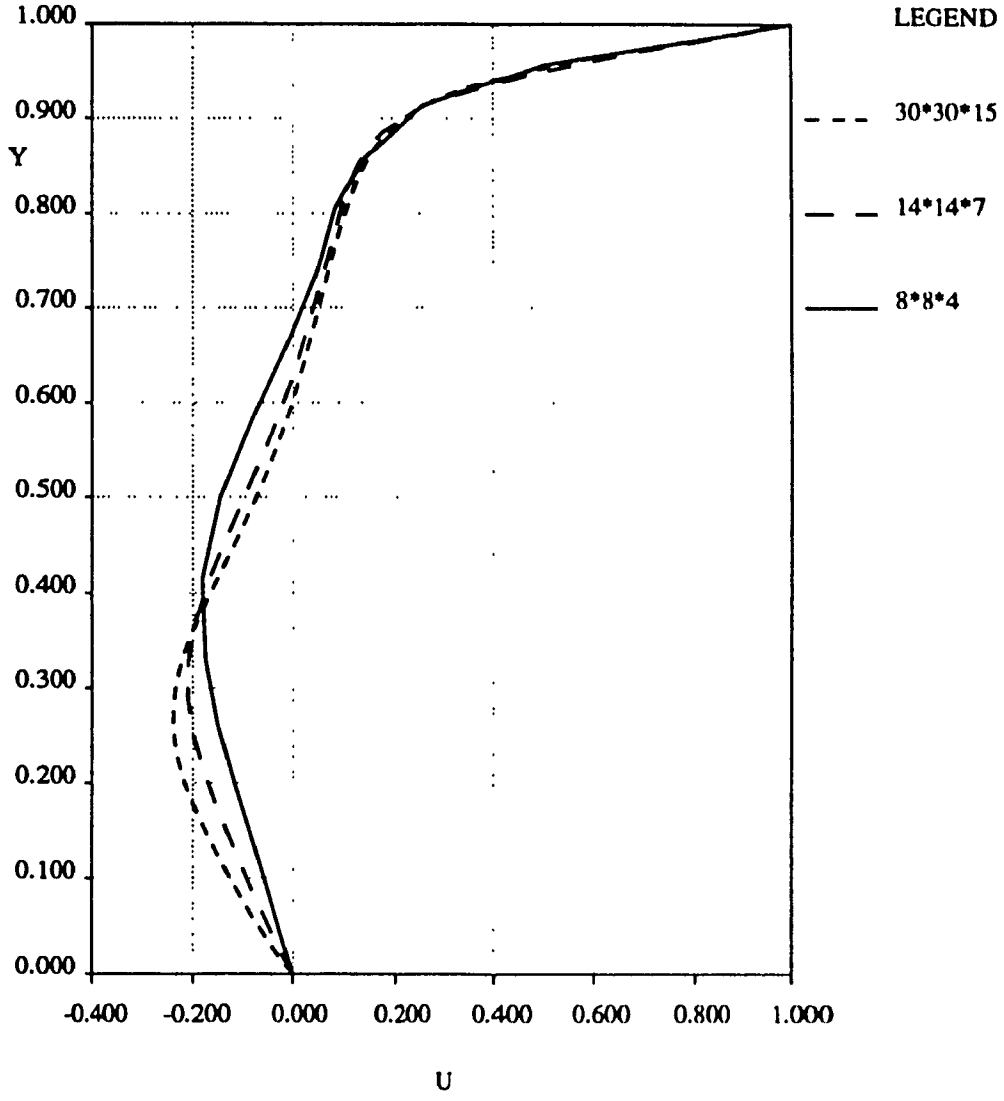

Figure 6.23 Centerline velocities for 3-D driven cavity, effect of grid size, $Re = 400$.

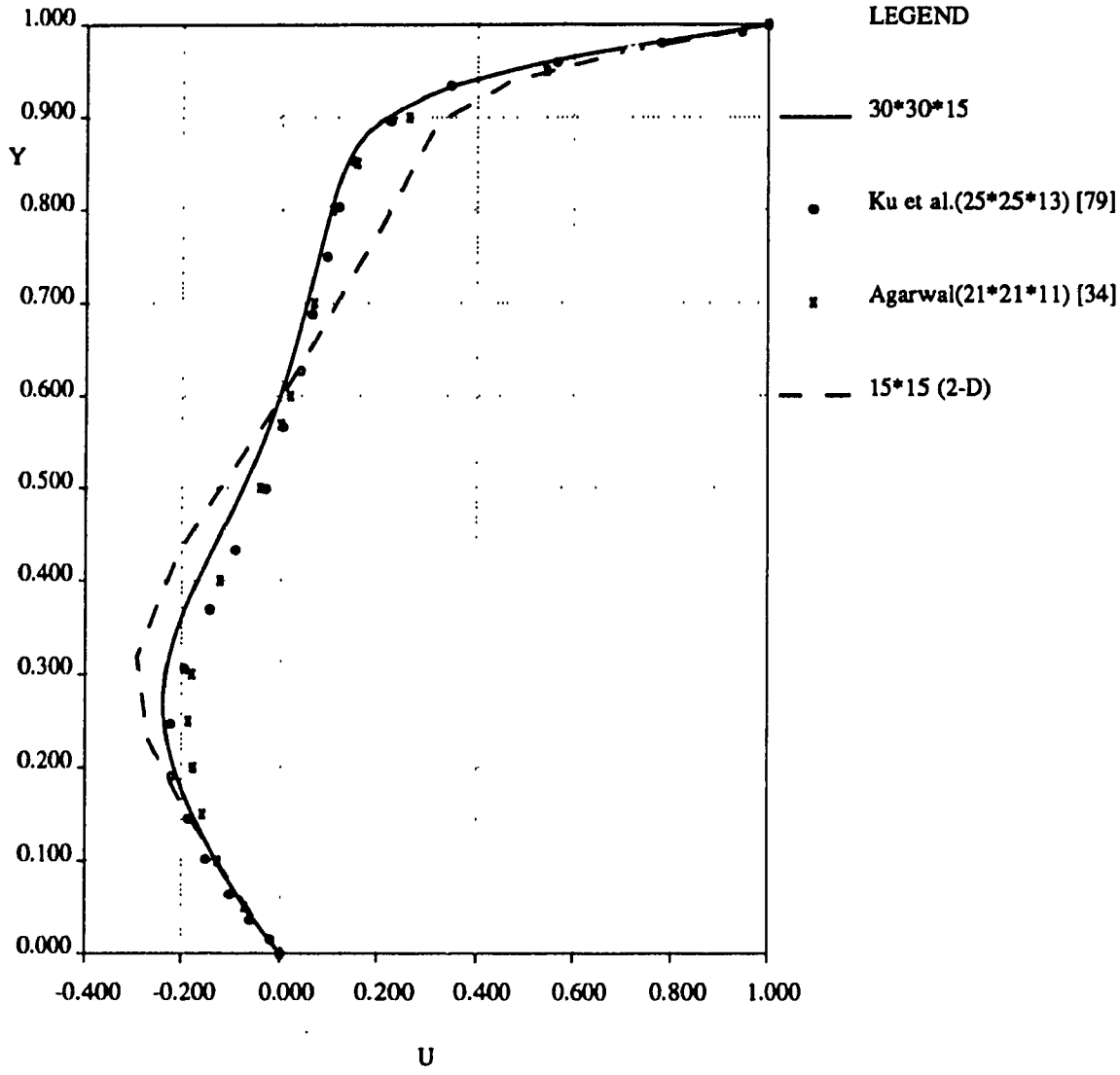

Figure 6.24 Centerline velocities for 3-D driven cavity, *Re* =400.

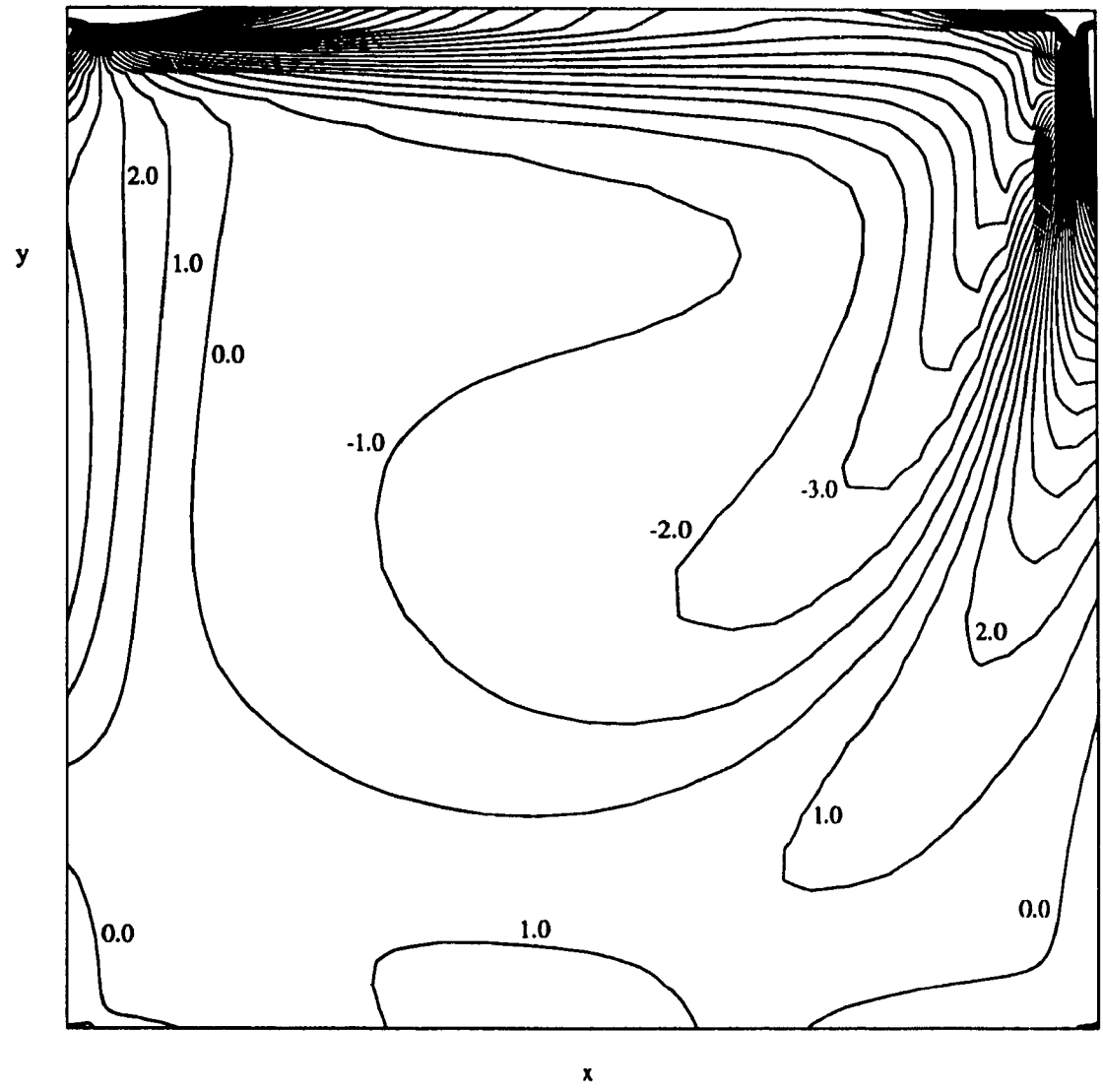

Figure 6.25a 3-D driven cavity, Re = 400,

Mid-plane normal vorticity lines, Streamwise.

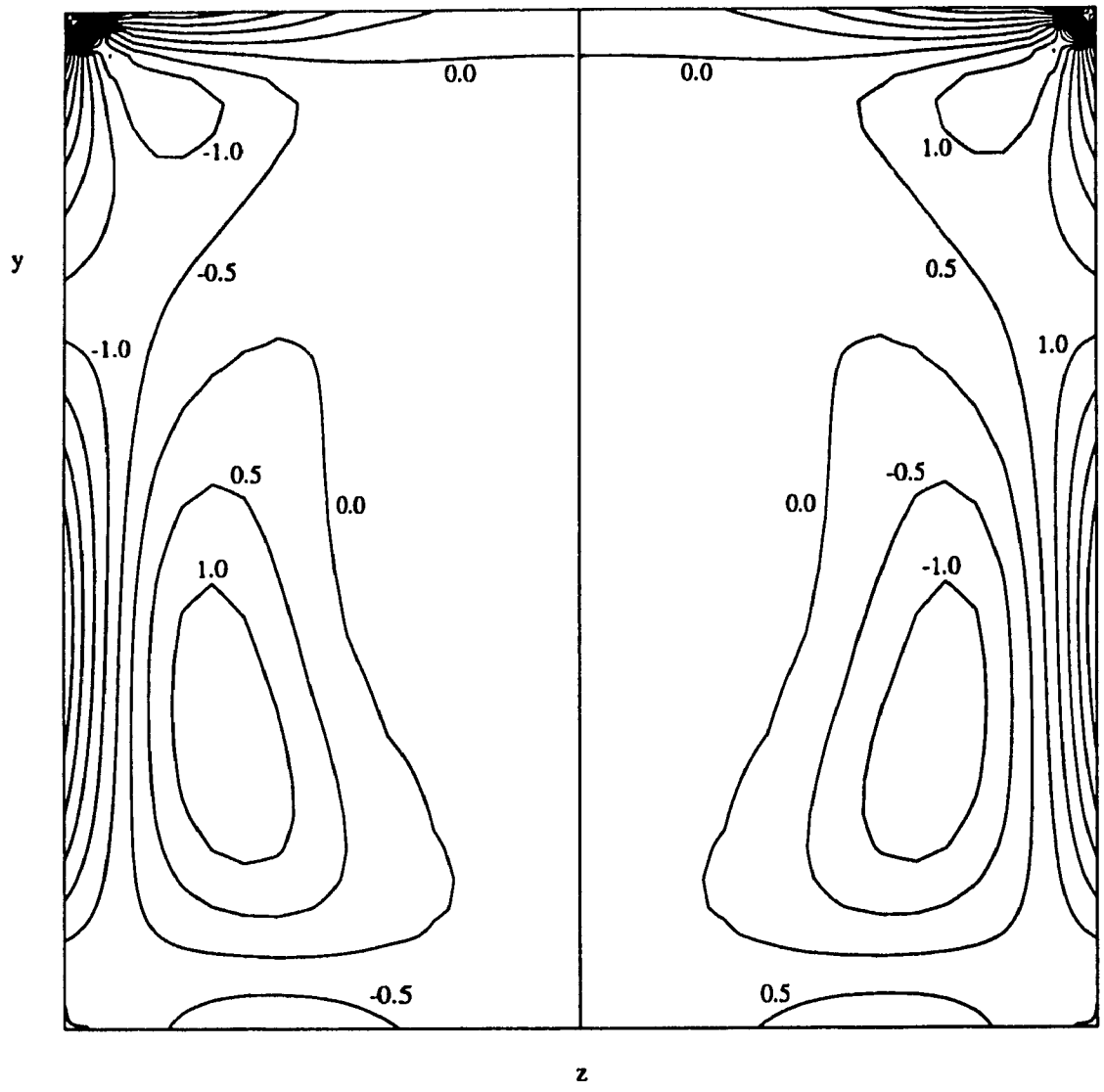

Figure 6.25b 3-D driven cavity, $Re = 400$,

Mid-plane normal vorticity lines, Spanwise.

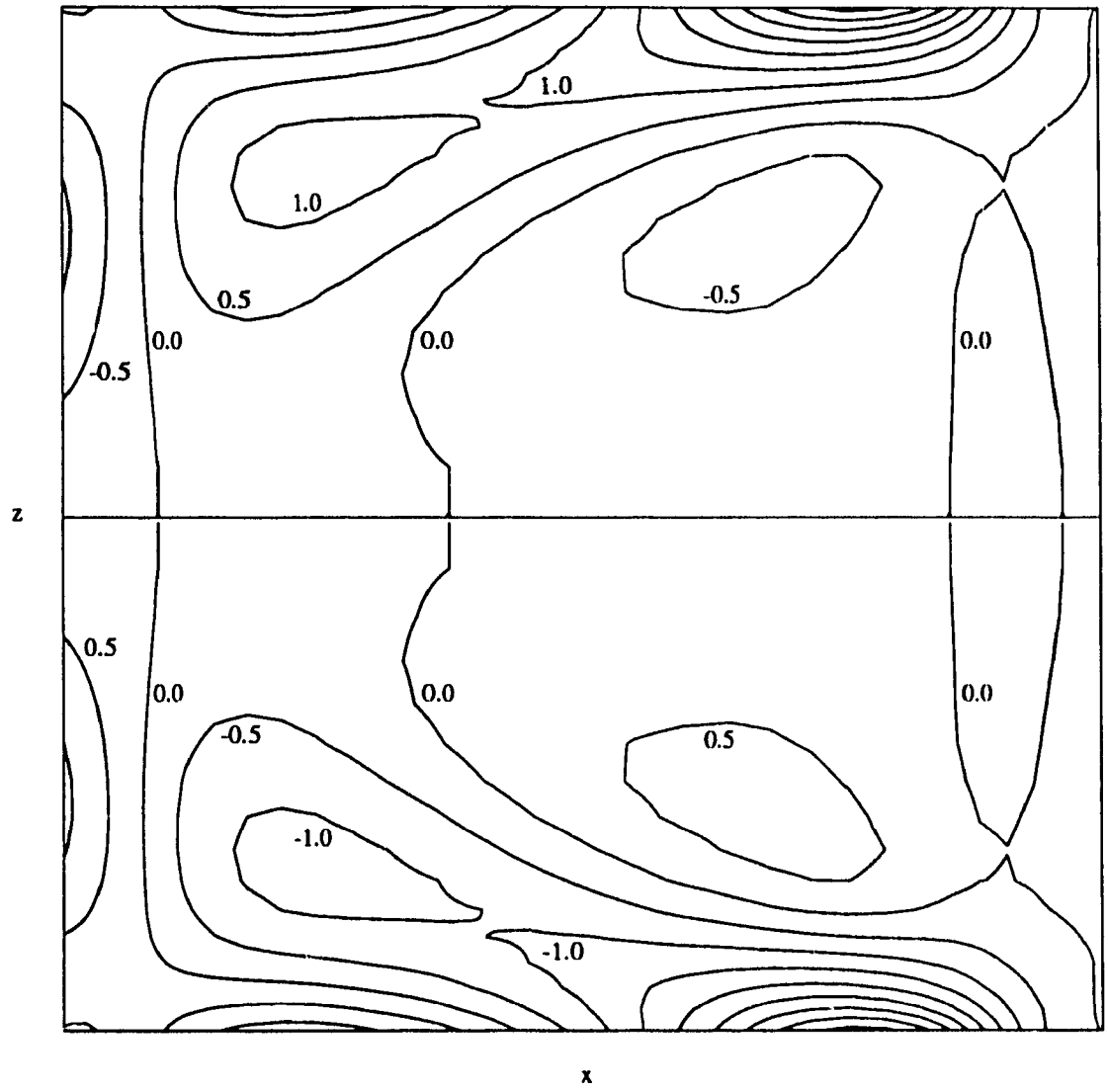

Figure 6.25c 3-D driven cavity, *Re* = 400,

Mid-plane normal vorticity lines, Horizontal.